NUMERICAL CALCULATION OF THE RESPONSE OF COASTAL WATERS
TO STORM SYSTEMS - WITH APPLICATION TO HURRICANE CAMILLE
OF AUGUST 17-22, 1969

By

Bryan Rowell Pearce

A DISSERTATION PRESENTED TO THE GRADUATE
COUNCIL OF THE UNIVERSITY OF FLORIDA IN PARTIAL
FULFILLMENT OF THE REQUIREMENTS FOR THE DEGREE OF
DOCTOR OF PHILOSOPHY

UNIVERSITY OF FLORIDA
1972

DEDICATION

This dissertation is dedicated to my son,
Nicholas James, born August 14, 1972.

ACKNOWLEDGEMENTS

TABLE OF CONTENTS

LIST OF FIGURES

LIST OF SYMBOLS

a_n	Fourier coefficients
B_n	Fourier coefficients for forcing function
c	wave celerity, $\sqrt{gh}$
c_1, c_2	constant coefficients used in moving wind stress development
C	storm or forcing function velocity
CDT	central daylight time
c^*	C/c
D	total depth
f	Darcy-Weisbach friction factor
f_L	linear friction factor
F,F'	forcing function
F_x, F_y	resistance coefficients for x and y equations of motion
g	gravitational acceleration
GMT	Greenwich Mean Time
h	water depth, referenced to Mean Sea Level (MSL)
h_o	water depth at shelf break
h_1	water depth at coastline
H_1, H_2	definitions used to simplify moving wind stress development
H_F	hindcast wave height
i	indicial functional parameter
k	wind stress coefficient
ℓ	shelf width

m	bottom slope
MSL	mean sea level
n	indicial functional parameter
p	pressure
p_0	surface pressure at center of hurricane
p_∞	surface pressure far from storm
p_η	surface pressure
q	water transport
q_n	water transport component normal to boundary
q_x, q_y	water transport components in x and y directions
r	distance from center of hurricane
R	radius to maximum winds
t	time variable
t*	dimensionless time variable, t/T
t'	dummy variable
t_0	initial time
t_1, t_2, t_3	time that zeros of idealized forcing function cross shelf break
T	function of time; $4\ell/C$
T_F	hindcast wave periods
u	component of water velocity in x direction
$\bar{u}$	time average of u
u'	instantaneous fluctuation of u
U	wind velocity at 30 feet above the surface
$U_{x,y}$	x and y components of U
U_{cr}	U critical, in Van Dorn's expression for wind stress coefficient

U_c	cyclostrophic wind
U_g	geostrophic wind
U_G	gradient wind
v	component of water velocity in y direction
$\bar{v}$	time average of v
v'	instantaneous fluctuation of v
V	forward velocity of storm
V'	$V \sin\theta$
w	component of water velocity in z direction; wind field breadth
$\bar{w}$	time average of w
w'	instantaneous fluctuation of w
$w^\star$	lateral dimension of shelf incorporated into numerical model
x, x_1	horizontal coordinate, normal to coast
$x^\star, x'$	dimensionless horizontal coordinates, x/ℓ
x_c	coordinate of coastline
X	function of x; dimensionless depth, x/x_B
X_s	starting point of storm as distance from landfall
y, x_2	horizontal coordinate, parallel to shore
y'	dimensionless horizontal coordinate, y/ℓ
z, x_3	vertical coordinate
α_B	angle between breaking waves and shoreline
α_n	coefficient in moving wind stress analytical development
$\alpha^\star$	dimensionless parameter, $w/w^\star$
$\alpha^{\star\star}$	dimensionless parameter, $\ell/w^\star$
β	constant, $\tau_{n_x}/\rho g$

γ	ρg
δ	impulse function
Δp	central pressure index
Δt	time increment
$\Delta x, \Delta y$	grid element dimensions
$\Delta \tau$	shear stress increment
ζ	dimensionless parameter, mh/β
ζ_0	dimensionless parameter, mh_0/β
ζ_1	dimensionless parameter, mh_1/β
η	surge height, referenced to MSL
η'	dimensionless surge height
θ	angle between point of observation and line of storm movement
κ	shear stress parameter
λ	width of idealized storm
λ^*	dimensionless storm width, λ/ℓ
μ	molecular viscosity
ξ	$m\eta/\beta$; dummy variable
ρ	density of seawater
ρ_a	density of air
σ, σ_n	$cn\pi/2\ell$
σ', σ_n'	$Cn\pi/2\ell$
τ	shear stress
τ_η	surface shear stress
$\tau_{x,y,z}$	components of shear stress
$\tau_{\eta_{x,y}}$	x and y components of surface shear stress

$\tau_{b_{x,y}}$ x and y components of bottom shear stress

$\tau'_{x_i x_j}$ Reynolds stress

ϕ latitude

ω the earth's angular velocity

∇ gradient operator

∇^2 Laplacian operator

Abstract of Dissertation Presented to the
Graduate Council of the University of Florida in Partial
Fulfillment of the Requirements for the Degree of Doctor of Philosophy

NUMERICAL CALCULATION OF THE RESPONSE OF COASTAL WATERS
TO STORM SYSTEMS - WITH APPLICATION TO HURRICANE CAMILLE
OF AUGUST 17-22, 1969

By

Bryan Rowell Pearce

August, 1972

Chairman: Robert G. Dean
Cochairman: Bent A. Christensen
Major Department: Civil and Coastal Engineering

A numerical model is employed to describe the water motion in a

coastal region associated with the passage of a hurricane or severe

storm. The model is two-dimensional, employs the vertically integrated

or "tidal" equations of motion, and is used to describe the specific

case of Hurricane Camille of August 1969. Two models are employed, a

large grid with 16 nautical mile grid elements and a small grid model

with 6 nautical mile grid elements. The results of the two models were

not significantly different. The maximum storm surge or maximum

water level above mean sea level was calculated and found to agree to

within twenty per cent with maximum surge heights determined from

high water marks. Calculated surge height was found to be insensitive

to bottom friction coefficients varying from .005 to .02. Inclusion

of the nonlinear convective terms affected the calculated surge
height maximum for Hurricane Camille by less than two per cent and
affected the surge in any grid element adjacent to the coast by less
than five per cent. Two-dimensional storm surge plots at different
times are presented.

Hurricane generated currents were calculated and compared to data
taken off the Florida coast. It is concluded that more actual current
data are necessary before hurricane generated currents can be cal-
culated with confidence. The current calculations were found to be
sensitive to bottom friction and subject to "wind-up".

In addition to numerical calculations, basic analytical cases
are covered, including the response of a shelf of uniform depth to
a triangular wind stress distribution moving with constant velocity.

CHAPTER 1

INTRODUCTION

The problem of predicting the response of coastal waters to extreme wind systems is becoming increasingly important as the coastal regions of this country are developed for residential, recreational and industrial uses. Disasters such as the ones occurring in recent years at Galveston as a result of Hurricane Carla and along the Mississippi coast as a result of Hurricane Camille demonstrate that action should be taken to minimize the tragic consequences of such events. Prediction of the vulnerability of particular areas to flooding in similar storms would be of considerable interest to local residents and governments as well as insurance underwriters. Moreover, real time forecasting of storm surge elevation, with confidence, for an approaching storm would be of great value in planning and implementing evacuation and other measures to minimize damage. This is clearly illustrated by Hurricane Agnes (1972). Agnes was a hurricane of large areal extent but relatively low intensity. Little attention was paid to surge forecasting, and as a result the residents of some areas on the west coast of Florida were surprised by a storm tide 3 to 8 feet above normal. Damage in the Tampa-St. Petersburg area was estimated at about $20 million. Undoubtedly some of this could have been prevented if adequate real time surge forecasts had been available.

The design of permanent facilities at or near the shoreline must include consideration of the maximum and minimum tides that may occur as well as the wave action. In the operation of nuclear power plants, for example, one consideration is the availability of sufficient cooling water to ensure an orderly shut down prior to a low tide occurence below the level necessary for plant operation. Thus, a proper study of the situation would establish a maximum elevation at which the inlet facilities could be placed.

Various approaches are used in solving this type of problem. The purely analytical approaches are limited to idealized wind stresses, pressure distributions, and topography. Lamb [1] considers the case of "free" long waves in an infinite canal of uniform depth. In addition to gravity, small disturbing forces are considered to be acting on the fluid, which vary only by a small fraction of their value within distances comparable to the depth. This leads to an in-homogeneous wave equation similar to that of Section 3-e of the text. Lamb then finds a solution for a pressure distribution that travels with unchanged form at constant velocity. The presence of boundary or terminal conditions greatly complicates the solution. The case of a finite shelf is considered in the text.

Reid [2] presents the approximate response of a sloping shelf due to a triangular shear stress distribution traveling directly on-shore. The results, obtained at the shoreline, are based upon the linear one-dimensional wave equation. The solutions are obtained using a graphical technique and the method of characteristics. He considers many different cases of fetch lengths and storm speed and summarizes his results in graphical and tabular form.

Further analytical work in the area of storm surges has been and will be done, yet the complexities of the actual forcing functions and coastal topographies lead one to realize that another approach is necessary, if realistic solutions to actual problems are to be obtained. Hansen [3,4] is one of the pioneers of storm surge calculations. He calculated surges arising from storms occurring in the North Sea, using the linearized equations of motion. That is, he ignored surge height with respect to depth and ignored the convective terms. He laid the foundation, however, for the present work in numerical surge calculations. Many contemporary investigators still use, in some form, the staggered integration scheme he devised.

Platzman [5] analyzes the case of a pressure distribution or squall line moving over Lake Michigan causing a surge of more than six feet on the Chicago lake front. The volume transport or vertically integrated equations of motion were used in central difference form in conjunction with a two-dimensional bathymetry and a moving pressure disturbance. Platzman's calculated surge is about one-half of the observed surge and he concludes that this is probably due to the omission of wind stress.

Miyazaki [6] treats the Gulf of Mexico as a closed basin, assuming the surge height to be zero at the mouth between Yucatan, Cuba and Florida. This procedure eliminates the difficult problem of specifying lateral boundary conditions in open water. The grid he uses is variable and finest at points of interest in the coastal regions. He includes bottom stress in a form given by Reid [7] which is a function of both flux, q, and of surface shear stress, τ_η.

Marinos and Woodward [8] calculate storm surges using the

assumption of bathystrophic flow (currents parallel to the bottom contours). They arrive at a "quasi-one-dimensional" scheme which considers only one-dimensional depth profiles but includes the Coriolis effect. The bathystrophic procedure was originally developed by Freeman, Baer and Jung [9].

Reid and Bodine [10] present a detailed numerical model for the prediction of surges in Galveston Bay, Texas. The bay is treated as a nearly closed system which, again, eliminates the problem of open water, lateral boundary conditions. Measured tidal data at the entrances to the bay are used as an input to the model and flow through these areas is allowed. The model includes bottom friction and allows for over-topping and flooding of adjacent low-lying areas.

Harris and Jelesnianski [11] and Jelesnianski [12,13,14,15] have presented a series of papers concerning storm surge calculations. The numerical technique follows that of Platzman. In the paper "Numerical Computations of Storm Surges with Bottom Stress," Jelesnianski [14] includes bottom stress in his calculation, using an eddy viscosity and a slip coefficient. Jelesnianski notes that for a storm not moving too slowly, the bottom friction term is not important and may be omitted, but for slow storms or storms moving parallel to the coast bottom friction must be included. In the paper "Bottom Stress Time-History in Linearized Equations of Motion for Storm Surges," Jelesnianski [15] abandons the slip coefficient and maintains the eddy viscosity with the assumption that it is constant in both the vertical and horizontal. Good agreement is obtained between surge height data and the calculations. He notes, however, that "currents are only of casual interest compared to the slope or

height variations." In general this is true, yet, it is becoming apparent that the currents are very important in terms of beach erosion and forces on various ocean structures. The development of a more generally applicable dissipation mechanism would decrease the sensitivity of the current calculations thus decreasing the necessity for "calibrating" a model which may mask errors and deficiencies in the model by appropriately selecting bottom friction coefficients.

The volume transport equations are formulated in terms of flux components and do not describe the velocity distribution near the bottom, which is related to the bottom friction. Jelesnianski [15] deals with the problem of bottom friction by providing bottom shear stress as a convolution integral of the surface shear stress function. In this technique he linearizes the equation of motion by making the assumption that the surge height is very small compared to the depth, $\eta << h$. In doing so he precludes flooding in low-lying areas and calculations for very shallow waters. In this report it is antici-pated that the modeling of flooding in low-lying areas and surge calculations in very shallow water will both be desirable, thus a quadratic bottom friction function which allows the use of the non-linear equations is used. This is equivalent to making the assumption that the vertical velocity profile is maintained in a near steady state condition. Future development of the model will rely on measure-ments to provide insight into the processes involved.

Surprisingly little work has been done in measuring hurricane phenomena. The storm surge data available are primarily from high water marks. Tidal records are predominantly from enclosed bays and rivers making comparison to the numerical model difficult. The only

known current data for Hurricane Camille were taken by Murray [16,17] on the Florida Panhandle. These currents, measured in the surf zone, were due to wave-induced mass transport as well as wind shear stress and water slope. Clearly more data of this type are needed.

The difficulty of reaching offshore areas in a hurricane makes manned observation of these phenomena nearly impossible, so alternate measures must be found. The appropriate instrumentation must be either in place continuously waiting for a storm or it must be placed in the path of the storm prior to the development of adverse sea conditions in that area. In the first case, the instrumentation sites must be periodically serviced with the knowledge that the wait for a hurricane may be a long one. In both cases, there is the problem of instrument recovery. An inexpensive underwater gage and integrating current meter have been developed and are described in the report.

CHAPTER 2

STORM SURGE CALCULATIONS - THEORY

a. Volume Transport Equations

The equations of motion and continuity as used in the development of the storm surge model are developed qualitatively in this section with the details of the integration over depth presented in Appendix A. The coordinate system and nomenclature are presented in Figure 2-1. The origin of the coordinate system is arbitrarily chosen at the shelfbreak and is approximately centered in the region of interest. The x axis is directed toward shore, y is oriented approximately parallel to the coast and z is positive upwards. The Navier-Stokes or momentum equations for fluid motion are the governing dynamic equations:

$$\frac{\partial u}{\partial t} + u\frac{\partial u}{\partial x} + v\frac{\partial u}{\partial y} + w\frac{\partial u}{\partial z} - 2\omega(\sin\phi)v = -\frac{1}{\rho}\frac{\partial p}{\partial x} + \frac{\mu}{\rho}\nabla^2 u \quad (2\text{-}1a)$$

$$\frac{\partial v}{\partial t} + u\frac{\partial v}{\partial x} + v\frac{\partial v}{\partial y} + w\frac{\partial v}{\partial z} + 2\omega(\sin\phi)u = -\frac{1}{\rho}\frac{\partial p}{\partial y} + \frac{\mu}{\rho}\nabla^2 v \quad (2\text{-}1b)$$

$$\frac{\partial w}{\partial t} + u\frac{\partial w}{\partial x} + v\frac{\partial w}{\partial y} + w\frac{\partial w}{\partial z} = -\frac{1}{\rho}\frac{\partial p}{\partial z} + \frac{\mu}{\rho}\nabla^2 w - g \quad (2\text{-}1c)$$

where u, v and w are the components of the water velocity in the x, y and z directions respectively, t is time, ρ is the water density, p is pressure, μ is molecular viscosity, ω is the angular velocity of the
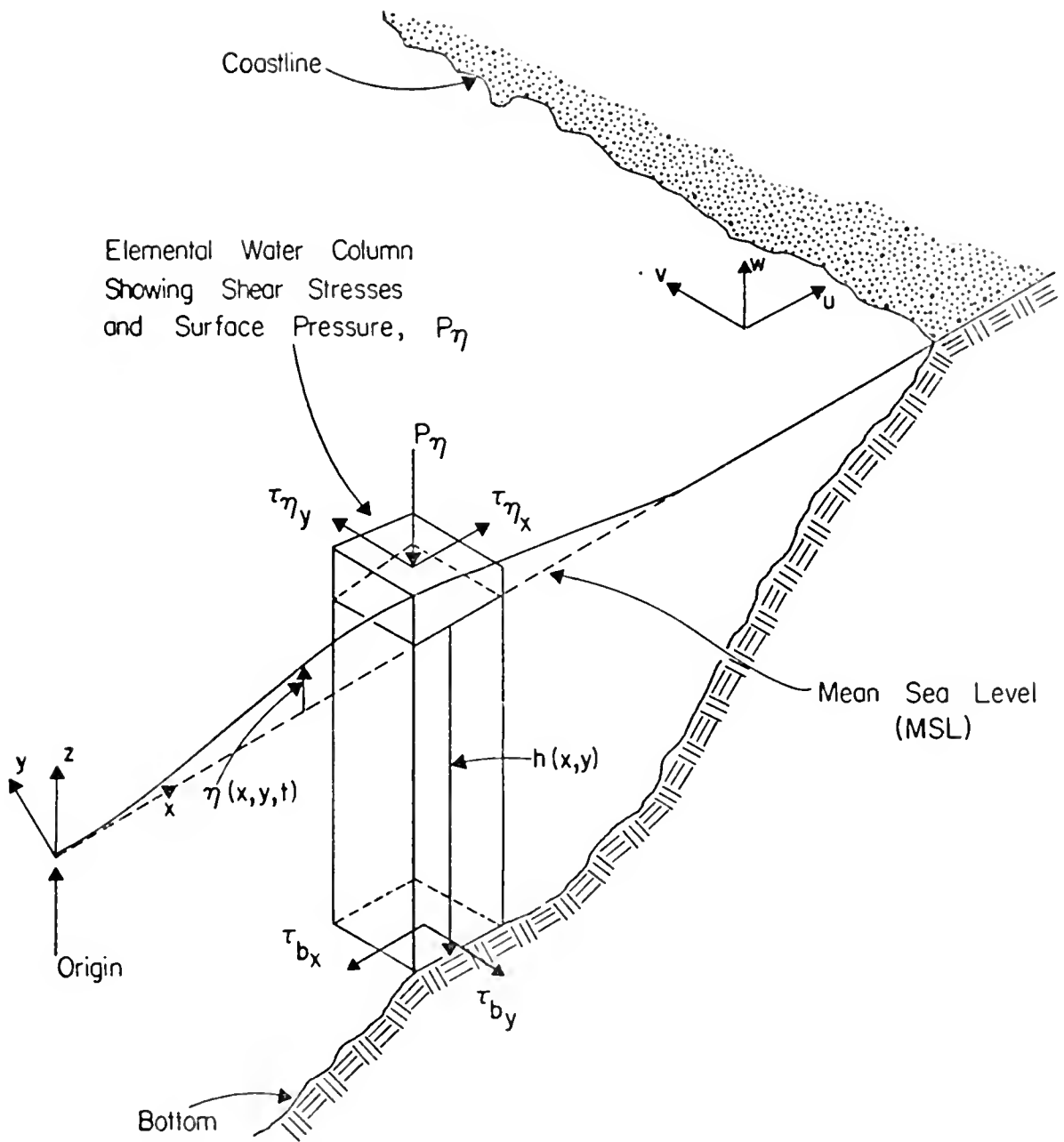
FIGURE 2-1   PERSPECTIVE OF NEARSHORE ZONE
SHOWING COORDINATE SYSTEM AND
NOMENCLATURE

Earth, ϕ is the latitude, ∇^2 is the Laplacian operator $\nabla^2 = \frac{\partial^2}{\partial x^2}$ $+ \frac{\partial^2}{\partial y^2} + \frac{\partial^2}{\partial z^2}$, and the fluid has been assumed incompressible. The continuity equation is:

$$\frac{\partial u}{\partial x} + \frac{\partial v}{\partial y} + \frac{\partial w}{\partial z} = 0 \qquad (2\text{-}1d)$$

Equations (2-1a) through (2-1c) portray explicitly only the laminar processes. In this development, the turbulent effects are dominant, especially the turbulent or Reynolds stresses. Although it is impossible to describe the turbulent motion in detail, it is useful to separate the effects of the mean and fluctuating velocity components. By describing the variables in Equations (2-1) as the sum of a time mean value and a fluctuation and then taking a time mean, the turbulent equations of motion result. Thus setting $u = \bar{u} + u'$, $v = \bar{v} + v'$, $w = \bar{w} + w'$, and $p = \bar{p} + p'$ leads to the x-equation of motion

$$\frac{\partial \bar{u}}{\partial t} + \bar{u}\frac{\partial \bar{u}}{\partial x} + \bar{v}\frac{\partial \bar{u}}{\partial y} + \bar{w}\frac{\partial \bar{u}}{\partial z} = -\frac{1}{\rho}\frac{\partial \bar{p}}{\partial x} + \frac{\mu}{\rho}\nabla^2\bar{u} - \left(\frac{\partial \overline{u'^2}}{\partial x} + \frac{\partial \overline{u'v'}}{\partial y} + \frac{\partial \overline{u'w'}}{\partial z}\right) \quad (2\text{-}2)$$

where

$$\overline{u'_i u'_j} = \frac{1}{T}\int_0^T u'_i u'_j \, dt$$

and u'_1, u'_2 and u'_3 indicate u', v' and w' respectively. The terms in parenthesis are the turbulent stresses and T is a period large compared to the period of a turbulent fluctuation but small compared to any change in $\bar{u}$ or $\bar{v}$. It is assumed here that terms of the form $\frac{\mu}{\rho}\nabla^2\bar{u}$ are negligible when compared to the turbulent stresses. Thus the turbulent equations to be used are:

$$\frac{\partial u}{\partial t} + u\frac{\partial u}{\partial x} + v\frac{\partial u}{\partial y} + w\frac{\partial u}{\partial z} - 2\omega(\sin\phi)v = -\frac{1}{\rho}\frac{\partial p}{\partial x} + \frac{1}{\rho}(\frac{\partial \tau'_{xx}}{\partial x} + \frac{\partial \tau'_{xy}}{\partial y} + \frac{\partial \tau'_{xz}}{\partial z}) \quad (2\text{-}3a)$$

$$\frac{\partial v}{\partial t} + u\frac{\partial v}{\partial x} + v\frac{\partial v}{\partial y} + w\frac{\partial v}{\partial z} + 2\omega(\sin\phi)u = -\frac{1}{\rho}\frac{\partial p}{\partial y} + \frac{1}{\rho}(\frac{\partial \tau'_{xy}}{\partial x} + \frac{\partial \tau'_{yy}}{\partial y} + \frac{\partial \tau'_{yz}}{\partial z}) \quad (2\text{-}3b)$$

$$\frac{\partial w}{\partial t} + u\frac{\partial w}{\partial x} + v\frac{\partial w}{\partial y} + w\frac{\partial w}{\partial z} = -\frac{1}{\rho}\frac{\partial p}{\partial z} - g + \frac{1}{\rho}(\frac{\partial \tau'_{xz}}{\partial x} + \frac{\partial \tau'_{yz}}{\partial y} + \frac{\partial \tau'_{zz}}{\partial z}) \quad (2\text{-}3c)$$

where it is now understood that u, v, w, p, $\tau'_{x_i x_j}$ indicate time mean values. $\tau'_{x_i x_j}$, the Reynolds stress, is represented by $-\rho\overline{u'_i u'_j}$ where $\rho\overline{u'_i u'_j} = \rho\overline{u'_j u'_i}$. This is explained in detail in reference [18]. The continuity equation in turbulent form is unchanged

$$\frac{\partial u}{\partial x} + \frac{\partial v}{\partial y} + \frac{\partial w}{\partial z} = 0 \quad (2\text{-}3d)$$

Frequently a Boussinesq approximation is used for the expression in parenthesis in Equation (2-2) which maintains the original form of Equation (2-1). The equations remain intractable either in the form (2-1)or(2-3). Since the velocity gradients in the vertical are antici-pated to be, in most cases, an order of magnitude larger than the velocity gradients in the horizontal, the lateral stresses are neglected. Thus it is assumed that $\tau'_{xy} = \tau'_{yx} \approx 0$. The normal stress terms of the form $\frac{\partial \tau'_{x_i x_i}}{\partial x_i}$ are assumed small compared to the surface pressure term $-\frac{1}{\rho}\frac{\partial p_n}{\partial x}$ and the hydrostatic pressure. To further simplify Equations (2-3) the assumption is made that the vertical accelerations are small, or as a consequence that the pressure distribution in the vertical is hydrostatic. Thus,

$$p(x,y,z,t) = p_\eta(x,y) + \gamma(\eta(x,y,t)-z) \quad (2\text{-}4)$$

where $\eta(x,y,t)$ is the free surface displacement from mean sea level (MSL), $p_\eta(x,y)$ is the pressure at the free surface, and $\gamma = \rho g$ is the specific weight of water.

The Equations (2-3) are now integrated over the vertical from $-h$ to η where $-h$ is the z coordinate of the bottom. This procedure together with Equation (2-4) and the free surface and bottom boundary conditions leads to the vertically integrated or tidal equations of motion. The details carried out in Appendix A are straightforward and with approximations to be defined later lead to the following, using Leibnitz's rule,

$$\frac{\partial q_x}{\partial t} + \frac{q_x}{D}\frac{\partial q_x}{\partial x} + \frac{q_y}{D}\frac{\partial q_x}{\partial y} - 2\omega(\sin\phi)q_y = -\frac{D}{\rho}\frac{\partial p_\eta}{\partial x} - gD\frac{\partial \eta}{\partial x} + \frac{1}{\rho}(\tau_{n_x} - \tau_{b_x}) \quad (2\text{-}5a)$$

$$\frac{\partial q_y}{\partial t} + \frac{q_x}{D}\frac{\partial q_y}{\partial x} + \frac{q_y}{D}\frac{\partial q_y}{\partial y} + 2\omega(\sin\phi)q_x = -\frac{D}{\rho}\frac{\partial p_\eta}{\partial y} - gD\frac{\partial \eta}{\partial y} + \frac{1}{\rho}(\tau_{n_y} - \tau_{b_y}) \quad (2\text{-}5b)$$

$$\frac{\partial q_x}{\partial x} + \frac{\partial q_y}{\partial y} + \frac{\partial \eta}{\partial t} = 0 \quad (2\text{-}5c)$$

where the subscripts, η, and b indicate the subscripted quantities are to be evaluated at the surface and bottom respectively. D, q_x and q_y are defined as follows:

$$D(x,y) = h(x,y) + \eta(x,y,t)$$

$$q_x(x,y,t) = \int_{-h(x,y)}^{\eta(x,y,t)} u(x,y,t)\, dz$$

$$q_y(x,y,t) = \int_{-h(x,y)}^{\eta(x,y,t)} v(x,y,t)\, dz$$

It should be noted also that the convective terms of the form $\frac{q_y}{D} \frac{\partial q_x}{\partial y}$ as written are only approximate; the actual terms resulting from the integration are of the form

$$\frac{\partial}{\partial y} \int_{-h}^{\eta} uv \, dz,$$

but are written in the differential form in analogy to Equations (2-1). The convective terms will be neglected in the further development of the model until considered again in Appendix B. In summary, the equations of motion in the final form to be used are:

$$\frac{\partial q_x}{\partial t} - 2\omega(\sin\phi)q_y = -\frac{D}{\rho} \frac{\partial P_\eta}{\partial x} - gD \frac{\partial \eta}{\partial x} + \frac{1}{\rho} (\tau_{\eta_x} - \tau_{b_x}) \qquad (2\text{-}6a)$$

$$\frac{\partial q_y}{\partial t} + 2\omega(\sin\phi)q_x = -\frac{D}{\rho} \frac{\partial P_\eta}{\partial y} - gD \frac{\partial \eta}{\partial y} + \frac{1}{\rho} (\tau_{\eta_y} - \tau_{b_y}) \qquad (2\text{-}6b)$$

The form of the continuity equation is:

$$\frac{\partial q_x}{\partial x} + \frac{\partial q_y}{\partial y} + \frac{\partial \eta}{\partial t} = 0 \qquad (2\text{-}6c)$$

b. Assumptions and Boundary Conditions

The equations of motion were developed in the preceding section. To specify a particular problem, various conditions must be imposed on the boundaries of the model. On the water surface a forcing function consisting of a normal pressure and a shear stress is applied. At the bottom, a shear stress or friction dependent on the water velocity is imposed. In addition conditions on the surge height and water transport are necessary at the areal boundaries of the model.

The shear stress at the free surface is calculated by the method proposed by Van Dorn [19]. The shear stress is based on the wind velocity and is given as follows:

$$\tau_{n_x} = \rho k |U| U_x$$

$$\tau_{n_y} = \rho k |U| U_y$$

(2-7)

where $U = \sqrt{U_x^2 + U_y^2}$ and U_x and U_y are the x and y components of the wind velocity, respectively, at a reference elevation of approximately 10 meters. The constant k has been determined by Van Dorn as the following function of velocity:

$$k = \begin{cases} k_1 \; ; \; U < U_{cr} \\ \\ k_1 + k_2(1 - U_{cr}/U)^2 \; ; \; U \geq U_{cr} \end{cases}$$

(2-8)

where

$$k_1 = 1.1 \times 10^{-6}$$

$$k_2 = 2.5 \times 10^{-6}$$

$$U_{cr} = 14 \text{ knots} = 23.6 \text{ feet/second}$$

There are uncertainties in applying Van Dorn's results to hurricane winds. Van Dorn's data are generally for wind speeds low in comparison to the wind speeds of a large hurricane. Although there is no proof that the results are directly applicable, they are used here because the associated measurements showed little scatter and the results are reasonably consistant with other data sources. Wu [20] has published more recent information concerning the wind stress coefficient, k. Figure 2-2 summarizes available data. Van Dorn's k, calculated from Equation (2-8), is also plotted in Figure 2-2 to provide a comparison. Since the hurricane model to be discussed requires a shear stress field as input, a better shear stress model, if it becomes available, can be easily incorporated into the surge model without changes in concept or approach. The wind velocity input will be discussed in Section 2-c.

The treatment of the bottom friction, τ_{b_x}, τ_{b_y} is a much more difficult problem. In making storm surge calculations the simplest assumption is to consider $\tau_{b_x} = \tau_{b_y} = o$. This is employed in many developments of storm surge calculations, especially the earlier ones. Under appropriate conditions this is a justifiable assumption. For the case of a rapidly moving storm traveling perpendicular or nearly perpendicular to the shore it is a good assump-
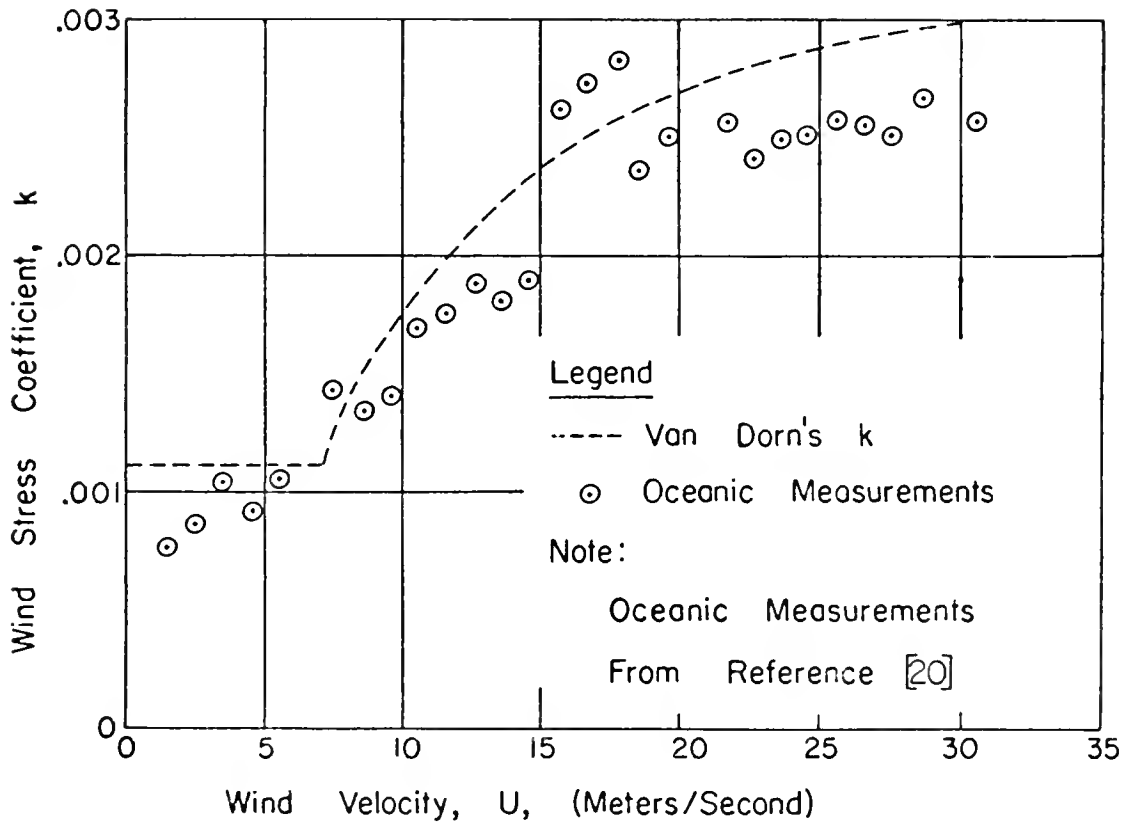
FIGURE 2-2   COMPARISON OF VAN DORN'S k
WITH OCEANIC WIND STRESS
MEASUREMENTS

tion since there is little time for "wind-up" and the friction
effects are small due to low water velocities [13].

A better assumption in some cases is that of a linear or
"linearized" bottom stress of the form $f_L q_x$, $f_L q_y$ where f_L is a
linearized friction factor. This is the type of friction used, for
example, by Dean and Pearce [21]. A "linearized" friction term is
generally necessary if friction is required and any type of analytical
solution is desired. The bottom shear stress employed in this model
is the Darcy-Weisbach expression and is the most accurate of the
three,

$$\tau_{b_x} = \frac{\rho f |u| u_x}{8} \quad ; \quad \tau_{b_y} = \frac{\rho f |u| u_y}{8}$$

or in terms of volume transport

$$\tau_{b_x} = \frac{\rho f |q| q_x}{8D^2} \quad ; \quad \tau_{b_y} = \frac{\rho f |q| q_y}{8D^2}$$

where $u = \sqrt{u_x^2 + u_y^2}$, $q = \sqrt{q_x^2 + q_y^2}$, and f is the quadratic
bottom friction factor. In incorporating this steady state rela-
tionship into the model it is assumed that the law is valid for the
propagation of long waves of the period of interest. This is
equivalent to assuming that the velocity variation over depth is
nearly the same for slowly varying flows as for steady state.
Although this technique has limitations, especially in deep water,
it is the best method available that can be used in conjunction with
the nonlinear equations to allow for flooding and to permit cal-
culations in very shallow water. Another important consideration is
that in deep water the friction is relatively less important than in

shallow water since the water velocities are in general much smaller. As an illustrative example, the response of a water column to an impulsive wind is depicted in Figure 2-3.

Returning to the problem specification, the boundary conditions are illustrated in Figure 3-5. At the seaward boundary, the wind setup is assumed zero as a result of considering an infinite depth at that point. The barometric tide still exists at the seaward boundary and is given by $\eta(x,y) = 1.15(p_\infty - p_\eta(x,y))$ where p_∞ designates the barometric pressure at a distance large compared to the storm dimension, where η is in feet, and the pressure p is in inches of mercury.

At any land-sea boundary the flux normal to that boundary is zero, $q_n = 0$, where the subscript n indicates the component normal to that boundary.

Most difficult from a physical standpoint are the lateral boundary conditions. They are, however, necessary to carry out the calculations. Since no real physical limitations exist, conditions must be chosen that least disturb the model and therefore allow a realistic solution to be obtained. A further condition is then imposed that the boundaries are at a distance large compared to a characteristic dimension of the storm. This means, in effect, that the boundary conditions on the lateral boundaries become a second order effect if they are far away. The boundary conditions used at the lateral boundaries of this model are: the flow in the x direction is equal to zero, $q_x = 0$, and the surge height η is set equal to the barometric tide at the lateral boundaries.
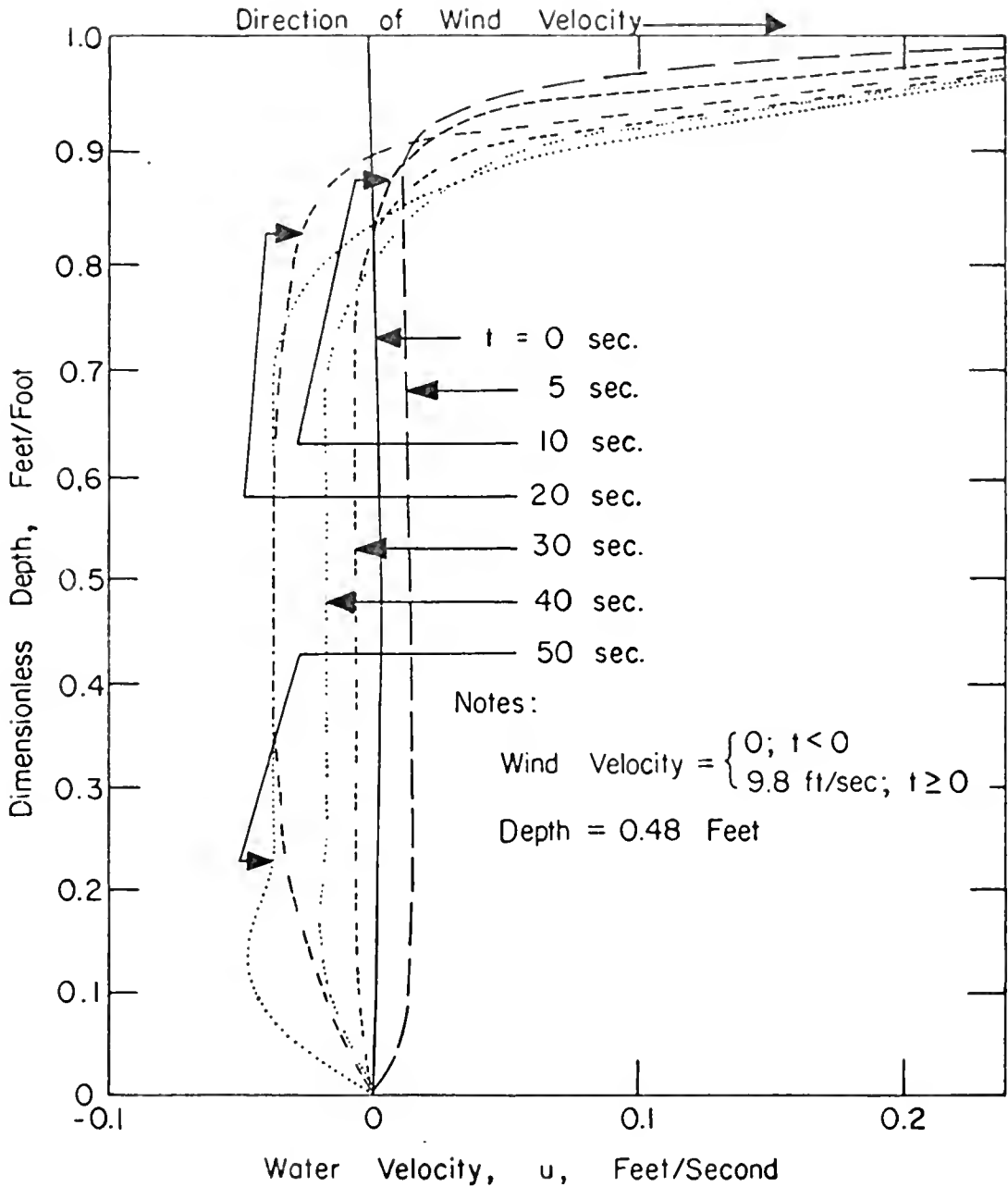
FIGURE 2-3   TRANSIENT WATER VELOCITY
DISTRIBUTION IN A CLOSED CHANNEL
DUE TO IMPULSIVE WIND (FROM
REFERENCE [22])

The initial conditions are simply a quiescent system. The surge heights can be initially zero or in barometric equilibrium; this makes little difference since the storm is initially far from the region of interest. Initial barometric equilibrium is used in this study. More importantly the storm is assumed to start at a distance offshore large enough that the effects due to model start-up are negligible. The effects of various starting points can be seen in Figures 4-5 and 4-10, where the surge height is relatively insensitive but the currents exhibit wind-up.

c.   The Hurricane Model

The actual storm surge model uses τ_{n_x}, τ_{n_y} and p_n as input. Since the measured wind shear stress is in general not available, Van Dorn's technique is used to convert U_x and U_y to τ_{n_x} and τ_{n_y} as discussed in Section 2-b.   Actual wind fields may be applied or an idealized model used to represent the storm.   In this section an analytical model is used to represent wind velocity and pressure fields. Since the actual surge model is the primary objective of this study, the hurricane model will be presented and used without further comment, except for a short note on the numerical technique in Chapter 3.

The hurricane representation used is not unique and a different one could be substituted into the numerical model.   The hurricane model used is that presented by Wilson [23].   The important parameters of an idealized hurricane are: the central pressure index CPI or equivalently the central pressure anomaly $\Delta p = p_\infty - p_0$ (where p_∞ is the normal pressure or the pressure at a large distance from the hurricane center and p_0 is the central pressure of the hurricane), the distance from the hurricane center to the point of maximum winds R, and the forward velocity V of the hurricane.   These parameters Δp, R, and V are reported by the National Weather Service when characterizing a storm, thereby providing a method to approximate a hurricane. The isobars are assumed circular and the pressure distribution at the surface is taken as $p_n = p_0 + \Delta p e^{-R/r}$.   The streamlines are

assumed circular for a stationary storm. The equations presented include the effect of a constant translational velocity, V, superimposed on the storm as shown in Figure 2-4. Using Wilson's notation:

$$U_G = U_c \left(\sqrt{\gamma^2 + 1} - \gamma \right)$$

where

$$\gamma = 1/2 \left(\frac{V'}{U_c} + \frac{U_c}{U_g} \right)$$

and

$$U_c = \sqrt{ \frac{\Delta p}{\rho_a} \frac{R}{r} e^{-R/r} }$$

$$U_g = \frac{\frac{\Delta p}{\rho_a} \frac{R}{r^2} e^{-R/r}}{2\omega(\sin\phi)}$$

$$V' = V(\sin\theta)$$

The subscript G refers to gradient wind, c to cyclostrophic wind, and g to geostrophic wind. ρ_a is the density of air, V the forward velocity of the storm, θ is defined in Figure 2-4 and $2\omega(\sin\phi)$ is the Coriolis parameter as used in Equations (2-1). The gradient wind U_G is the desired parameter. These winds are calculated at a point high enough above the surface to allow the assumption of zero friction. To reduce these to the 10 meter elevation a reduction factor is needed. The factor depends on latitude, divergence of wind direction from the isobars and other factors. In this study a constant factor of 0.83 was used. See references [24,25].
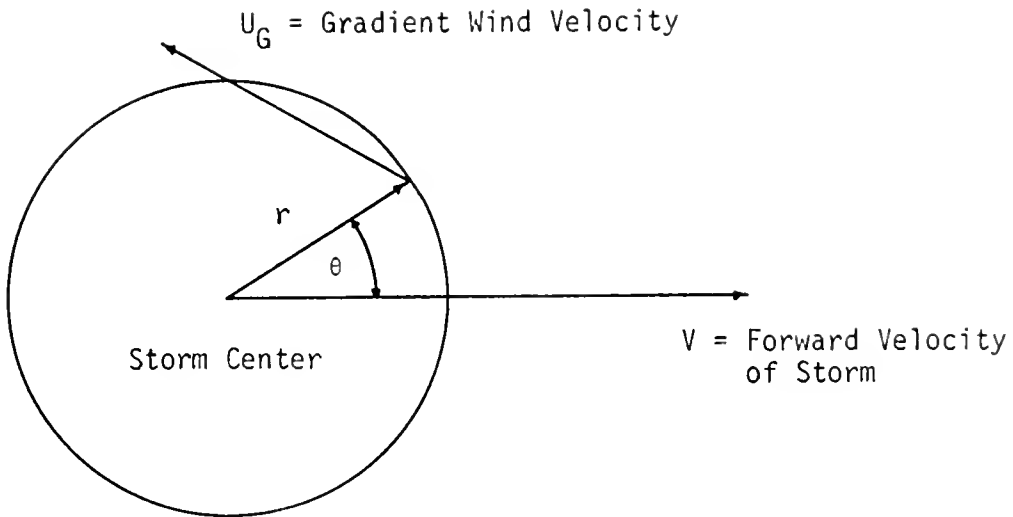
FIGURE 2-4   DEFINITION SKETCH FOR STORM TRAVELING AT CONSTANT VELOCITY

The winds of Hurricane Camille are evaluated using this method. The hurricane position as a function of time is given in Figure 2-5. The central pressure p_o, and the peripheral pressure p_∞, are given as functions of time in Figure 2-6a. Figure 2-6b depicts radius to maximum winds R, and forward speed of the storm V, as functions of time. Figure 2-6c gives maximum sustained wind speeds in knots as a function of time. These data are from the National Weather Service [26,27]. Figures 2-7a through 2-7c present comparisons, at different times, of the surface wind fields for Hurricane Camille as developed by the National Weather Service [27] with the wind fields calculated by the above model.
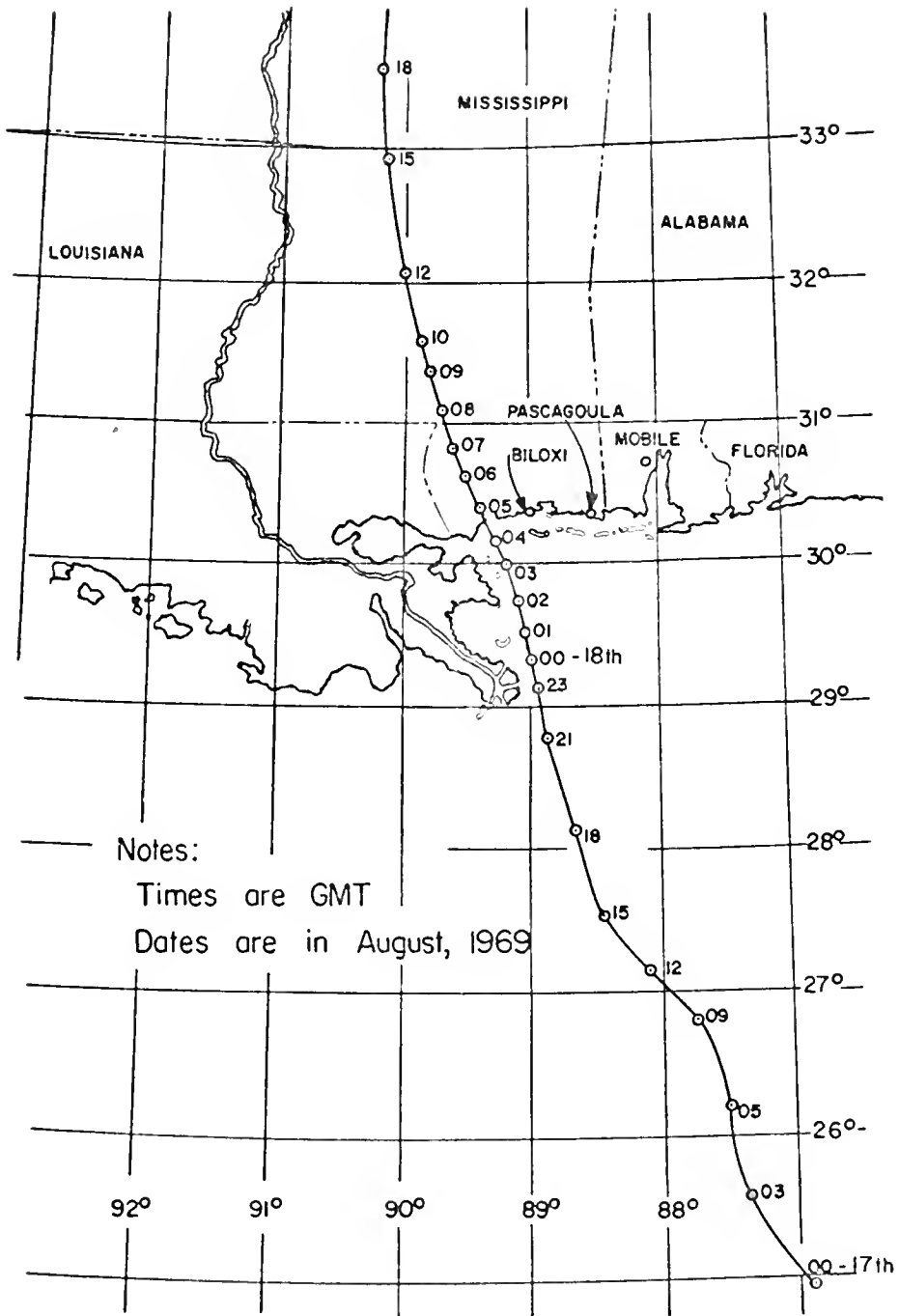
FIGURE 2-5 STORM TRACK FOR HURRICANE
CAMILLE, AUGUST 16-18, 1969
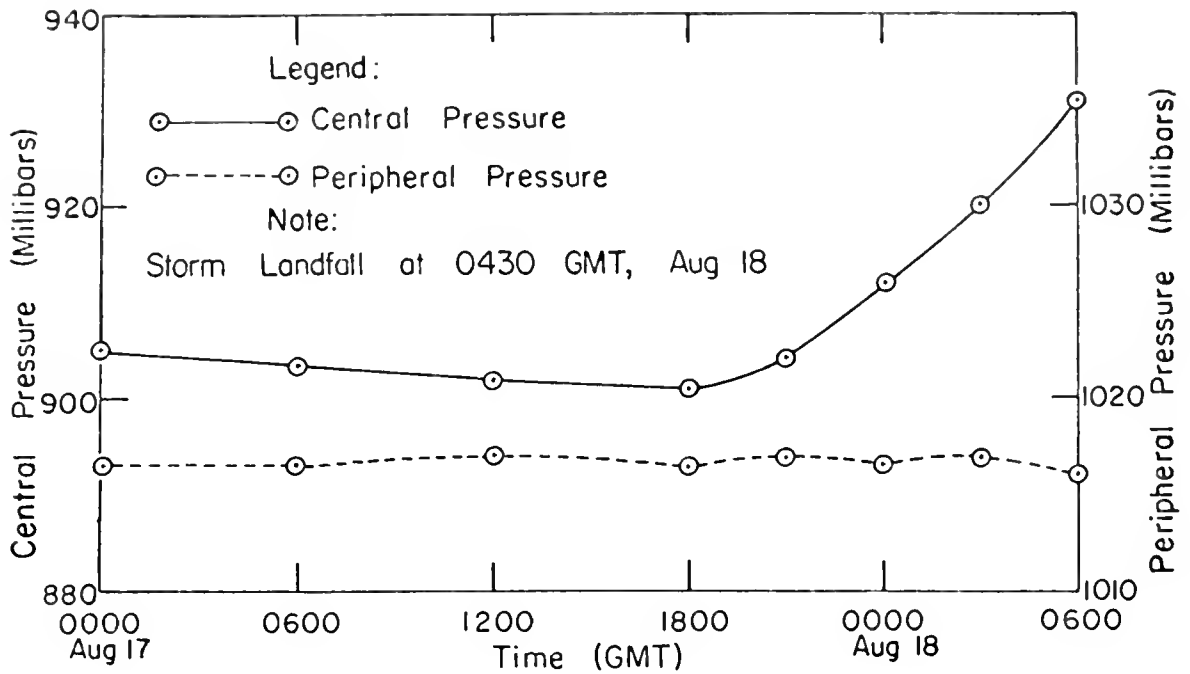
FIGURE 2-6a   PRESSURE   CHARACTERISTICS   OF
HURRICANE   CAMILLE   AS   A
FUNCTION   OF   TIME
(DATA   FROM   REFERENCE   [26])
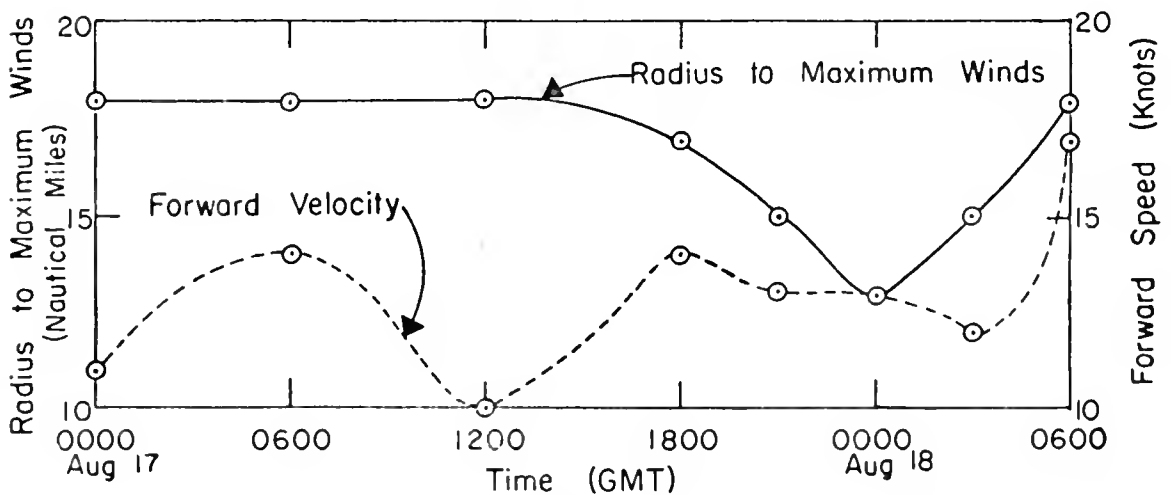
FIGURE 2-6b   RADIUS   TO   MAXIMUM   WINDS   AND
FORWARD   SPEED   OF   HURRICANE
CAMILLE   AS   FUNCTIONS   OF   TIME
(DATA   FROM   REFERENCE   [26])
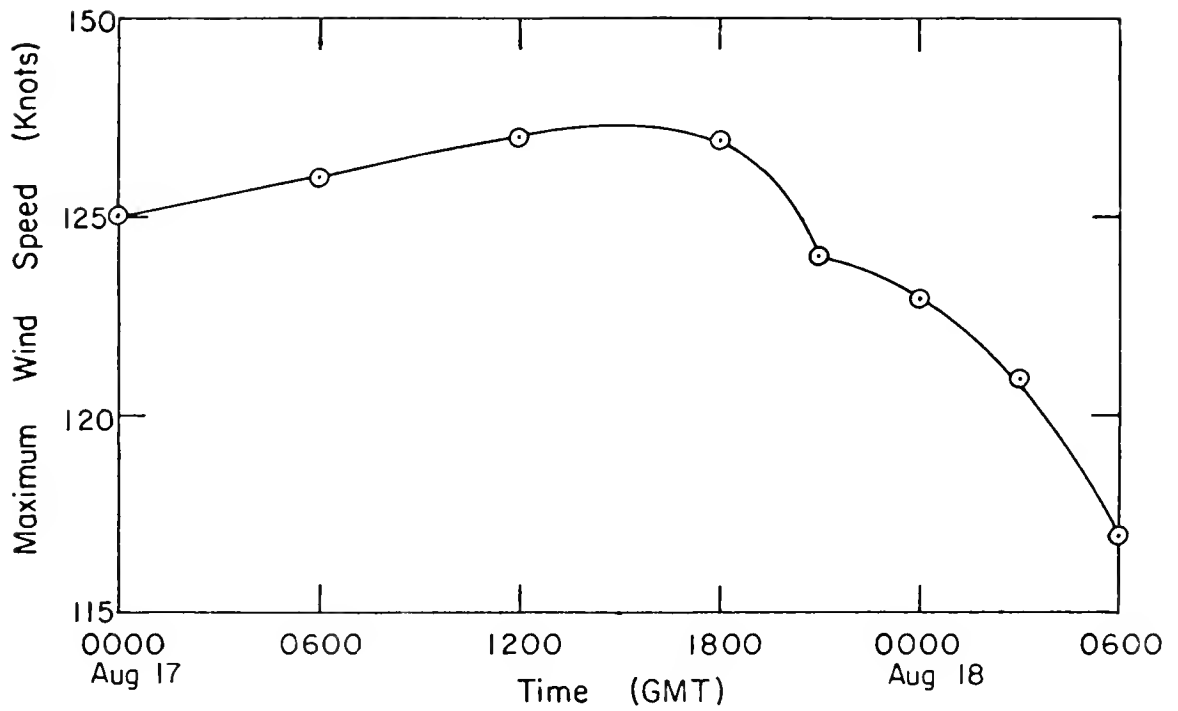
FIGURE 2-6c MAXIMUM WIND SPEED IN HURRICANE
CAMILLE AS A FUNCTION OF TIME
(DATA FROM REFERENCE [26])
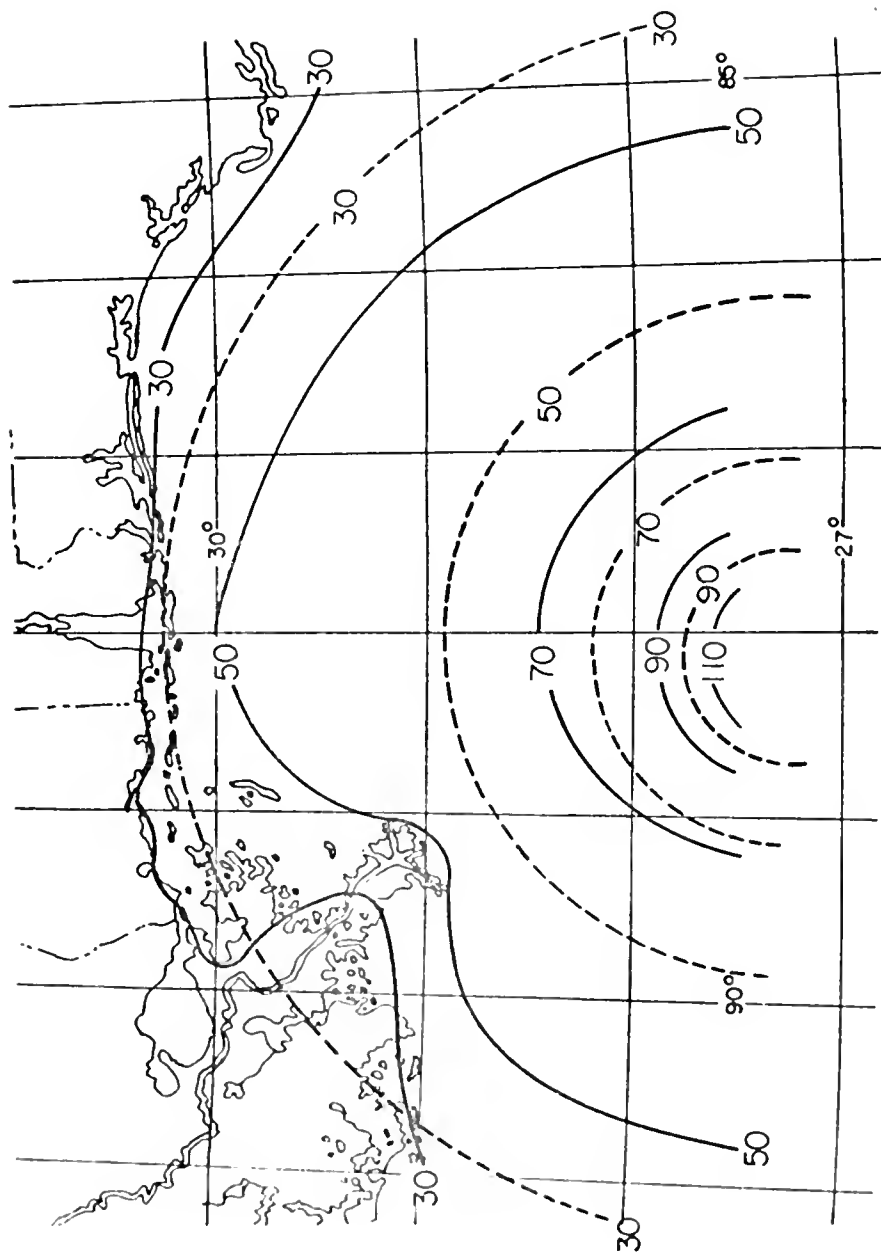
Legend

----- 30 Foot Surface Isotachs-Calculated

——— 30 Foot Surface Isotachs-From Reference [27]

Note: 1200 Hours GMT August 17, 1969

FIGURE 2-7a   COMPARISON OF 30 FOOT SURFACE ISOTACHS - 8/17/1200

FIGURE 2-7b COMPARISON OF 30 FOOT SURFACE ISOTACHS - 8/17/1800
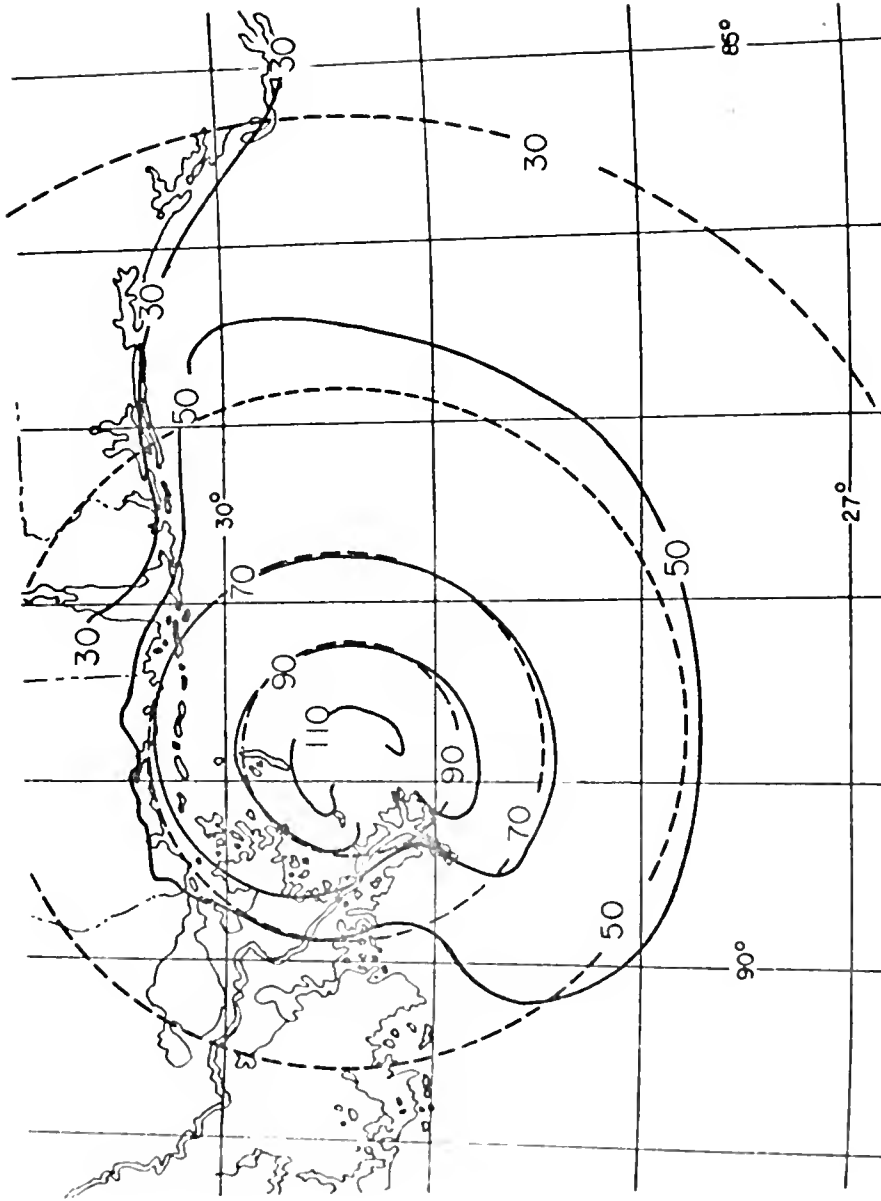
Note: 1800 Hours GMT August 17, 1969

Legend

----- 30 Foot Surface Isotachs-Calculated

——— 30 Foot Surface Isotachs-From Reference [27]

28

Legend

------ 30 Foot Surface Isotachs-Calculated

——— 30 Foot Surface Isotachs-From Reference [27]

Note: 0000 Hours GMT August 18, 1969

FIGURE 2-7c COMPARISON OF 30 FOOT SURFACE ISOTACHS - 8/18/0000

d. Analytical Treatment-Steady State, Without Bottom Friction

i. Problem Definition

Having defined the problem and established equations of motion and boundary conditions, it remains to find a solution for a particular storm and affected coastal region. Before presenting the numerical approach necessary to attain a solution of complicated prototype conditions and geometry, several simplified analytical approaches will be considered. These will serve three basic purposes. First, they allow highly simplified calculations for basic engineering purposes. Second, they allow intuitive investigations into the physical processes involved. Third, they produce solutions with which to check the numerical approaches.

Figure 2-8 is a definition sketch for this section. The present treatment includes only motions in the x-direction; Equations (2-5a) and (2-5c) therefore reduce to Equations (2-9a) and (2-9b) respectively.

$$\frac{\partial q_x}{\partial t} + \frac{q_x}{D} \frac{\partial q_x}{\partial x} = - \frac{D}{\rho} \frac{\partial p_n}{\partial x} - gD \frac{\partial \eta}{\partial x} + \frac{1}{\rho} (\tau_{n_x} - \tau_{b_x}) \tag{2-9a}$$

$$\frac{\partial q_x}{\partial x} + \frac{\partial \eta}{\partial t} = 0 \tag{2-9b}$$
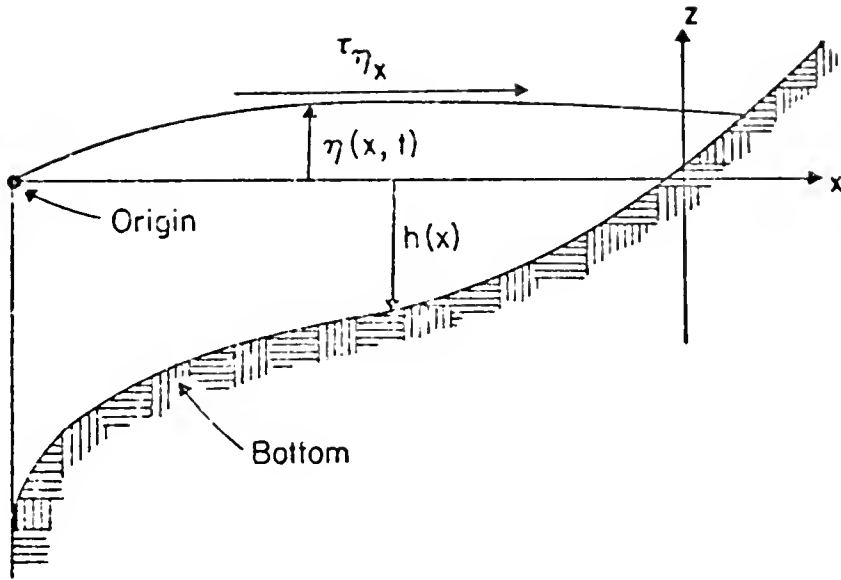
FIGURE 2-8   NOTATION FOR ONE-DIMENSIONAL PROBLEM

The solution is now independent of y. Two cases will be considered,

the uniform depth case $h(x) = h$ = constant and the case of $h(x) = h_o$ -

mx or uniform slope. In both cases it will be assumed that the wind

stress on the surface is uniform. For the steady state case, the

case of no net transport in the x-direction, $q_x = 0$ and therefore the

shear stress $\tau_{b_x} = 0$, regardless of f, the bottom friction coefficient.

(Note: it is assumed here that there is zero velocity over the entire

depth.)   For this problem the $\frac{q_x}{D} (\frac{\partial q_x}{\partial x})$ term is zero and the atmospheric

pressure gradient $\frac{\partial p_n}{\partial x}$ is assumed small in relation to the other terms.

ii.   Uniform wind stress Acting Over a Shelf of Uniform Depth

In the first example $h(x)$ is uniform (=h) as shown in Figure

2-9.
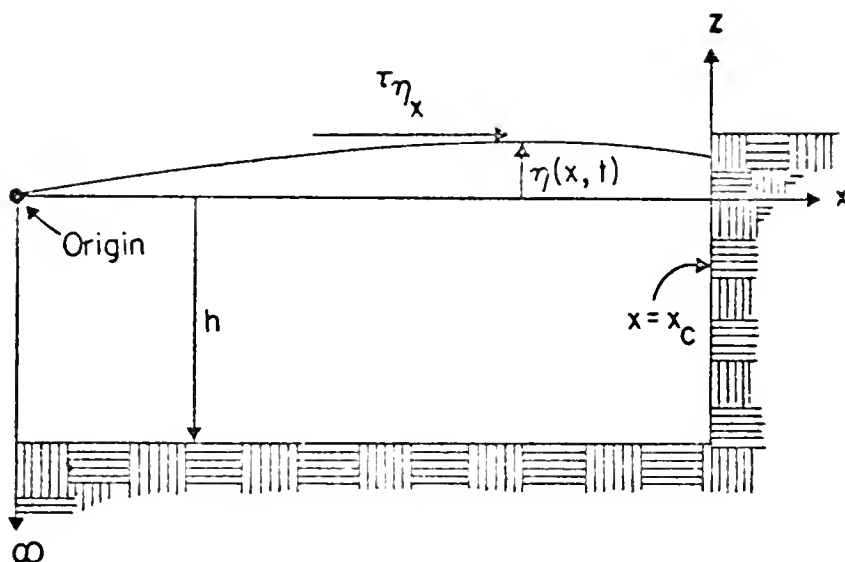
FIGURE 2-9   ONE-DIMENSIONAL SHELF WITH UNIFORM DEPTH

The further assumption is made that the shear stress is uniform and constant at the water surface $z = \eta$. The problem can be stated as follows:

$$-gD \frac{\partial \eta}{\partial x} + \frac{\tau_{\eta_x}}{\rho} = 0$$

$$q_x = \frac{\partial q_x}{\partial t} = 0$$

Since $D = h + \eta$

$$\rho g (h+\eta) \frac{\partial \eta}{\partial x} = \tau_{\eta_x} \qquad\qquad (2\text{-}10)$$

Rewriting Equation (2-10) leads to

$$\frac{\partial \eta}{\partial x} = \frac{\tau_{\eta_x}}{\rho g (h+\eta)} \qquad\qquad (2\text{-}11)$$

At $x = 0$, the boundary condition for η is determined by noting that seaward of that point $h \rightarrow \infty$ and therefore

$$\frac{\partial \eta}{\partial x} \rightarrow 0 \quad \text{as} \quad h \rightarrow \infty$$

Thus η = constant as $h \rightarrow \infty$, and $\eta = 0$ is chosen as the boundary condition at the shelf break, $x = 0$. Solving for η yields

$$\eta(h + \eta/2) = \frac{\tau_{\eta_x}}{\rho g} x$$

or

$$\eta = -h + \sqrt{h^2 + \frac{\tau_{\eta_x}}{\rho g} 2x}$$

Evaluating τ_{η_x}, using Van Dorn's constants, completes the solution. An even simpler procedure is frequently the basis for storm surge calculations. Assuming that the storm surge, η, is small compared to the undisturbed depth (i.e. $h + \eta \approx h$) leads to the solution

$$\eta = \frac{\tau_{\eta_x}}{\rho g h} x$$

Designating x_c as the fetch or shelf width and h as depth leads to the storm surge at the coastline $x = x_c$

$$\eta|_{x=x_c} = \frac{\tau_{\eta_x}}{\rho g} \frac{\text{Fetch}}{\text{Depth}}$$

Figure 2-10 provides a simplified procedure for making these calculations and is based on the latter solution. As an example, assume a depth of 50 feet for a 50 mile shelf width (or fetch) and a wind speed of 50 knots, then the storm surge calculated from Figure 2-10 is 3.23 feet.
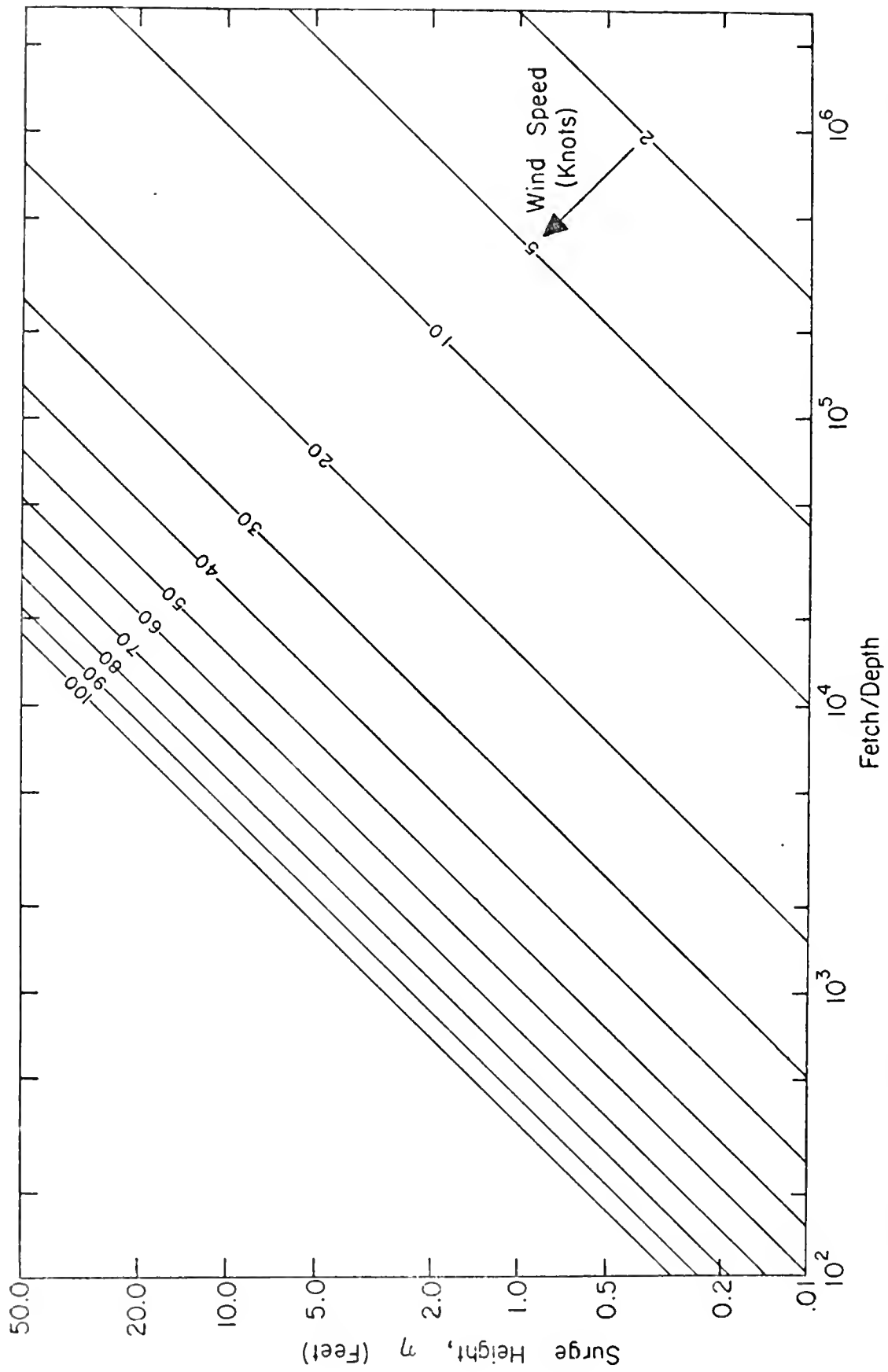
FIGURE 2-10   SURGE HEIGHT VERSUS FETCH / DEPTH FOR UNIFORM DEPTH

iii. <u>Uniform Wind Stress Acting Over a Shelf of Uniform Slope</u>

As a slightly more realistic situation, the same assumptions are made as in the previous case except now a sloping bottom (or $h(x) = h_o - mx$) is considered as shown in Figure 2-11.
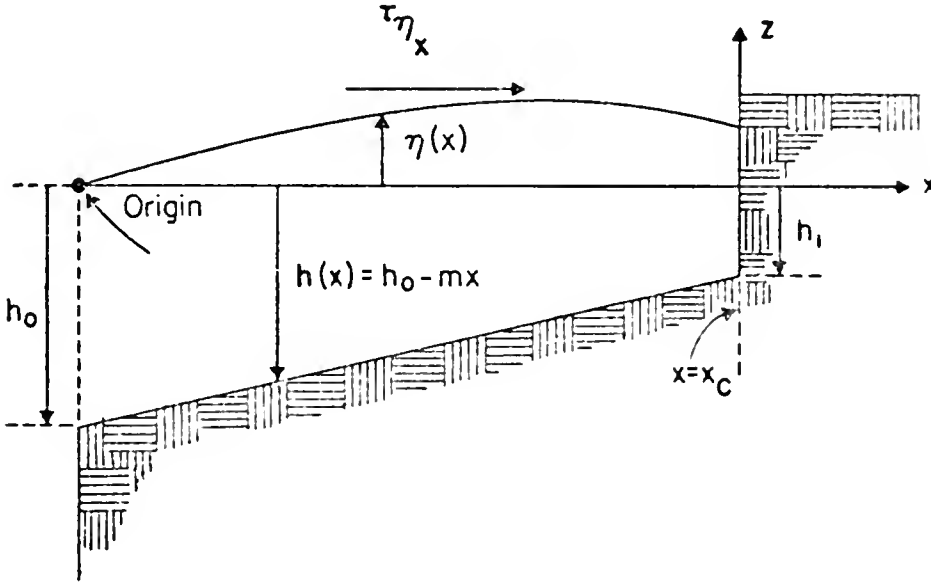
FIGURE 2-11 ONE-DIMENSIONAL SHELF WITH UNIFORMLY SLOPING BOTTOM

From Equation (2-11)

$$(h + \eta) \frac{\partial \eta}{\partial x} = \frac{\tau_{\eta_x}}{\rho g} = \text{constant} = \beta$$

and noting that $h(x) = h_o - mx$

$$D \frac{\partial D}{\partial x} = (h+\eta) \frac{\partial \eta}{\partial x} + (h+\eta) \frac{\partial h}{\partial x} = (h+\eta) \frac{\partial \eta}{\partial x} - m (h+\eta)$$

thus $dx = \frac{DdD}{\beta - mD}$. Integrate and apply the boundary condition $\eta = 0$ at $x = 0$ to obtain

$$\xi = \ln \left(\frac{1 - \zeta_o}{1 - \zeta - \xi} \right) \tag{2-12}$$

where

$$\xi = \frac{m\eta}{\beta}$$

$$\zeta = \frac{mh}{\beta}$$

$$\zeta_0 = \frac{mh_0}{\beta}$$

$$\zeta_1 = \frac{mh_1}{\beta}$$

To simplify the calculations obtain η at the coastline $x = x_c$. Equation (2-12) then reduces to

$$\xi = \ln \left(\frac{1 - \zeta_0}{1 - \zeta_1 - \xi}\right) \qquad (2-13)$$

Solutions to Equation (2-13) at $x = x_c$ are provided in Figure 2-12. As an example consider a shelf with $x_c = 50$ nautical miles, $h_0 = 80$ feet, and $h_1 = 20$ feet, this shelf has the same width and the same average depth as in case ii. For the same 50 knot wind, η at the coast is 3.53 feet. Heuristically, one would expect a larger η for the case of the sloping shelf.

Consider the location on the sloping shelf which has the same depth as the uniform depth shelf. For a point Δx towards shore there is a change in depth Δh and conversely for Δx away from shore. Thus

$$\Delta\eta^+ = \frac{\text{constant}}{h+\Delta h} = \frac{\text{constant}}{\bar{h}} \left[1 - \frac{\Delta h}{\bar{h}} + \left(\frac{\Delta h}{\bar{h}}\right)^2 - 0\,(\Delta h)^3\right]$$

$$\Delta\eta^- = \frac{\text{constant}}{h-\Delta h} = \frac{\text{constant}}{\bar{h}} \left[1 + \frac{\Delta h}{\bar{h}} + \left(\frac{\Delta h}{\bar{h}}\right)^2 + 0\,(\Delta h)^3\right]$$

Notes:

(1) Solutions at $h = h_1$ (Coastline)

(2) $\xi = \dfrac{m\eta}{\beta}$ $\zeta = \dfrac{mh}{\beta}$

$\zeta_0 = \dfrac{mh_0}{\beta}$ $\zeta_1 = \dfrac{mh_1}{\beta}$

(3) m = Bottom Slope

(4) $\beta = \dfrac{\tau\eta_x}{\rho g}$
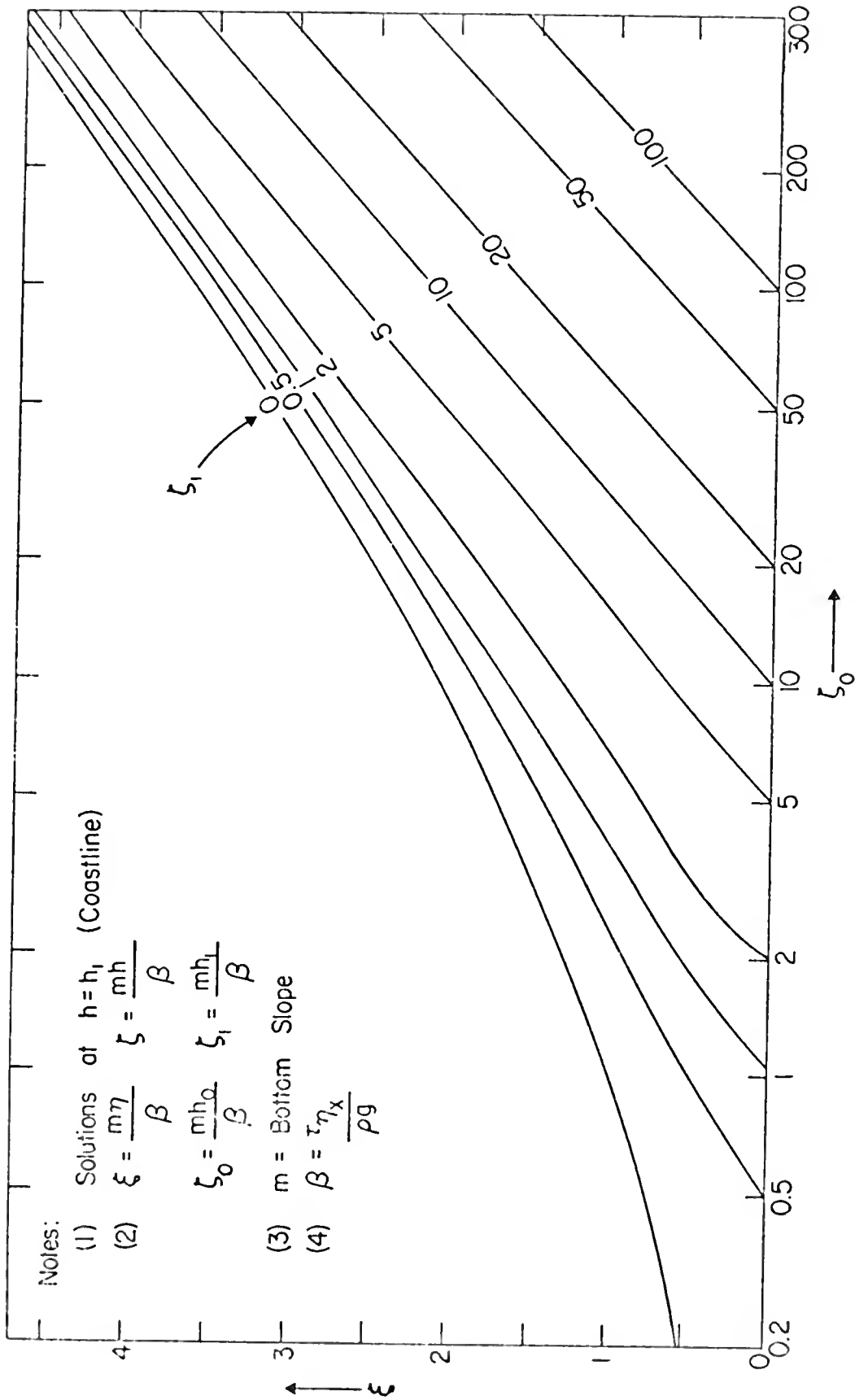
FIGURE 2-12   SOLUTIONS TO UNIFORM SLOPE CASE AT THE COASTLINE

and the total over $2\Delta x$ is

$$\delta\eta = \Delta\eta^+ + \Delta\eta^- = \frac{constant}{\bar{h}} \left[2 + 2\left(\frac{\Delta h}{\bar{h}}\right)^2 + 0 \ (\Delta h)^4 \right]$$

It can be seen, then, that a shelf of uniform depth will, in all cases, produce a smaller surge than a shelf of constant slope with the same average depth.

e. Analytical Treatment - Moving Wind Stress and Pressure Field

i. Problem Formulation

The purpose of this section is to contribute to the development of a simple procedure for the analysis of the dynamic effects involved in storm surge calculations. This analysis uses the one-dimensional tidal equations and the development will be for an arbitrary forcing function such as a hurricane. Also the bottom profile must be in an analytical form simple enough to allow a solution to the equations of motion. Conceptually, the approach is as follows: find the storm surge $\eta(x,t)$ resulting from an impulsive forcing function representing the wind shear stress, pressure gradient or both. If the impulse occurred at time t' and position x', the resulting surge at (x,t) could be written $\eta(x,t) = G(x,t; x',t')$; this is sometimes referred to as the Green's function. Having found the general form of the solution $G(x,t; x',t')$ for a simple offshore bathymetry one can then construct the solution for an arbitrary forcing function. This may be obtained by formal integration or the results may be obtained numerically.

The development in this section will be for the special case of a shelf of finite width and uniform depth as shown in Figure 2-13 and a triangular shear stress distribution as shown in Figure 2-15 .

For the equations of motion and continuity, consider Equations (2-5) where q_x is abbreviated as q, τ_{n_x} as τ_n, and τ_{b_x} as τ_b.

$$\frac{\partial q}{\partial t} + \frac{q}{D}\frac{\partial q}{\partial x} + gD\frac{\partial \eta}{\partial x} = -\frac{D}{\rho}\frac{\partial p_{\eta}}{\partial x} + \frac{1}{\rho}(\tau_{\eta} - \tau_{b}) \qquad (2\text{-}14a)$$

$$\frac{\partial q}{\partial x} + \frac{\partial \eta}{\partial t} = 0 \qquad (2\text{-}14b)$$

The convective acceleration terms will be neglected and the assumption $\eta << h$ is made, and since $D(x,t) = h + \eta(x,t) \simeq h$, Equations (2-14a) and (2-14b) reduce to

$$\frac{\partial q(x,t)}{\partial t} + gh\frac{\partial \eta(x,t)}{\partial x} = -\frac{h}{\rho}\frac{\partial p_{\eta}}{\partial x}(x,t) + \frac{1}{\rho}(\tau_{\eta}(x,t) - \tau_{b}(x,t))$$

$$\frac{\partial q(x,t)}{\partial x} + \frac{\partial \eta(x,t)}{\partial t} = 0$$

Ignoring the bottom friction term τ_{b} and letting $(\frac{1}{\rho}\tau_{\eta}(x,t) - \frac{h}{\rho}\frac{\partial p_{\eta}(x,t)}{\partial x}) = F'(x,t)$ we have:

$$\frac{\partial q}{\partial t} + gh\frac{\partial \eta}{\partial x} = F'(x,t) \qquad (2\text{-}15a)$$

$$\frac{\partial q}{\partial x} + \frac{\partial \eta}{\partial t} = 0 \qquad (2\text{-}15b)$$

The variables are described in Figure 2-13, where q is the volume transport per unit width. Differentiating Equation (2-15a) with respect to x and Equation (2-15b) with respect to t and subtracting, produces the inhomogeneous wave equation

$$\frac{\partial^2 \eta}{\partial t^2} - gh\frac{\partial^2 \eta}{\partial x^2} = -\frac{\partial F'(x,t)}{\partial x} = F(x,t) \qquad \cdot \qquad (2\text{-}16)$$
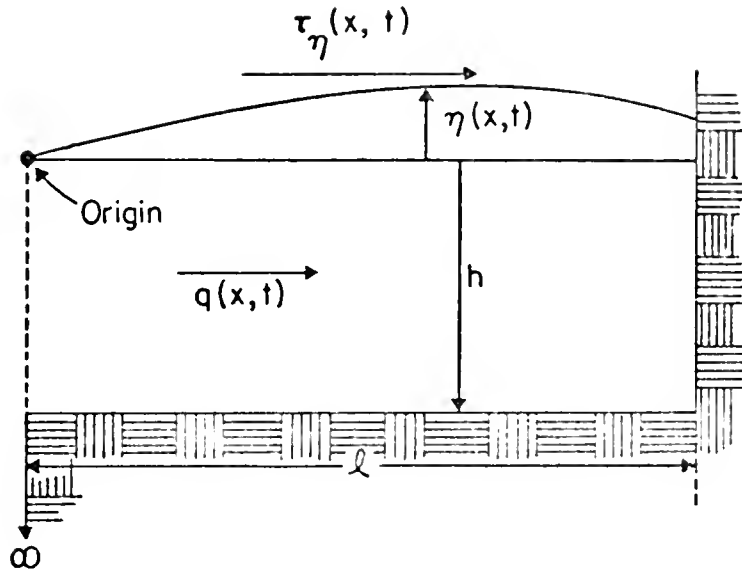
FIGURE 2-13   IDEALIZED SHELF BATHYMETRY

ii.   Solution

First a solution to the homogeneous problem $F(x,t) = 0$ is obtained.   Using separation of variables, let $\eta = X(x)T(t)$

For the spacial part of the problem, we obtain

$$- gh \frac{\partial^2 X}{\partial x^2} = \alpha_n^2 X \tag{2-17}$$

where α_n^2 is a constant as yet undetermined.   The solution to Equation (2-17) is

$$X = c_1 \sin \frac{\alpha_n}{\sqrt{gh}} x + c_2 \cos \frac{\alpha_n}{\sqrt{gh}} x \tag{2-18}$$

Referring to Figure 2-13 note that the depth is infinite at $x = 0^-$, and the surge must be zero at that point.   At $x = \ell$, there can be no flow through the wall and this leads to the condition $\frac{\partial \eta}{\partial x} = 0$ at $x = \ell$.

The condition $\eta = 0$ at $x = 0$ determines

$$c_2 \equiv 0 \text{ and } \frac{\partial \eta}{\partial x}\bigg|_{x=\ell} = \frac{c_1 \alpha_n}{\sqrt{gh}} \left(\cos \frac{\alpha_n \ell}{\sqrt{gh}}\right) T(t) = 0$$

leading to $\frac{\alpha_n \ell}{\sqrt{gh}} = (2n + 1) \frac{\pi}{2}$. The general case for the solution becomes a sum of the solutions in Equation (2-18). Thus the solution is taken to be in the form

$$\eta = \sum_{n=1,3,5\cdots}^{\infty} a_n(t) \sin \frac{n\pi x}{2\ell} \qquad (2\text{-}19)$$

Referring to the homogeneous form of Equation (2-16), obtain with Equation (2-19) the following:

$$\sum_{n=1,3,5\cdots}^{\infty} \left\{ \frac{\partial^2 a_n(t)}{\partial t^2} \sin \frac{n\pi x}{2\ell} + c^2 \left(\frac{n\pi}{2\ell}\right)^2 a_n(t) \sin \frac{n\pi x}{2\ell} \right\} = 0$$

From orthogonality, obtain

$$a_n''(t) + \sigma_n^2 a_n(t) = 0$$

where $\sigma_n = \frac{cn\pi}{2\ell}$ and $c = \sqrt{gh}$.

The two homogeneous solutions are of the form $a_n(t) = \sin \sigma_n t$, $\cos \sigma_n t$. Writing $F(x,t) = \sum_{n=1,3,5}^{\infty} B_n(t) \sin \frac{n\pi x}{2\ell}$ and $B_n(t) = \frac{2}{\ell}\int_0^{\ell} F(x,t) \sin \frac{n\pi x}{2\ell} dx$ for odd n, and using the method of variation of parameters, arrive at the following for the inhomogeneous equation; with the lower limit determined by the fact that $a_n(0) = 0$.

$$a_n(t) = \frac{\sin \sigma_n t}{\sigma_n} \int_0^t B_n(t') \cos\sigma_n t' dt' - \frac{\cos\sigma_n t}{\sigma_n} \int_0^t B_n(t') \sin\sigma_n t' dt'$$

$$a_n(t) = \int_0^t \frac{B_n(t')}{\sigma_n} \sin\sigma_n(t-t')dt'$$

$$\eta = \sum_{n=1,3,5}^{\infty} a_n(t) \sin\frac{n\pi x}{2\ell} = \sum_{n=1,3,5}^{\infty} \frac{1}{\sigma_n} \int_0^t B_n(t')\sin\sigma_n(t-t')dt'\sin\frac{n\pi x}{2\ell}$$

and finally

$$\eta(x,t) = \sum_{n=1,3,5}^{\infty} \frac{2}{\ell\sigma_n} \int_0^\ell \int_0^t F(x',t')\sin\sigma_n(t-t')\sin\frac{n\pi x'}{2\ell} dt'dx'\sin\frac{n\pi x}{2\ell} \quad (2\text{-}20)$$

Letting $F(x',t') = \kappa\delta(x'-x_0) \delta(t'-t_0)$ one then has an impulse function located at $x = x_0$ and $t = t_0$ where η represents the Green's function or response to this impulse function, and κ is a constant representing the strength of the instantaneous surface shear stress function

$$\eta(x,t) = G(x,t; x_0,t_0) =$$

$$\sum_{n=1,3,5}^{\infty} \frac{2}{\ell\sigma_n} \int_0^\ell \int_0^t \kappa\delta(x'-x_0) \delta(t'-t_0) \sin\sigma_n(t-t')\sin\frac{n\pi x'}{2\ell}dt'dx'\sin\frac{n\pi x}{2\ell}$$

$$G(x,t;x_0,t_0) = \sum_{n=1,3,5}^{\infty} \frac{2\kappa}{\ell\sigma_n} \sin\sigma_n (t-t_0) \sin\frac{n\pi x_0}{2\ell} \sin\frac{n\pi x}{2\ell} \quad (2\text{-}21)$$

It is now possible to construct a solution by the superposition of an appropriate series of impulses in space and time.

For some hurricane motions, a more convenient form of the Green's function is obtained by using an impulse function which travels with constant velocity and remains unchanged during its traverse over the

shelf. Assuming the forcing function to always start at x = 0, to travel at constant velocity C, and that the time that it crosses x = 0 is arbitrary at t_0, the impulse function is:

$$F(x,t) = \kappa\delta(x - C(t-t_0)) \quad 0 \le x \le \ell$$

Without loss of generality let $t = t + t_0$ which yields

$$F(x,t) = \kappa\delta(x - Ct) \qquad 0 \le x \le \ell$$

Thus for the case of a suddenly increased shear stress as shown in Figure 2-14, $\kappa = -\dfrac{\tau_0}{\rho}$, where τ_0 is the amount of the increase in shear stress.
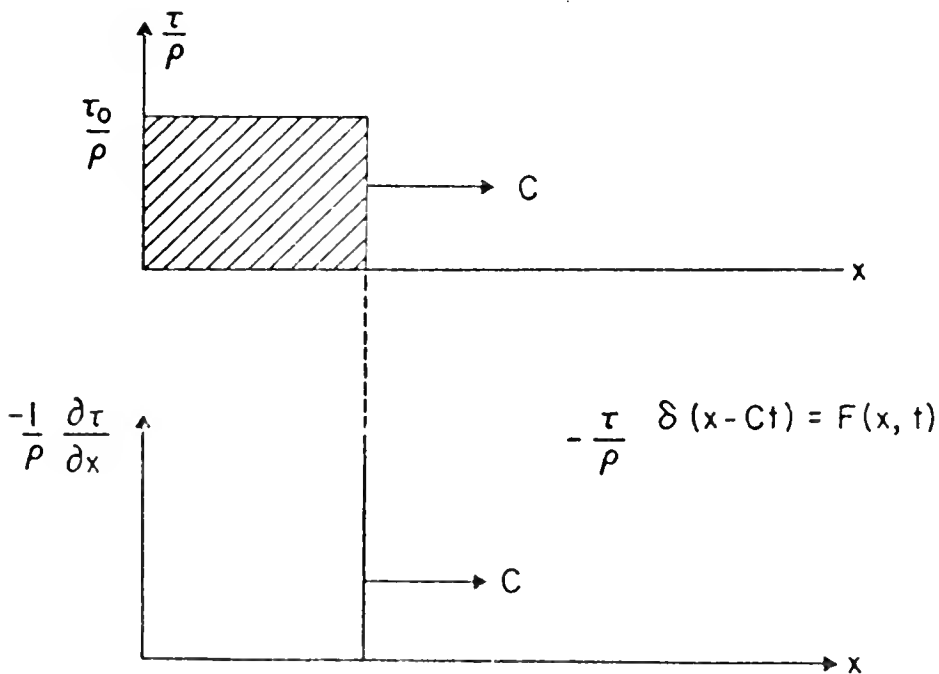
FIGURE 2-14   IMPULSIVE FORCING FUNCTION MOVING AT CONSTANT SPEED

For the case of an arbitrary shear stress distribution as shown in Figure 2-15a, locally $\Delta\tau = \frac{\partial\tau}{\partial x}\Delta x$
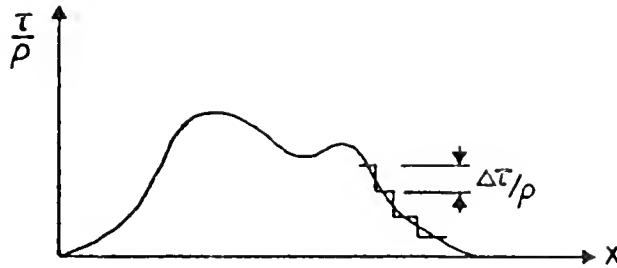
FIGURE 2-15a   ARBITRARY FORCING FUNCTION

For a triangular shear stress distribution as shown in Figure 2-15b
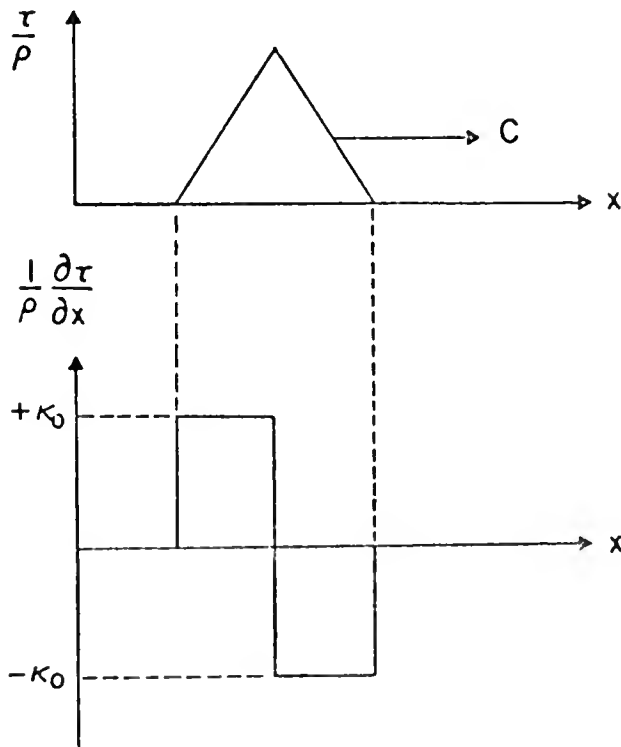
FIGURE 2-15b   TRIANGULAR FORCING FUNCTION

κ becomes $\frac{1}{\rho}\frac{\partial\tau}{\partial x}\,\delta x$, and the following is obtained.

$$F(x',t') = \frac{1}{\rho}\frac{\partial\tau}{\partial x}\,\delta(x'-Ct')\,dx = \frac{1}{\rho}\,\Delta\tau\,\delta(x'-Ct')$$

The resulting Green's Function can then be written in integral form as follows.

$$G(x,t;0,0)=\sum_{n=1,3,5}^{\infty}\frac{2}{\ell\sigma_n}\int_0^\ell\int_0^t\frac{\Delta\tau}{\rho}\,\delta(x'-Ct')\sin\sigma_n(t-t')\sin\frac{n\pi x'}{2\ell}dt'dx'\sin\frac{n\pi x}{2\ell}$$

Note that this is really the solution for an incremental element having a shear stress jump of $\Delta\tau$. Since $\delta(x'-Ct') \neq 0$ only when $x' = Ct'$

$$G(x,t;0) = \sum_{n=1,3,5}\frac{2\Delta\tau}{\rho\ell\sigma_n}\int_0^t\sin\sigma_n(t-t')\sin\frac{n\pi Ct'}{2\ell}\,dt'\,\sin\frac{n\pi x}{2\ell}$$

Letting $\sigma_n = \sigma = \frac{n\pi C}{2\ell}$, $\sigma_n' = \sigma' = \frac{n\pi C}{2\ell}$

and integrating yields

$$G(x,t;0) = \sum_{n=1,3,5}\frac{2\Delta\tau}{\rho\ell\sigma(\sigma'^2-\sigma^2)}\,[\sigma'\sin\sigma t - \sigma\sin\sigma't]\,\sin\frac{n\pi x}{2\ell}$$

Note that this is the solution for a solitary continuous impulse function traveling at speed C; at time $t > \ell/C$ the forcing function crosses the shelf, and the solution becomes periodic in time.

Letting $c^* = C/c$, $c = \sqrt{gh}$ and $\sigma' = \sigma\,c^*$ one arrives at

$$G(x,t;0) = \sum_{n=1,3,5}\frac{+2\Delta\tau}{\rho\ell\sigma^2(c^{*2}-1)}\,[c^*\sin\sigma t-\sin(\sigma c^*t)]\,\sin\frac{n\pi x}{2\ell}$$

with the constraints $t < \ell/C$ and $c^* \neq 1$. When $t > \ell/C$

$$G(x,t;0) = \sum_{n=1,3,5} \frac{2\Delta\tau}{\rho\ell\sigma} \int_0^{\ell/C} \sin\sigma(t-t') \sin\frac{n\pi Ct'}{2\ell} \, dt' \sin\frac{n\pi x}{2\ell}$$

where $\sigma' \, \ell/C = \frac{n\pi}{2}$

and

$$\left.\begin{array}{c} \cos\dfrac{n\pi}{2} = 0 \\[2em] \sin\dfrac{n\pi}{2} = (-1)^{\frac{n-1}{2}} \end{array}\right\} \qquad n = 1,3,5$$

$G(x,t; 0)$ thus becomes

$$G(x,t;0) = \sum_{n=1,3,5} \frac{2\Delta\tau\sin(n\pi x/2\ell)}{\rho\ell\sigma^2(c*^2-1)}[+c*\sin\sigma t - \cos\sigma(t-\ell/C)\,(-1)^{\frac{n-1}{2}}]$$

with the constraints $t > \ell/C$ and $c*^2 \neq 1$. If $\Delta\tau$ is written as $\frac{\partial\tau}{\partial x'} dx'$ and it is noted that $x = Ct$ then $\Delta\tau = C\frac{\partial\tau}{\partial x} dt$. Letting $t = t - t_o$ yields $G(x,t; t_o)$ where t_o represents the time at which $\delta(x-C(t-t_o))$ crosses the point $x = 0$. The desired result is then the sum or integral of the above solutions

$$n(x,t) = \int_{t_o} G(x,t; t_o)\, dt_o \tag{2-22}$$

The shear stress profile of a hurricane can be approximated by a triangular function [2]. The derivative of this is two rectangular pulses as indicated in Figures 2-15b. The response can be found using Equation (2-22) and remembering that $G(x,t; t_o)$ is represented by two functions depending on whether t is less than or greater than ℓ/C. The solution is straightforward but unfortunately tedious.

The solution is simplified by putting η into a dimensionless form. Letting

$$T = 4\ell/c$$

$$\sigma^* = \sigma T = 2n\pi$$

$$x^* = x/\ell$$

$$t^* = t/T$$

allows η' to be represented as Equation (2-23).

$$\eta'(x^*,t^*) = \frac{-\eta(x,t)\,(2\pi)^3}{(2\kappa'T^3/\ell)} \tag{2-23}$$

The appropriate variables and constants for the triangular stress distribution are illustrated in Figure 2-16, where t_1 has been arbitrarily set equal to zero for convenience,
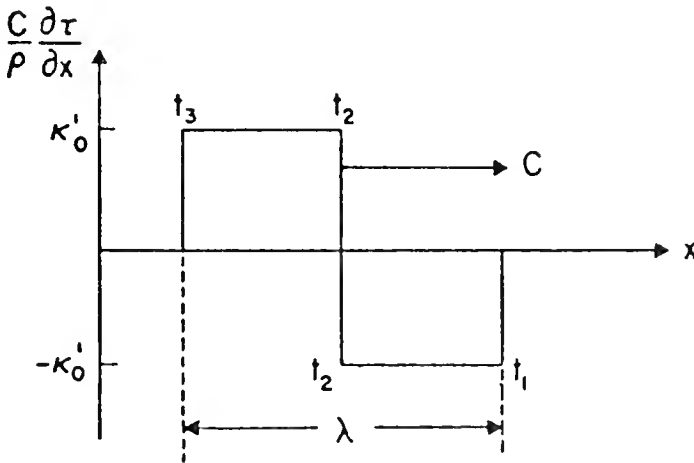
FIGURE 2-16   DEFINITION SKETCH FOR SHEAR STRESS DISTRIBUTION

and are defined as follows:

$$\kappa' = \frac{C}{\rho}\frac{\partial \tau}{\partial x}$$

$$t_1 = 0 \rightarrow t_1^* = 0$$

$$t_2 = \frac{\lambda}{2C} \rightarrow t_2^* = \frac{\lambda^*}{8c^*}$$

$$t_3 = \frac{\lambda}{C} \rightarrow t_3^* = \frac{\lambda^*}{4c^*}$$

$$\lambda^* = \frac{\lambda}{\ell}$$

$$\kappa' = -\kappa_0' \; ; \quad 0 < t_0 < \frac{\lambda}{2C}$$

$$\kappa' = \kappa_0' \; ; \quad \frac{\lambda}{2C} < t_0 < \frac{\lambda}{C}$$

$$\kappa' = 0 \; ; \quad \frac{\lambda}{C} < t_0$$

The solution must be presented as six different forms, each for a different time span. They are as follows:

(1) In the first case the storm has completely passed by the position, $x = \ell$, thus

$$t \geq \frac{\lambda + \ell}{C} \rightarrow t^* \geq \frac{\lambda^* + 1}{4c^*}$$

and the solution for η is

$$\eta'(x^*, t^*) =$$

$$\sum_{n=1,3,5} \frac{\sin(n\pi x/2\ell)}{n^3(c^{*2}-1)} \left[\sin\sigma_n((t-t_0)-\ell/C)\,(-1)^{\frac{n-1}{2}} + c^*\cos\sigma_n(t-t_0) \right]_{t_0=t_1}^{t_0=t_3}$$

By defining the contents of the brackets as $H_1(t_0)$, the response becomes

$$\eta'(x^*, t^*) = \sum_{n=1,3,5} \frac{\sin(n\pi x/2\ell)}{n^3(c^{*2}-1)} \left[H_1(t_3) + H_1(t_1) - 2H_1(t_2) \right]$$

where t_1, t_2, t_3 represent values of t_o and are defined in Figure 2-16.

(2) In case 2 the storm is completely on the shelf $0 < x < \ell$, thus

$$\lambda/C \leq t \leq \ell/C \quad \rightarrow \quad \frac{\lambda^*}{4c^*} \leq t^* \leq \frac{1}{4c^*}$$

and η can be written as follows

$$\eta'(x^*,t^*) =$$

$$\sum_{n=1,3,5} \frac{\sin(n\pi x/2\ell)}{n^3(c^{*2}-1)} \left[+c^*\cos(\sigma_n(t-t_o)) - \frac{1}{c^*}\cos(c^*\sigma_n(t-t_o)) \right] \Big|_{t_o=t_1}^{t_o=t_3}$$

Defining $H_2(t_o)$ as the contents of the brackets, as above, leads to

$$\eta'(x^*,t^*) = \sum_{n=1,3,5} \frac{\sin(n\pi x/2\ell)}{n^3(c^{*2}-1)} \left[H_2(t_3)+H_2(t_1) - 2H_2(t_2) \right]$$

The time periods from $0 < t < \lambda/C$ and $\ell/C < t < \frac{\lambda+\ell}{C}$ have not yet been covered since they introduce the additional complication of having only part of the forcing function in the region of interest. The solutions for these remaining time periods are:

(3)

$$\frac{\ell + \lambda/2}{C} < t < \frac{\ell + \lambda}{C} \quad \rightarrow \quad \frac{1 + \lambda^*/2}{4c^*} < t^* < \frac{1 + \lambda^*}{4c^*}$$

$$\eta'(x^*,t^*) =$$

$$\sum_{n=1,3,5} \frac{\sin(n\pi x/2\ell)}{n^3(c^{*2}-1)} \left[H_2(t_3)-H_2(t-\ell/C)+H_1(t-\ell/C)-2H_i(t_2)+H_1(t_1) \right]$$

(4)

$$\ell/C < t \leq \frac{\ell + \lambda/2}{C} \quad \rightarrow \quad \frac{1}{4c^*} < t^* \leq \frac{1 + \lambda^*/2}{4c^*}$$

$$\eta'(x^*,t^*) =$$

$$\sum_{n=1,3,5,\ldots} \frac{\sin(n\pi x/2\ell)}{n^3(c^{*2}-1)} [H_2(t_3)-2H_2(t_2) + H_2(t-\ell/C)-H_1(t-\ell/C)+H_1(t_1)]$$

(5)

$$\frac{\lambda}{2C} < t < \frac{\lambda}{C} \rightarrow \frac{\lambda^*}{8c^*} < t^* < \frac{\lambda^*}{4c^*}$$

$$\eta'(x^*,t^*) = \sum_{n=1,3,5,\ldots} \frac{\sin(n\pi x/2\ell)}{n^3(c^{*2}-1)} [H_2(t)+H_2(t_1)-2H_2(t_2)]$$

(6)

$$0 \le t \le \lambda/2C \rightarrow 0 \le t^* \le \frac{\lambda^*}{8c^*}$$

$$\eta'(x^*,t^*) = \sum_{n=1,3,5,\ldots} \frac{\sin(n\pi x/2\ell)}{n^3(c^{*2}-1)} [H_2(t_1) - H_2(t)]$$

$\eta'(x^*,t^*)$ has now been described for all t^*. It can be seen that η^* can be described as a function of three dimensionless quantities c^*, λ^*, and t^*.

Figure 2-17 shows profiles of η' on the shelf for various values of t^* and particular values of λ^* and c^*.

Figure 2-18, perhaps of more interest, shows η'_{max}, the maximum storm surge that occurs as a result of the storm passage as a function of both c^* and λ^*.

To determine the accuracy of both theory and calculations, an independent approach was utilized to obtain equivalent dimensionless surge heights. The one-dimensional tidal equation of motion and equation of continuity in finite difference form, as developed in
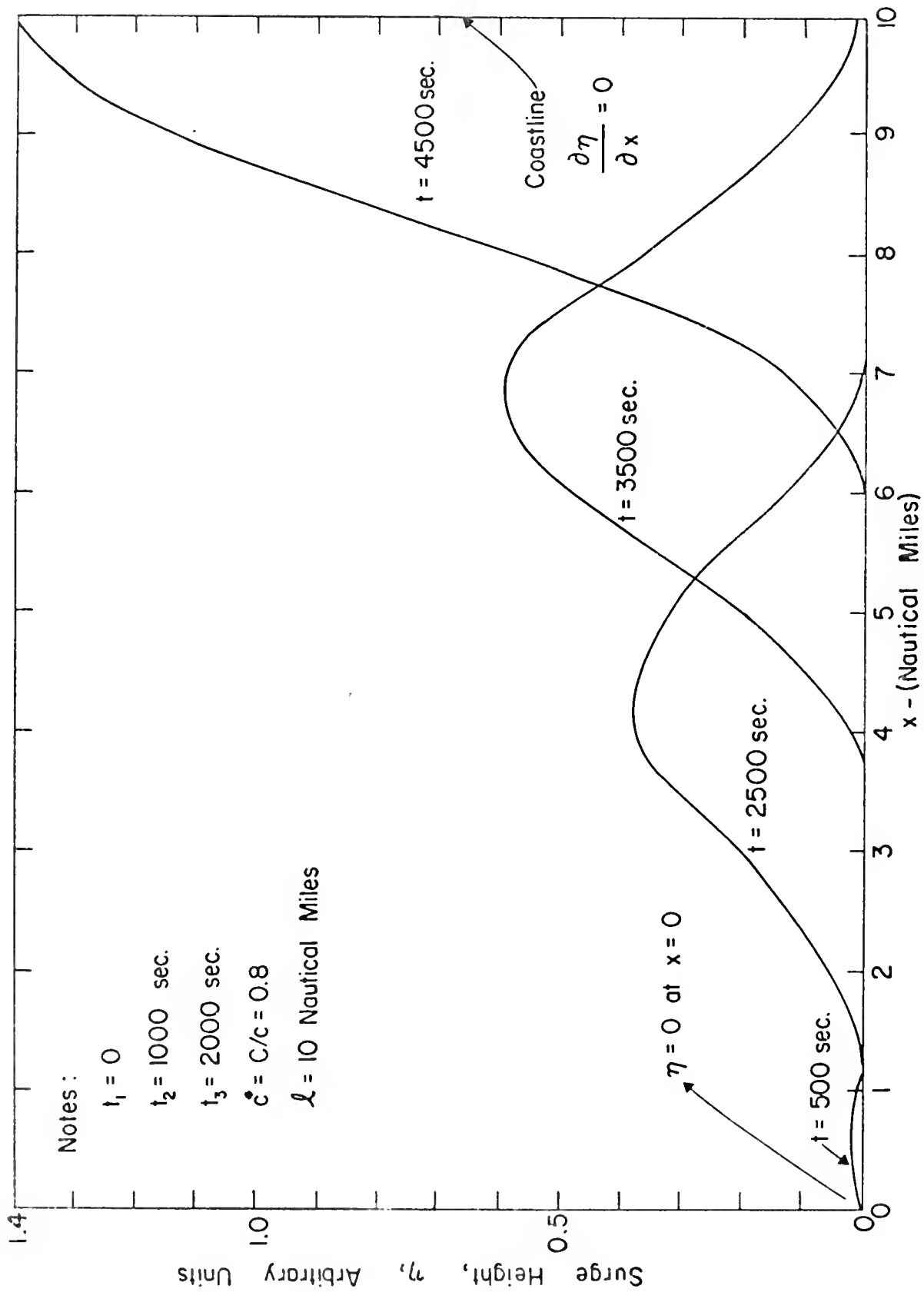
FIGURE 2-17   RESPONSE TO TRIANGULAR SHEAR STRESS DISTRIBUTION
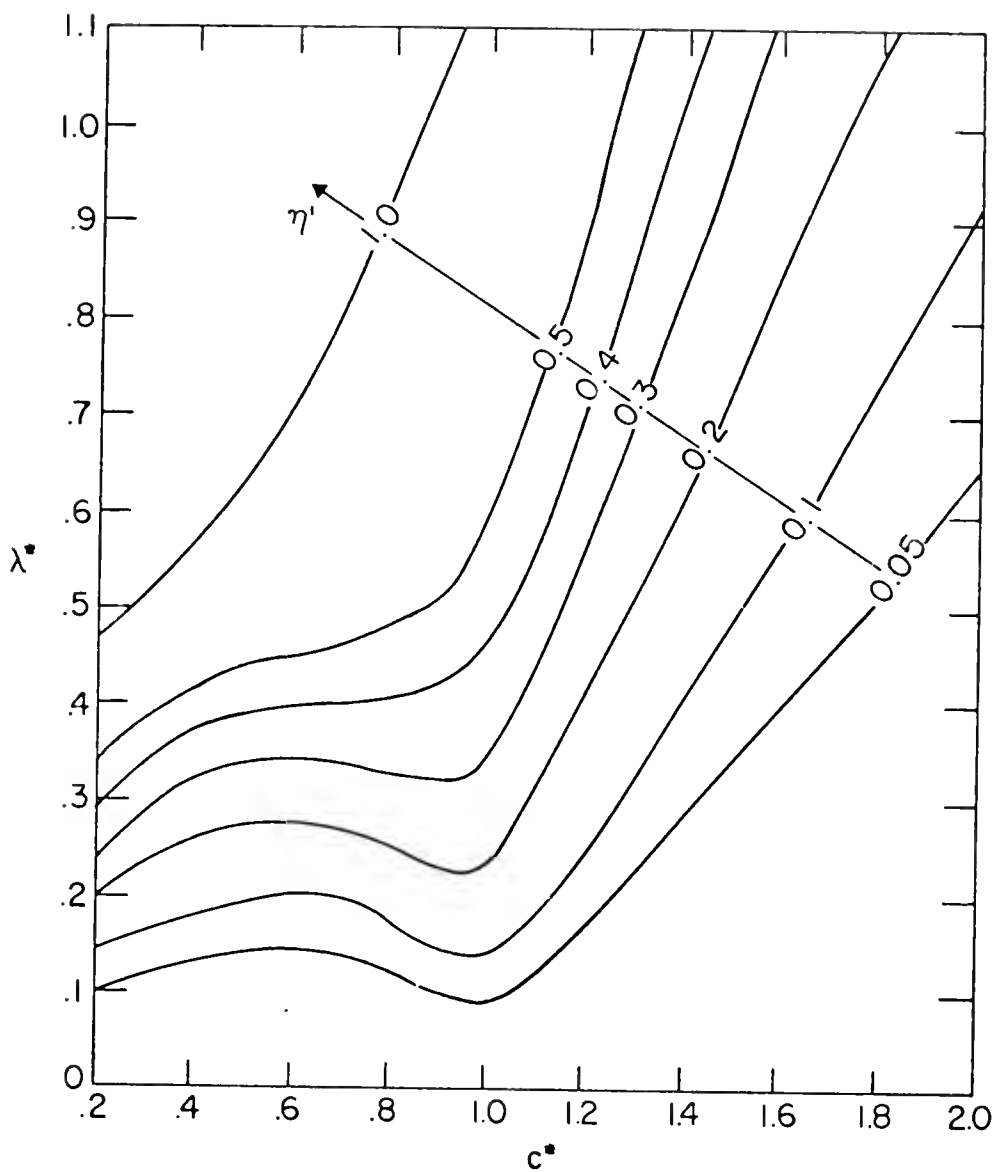
FIGURE 2-18 DIMENSIONLESS SURGE HEIGHT
MAXIMA AS A FUNCTION OF
DIMENSIONLESS STORM WIDTH AND
VELOCITY

Section 3-a , were used to obtain a numerical solution to this problem.
The equations were linearized $(D \simeq h)$ to agree with the assumptions
in this section, and the bottom friction neglected. The "no flow"
boundary condition $q_x = 0$ was prescribed at the coast with a boundary
condition $\eta = 0$ assumed at the shelf break. Note that the $q_x = 0$
condition is comparable to $\frac{\partial \eta}{\partial x} = 0$. Figure 2-19a depicts a shelf of
constant depth divided into 20 one-dimensional grid elements, as used
for the calculations. The "storm" or triangular shear stress dis-
tribution as illustrated in Figure 2-19b was moved over the shelf
waters at a constant speed, C. A slight approximation was used here.
Once the edge of a shear stress step encounters a new grid element,
the stress was assumed constant over that element for a time $\Delta t = \Delta x/C$,
or the time for the leading edge to traverse the grid element. The
numerical results were put into dimensionless form as in Equation (2-23)
and compared to the analytical results yielding Figure 2-20.

Notes:

(1) η Linearly Extrapolated to Coast

(2) Boundary Conditions

(a) $q = 0$ at Coast

(b) $\eta = 0$ in Grid (1)
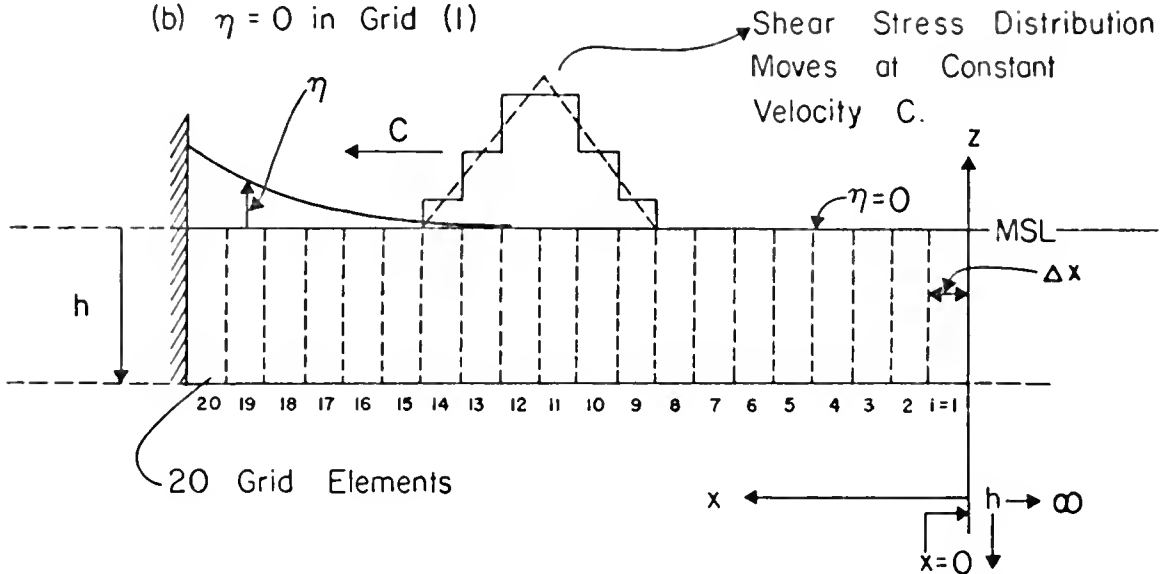
FIGURE 2-19a DEFINITION SKETCH FOR NUMERICAL CALCULATIONS
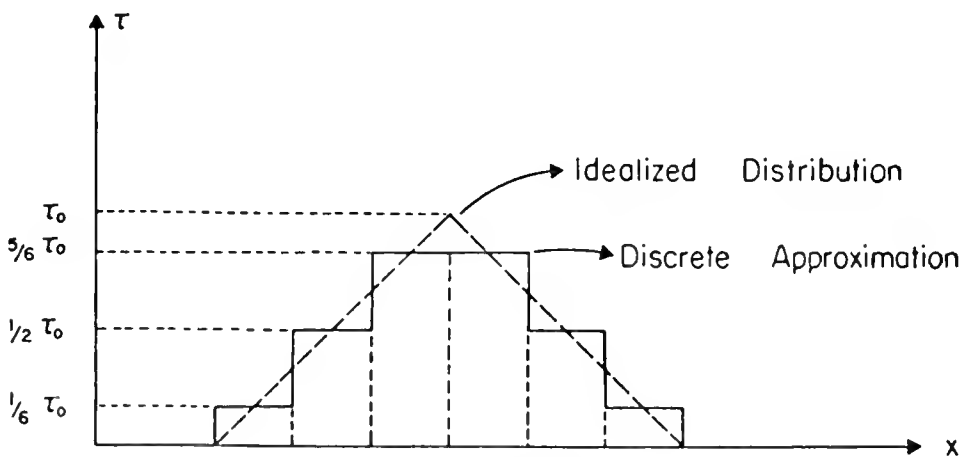
FIGURE 2-19b FINITE DIFFERENCE MODEL OF TRIANGULAR SHEAR STRESS DISTRIBUTION
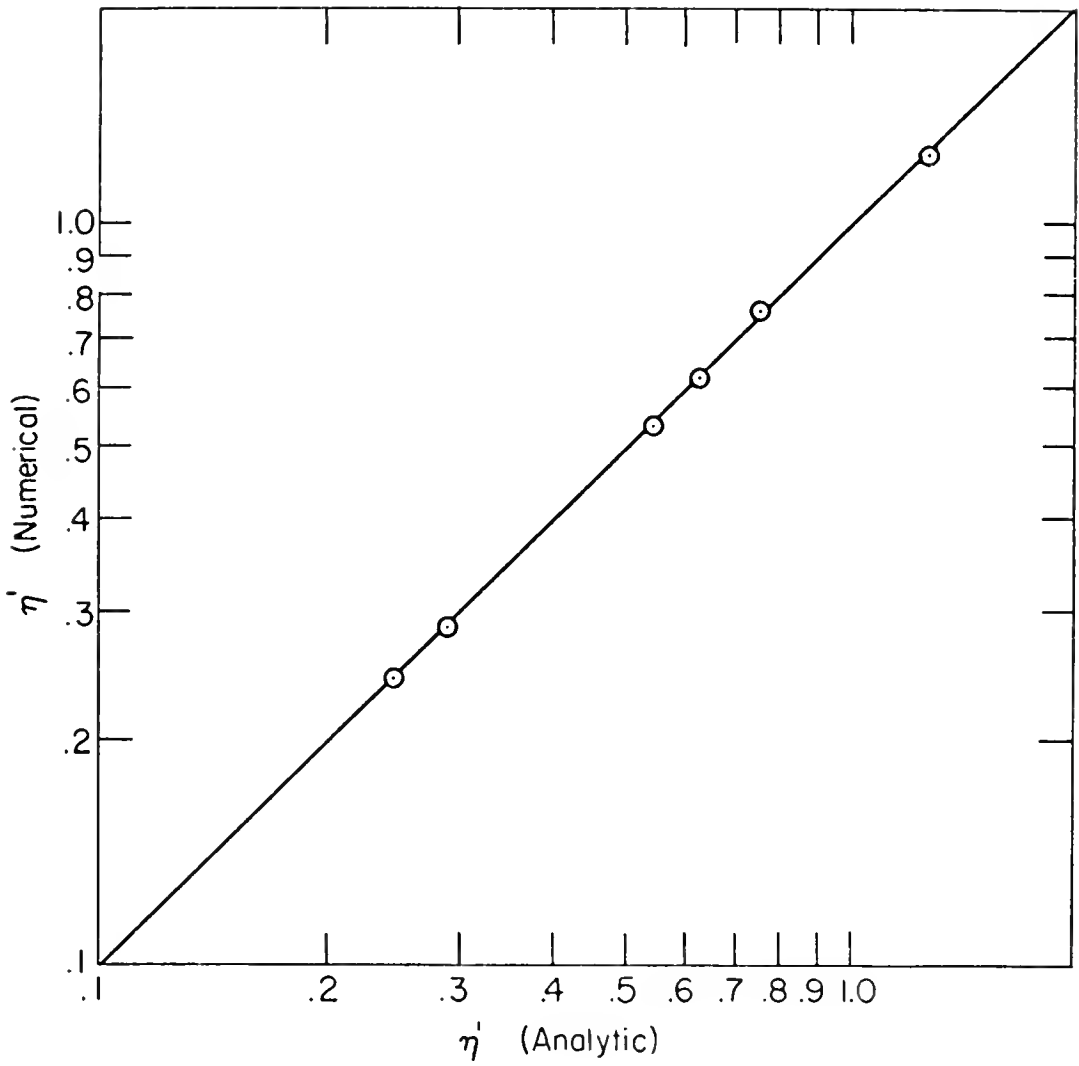
FIGURE 2-20   COMPARISON   OF   NUMERICAL   AND
ANALYTICAL SOLUTIONS

CHAPTER 3

THE NUMERICAL MODEL

a. <u>One-dimensional Numerical Model</u>

In most prototype situations it is unrealistic to make the simpli-
fying assumptions necessary for a successful analytical treatment of the
storm surge problem. To incorporate such features as an irregular coast-
line, irregular bathymetry, islands, and arbitrary wind stress patterns,
a numerical approach becomes necessary. The actual numerical approach or
algorithm is frequently referred to as a numerical model. Models may be
roughly categorized as one-, two-, and three-dimensional. One- and two-
dimensional models are presented in this chapter.

The one-dimensional model considers motion in only one direction,
e.g. along a perpendicular to the coastline. It is presented here for two
reasons: its simplicity allows physical insight into the problem and it
provides a check of the two-dimensional model, which can approach a
one-dimensional model as a limiting condition.

The development of the one-dimensional numerical model begins by
referring to Equations 2-6.

$$\frac{\partial q_x}{\partial t} - 2\omega(\sin\phi)q_y = -\frac{D}{\rho}\frac{\partial p_n}{\partial x} - gD\frac{\partial \eta}{\partial x} + \frac{1}{\rho}(\tau_{n_x} - \tau_{b_x}) \qquad (2\text{-}6a)$$

$$\frac{\partial q_y}{\partial t} + 2\omega(\sin\phi)q_x = -\frac{D}{\rho}\frac{\partial p_\eta}{\partial y} - gD\frac{\partial \eta}{\partial y} + \frac{1}{\rho}(\tau_{n_y} - \tau_{b_y}) \qquad (2\text{-}6b)$$

$$\frac{\partial q_x}{\partial x} + \frac{\partial q_y}{\partial y} + \frac{\partial \eta}{\partial t} = 0 \tag{2-6c}$$

Considering only motion in the x-direction leads to Equations (3-1a) and (3-1b)

$$\frac{\partial q_x}{\partial t} = -\frac{D}{\rho}\frac{\partial p_\eta}{\partial x} - gD\frac{\partial \eta}{\partial x} + \frac{1}{\rho}(\tau_{\eta_x} - \tau_{b_x}) \tag{3-1a}$$

$$\frac{\partial q_x}{\partial x} + \frac{\partial \eta}{\partial t} = 0 \tag{3-1b}$$

Using the quadratic friction law, $\tau_{b_x} = \dfrac{\rho f q_x |q|}{8D^2}$, Equations (3-1a) and (3-1b) can be written as

$$\frac{\partial q_x}{\partial t} = -\frac{D}{\rho}\frac{\partial p_\eta}{\partial x} - gD\frac{\partial \eta}{\partial x} + \frac{\tau_{\eta_x}}{\rho} - \frac{f|q_x|q_x}{8D^2} \tag{3-2a}$$

$$\frac{\partial q_x}{\partial x} + \frac{\partial \eta}{\partial t} = 0 \tag{3-2b}$$

These are the equations to be used for the one-dimensional calculations.

The finite difference integration scheme used for the numerical calculations is similar to that of Reid and Bodine [10] and Verma and Dean [28]. Figure 3-1 provides a schematic diagram of a typical coastal region showing the coordinate system and defining the variables in use. The vertical coordinate, z, is oriented positively upward and referenced to mean sea level, MSL; the horizontal coordinate x is oriented toward shore with x = 0 occurring at the shelf break. In the computations η, h, τ, and p are considered uniform over the grid width Δx, and centered at the midpoint of the segment. The quantity, q_x, denotes the flux in volume per unit width through the plane representing the seaward boundary of a grid element.
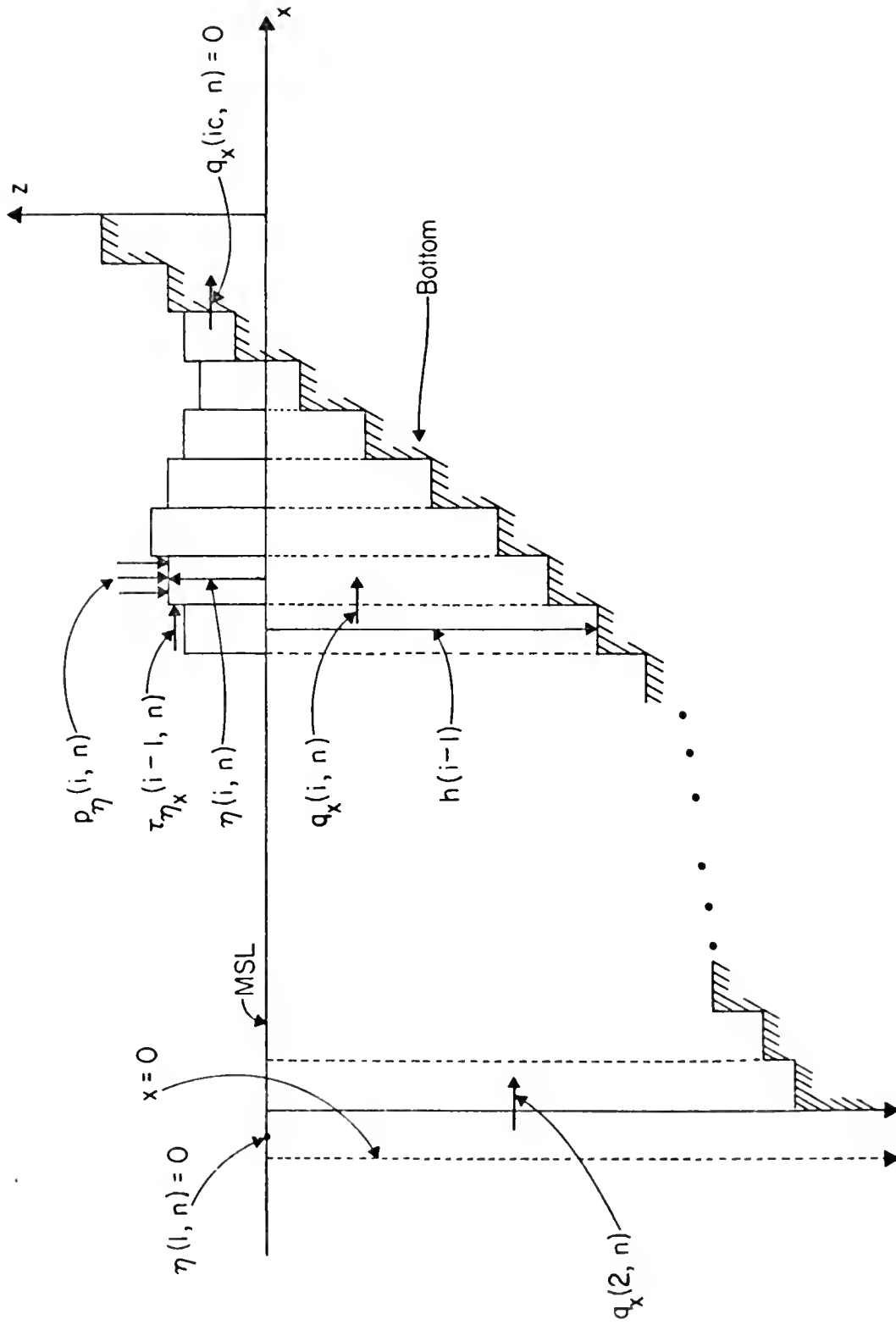
FIGURE 3-1   DEFINITION SKETCH FOR ONE-DIMENSIONAL CALCULATIONS,
SECTION NORMAL TO THE COAST

For clarity the variables are placed into an indicial form where $q_x(i+1,n)$ indicates the volume transport per unit width through the plane section at the location $x = i \Delta x$ and at time $n\Delta t$, i.e. flow into the grid designated by index $i+1$. Similarly, $n(i,n+1/2)$ indicates the value of n for the ith grid element. It is assumed to be centered at $x = (i+1/2)\Delta x$ and to be evaluated at time $t = (n+1/2)\Delta t$.

Following the scheme in Appendix A, the equations are placed in finite difference form as Equations (3-3a) and (3-3b)

$$q_x(i,n+1) = \frac{1}{F_x} [q_x(i,n) + \Delta t \{\frac{[D(i-1,n+1/2)+D(i,n+1/2)]}{2\Delta x}\} \cdot$$

$$\{[n(i-1,n+1/2) - n(i,n+1/2)] g + \frac{1}{\rho} [p_n(i-1,n+1/2) - p_n(i,n+1/2)]\}$$

$$+ \frac{\Delta t}{2\rho} [\tau_{n_x} (i-1,n+1/2) + \tau_{n_x} (i,n+1/2)]] \tag{3-3a}$$

where

$$F_x = 1 + \frac{\Delta t \, f}{2} |q_x(i,n)| [D(i-1,n+1/2)+D(i,n+1/2)]^{-2}$$

The continuity Equation (3-2b) provides, in finite difference form, the equation for the free surface,

$$n(i,n+3/2) = n(i,n+1/2) + \frac{\Delta t}{\Delta x} [q_x(i,n+1) - q_x(i+1,n+1)] \tag{3-3b}$$

To illustrate the calculation procedure assume that all values of q_x are available up to and including $t = n\Delta t$. Beginning at the seaward boundary, calculate q_x's at time $(n+1)\Delta t$ using Equations (3-3a). Next, calculate n's at $(n+3/2)\Delta t$ using Equation (3-3b), then advance the pressure and shear stress to $(n+3/2)\Delta t$ and calculate q_x's at time

$(n+2)\Delta t$, and so forth. In effect, averages over small segments are being made in both space and time to approximate the true solution. This results in a type of leapfrog method, since q_x's at time $(n+1)\Delta t$ are used to extend the solution from $\eta(i,n+1/2)$ to $\eta(i,n+3/2)$ and similarly η and D at $(n+3/2)$ are used to obtain $q_x(i,n+2)$. The process is continued until a desired time is reached, such as a surge maximum at the coast.

The seaward boundary condition, the barometric tide, is applied to grid $(1,n)$, where the wind setup is zero and $h(1,n) \to \infty$. This condition is written as $\eta(1,n) = 1.15 [p_\infty - p_\eta(1,n)]$ where η is in feet and p_∞ is the undisturbed pressure in inches of mercury far from the storm. The landward boundary condition of no flow requires $q_x(ic,n) = 0$. The initial conditions used will require all q_x's = 0 and the grid to be in barometric equilibrium. The only remaining data required for the calculations are the pressure and shear stress distributions as functions of time. Figure 3-2 shows the movement of such a system at constant velocity and with constant form. The required wind and pressure data are extrapolated linearly from the storm model described in Section 2-c.

The model also allows for the "flooding" or "draining" of a grid element. Consider the element (ic,n) in Figure 3-1, if $\eta(ic-1,n)$ <-h(ic) then the system is as shown, if $\eta(ic-1,n) > - h(ic)$ then the grid element (ic) must be flooded or activated. In practice when activating a grid element an instability can occur which results in switching between the activated and inactivated states. Also remember that at the moment of grid activation D = 0 causing trouble with the calculations at that point. To avoid these problems, the following steps are taken.

Surface Shear Stress Distribution Moves Toward Shore with Constant Velocity
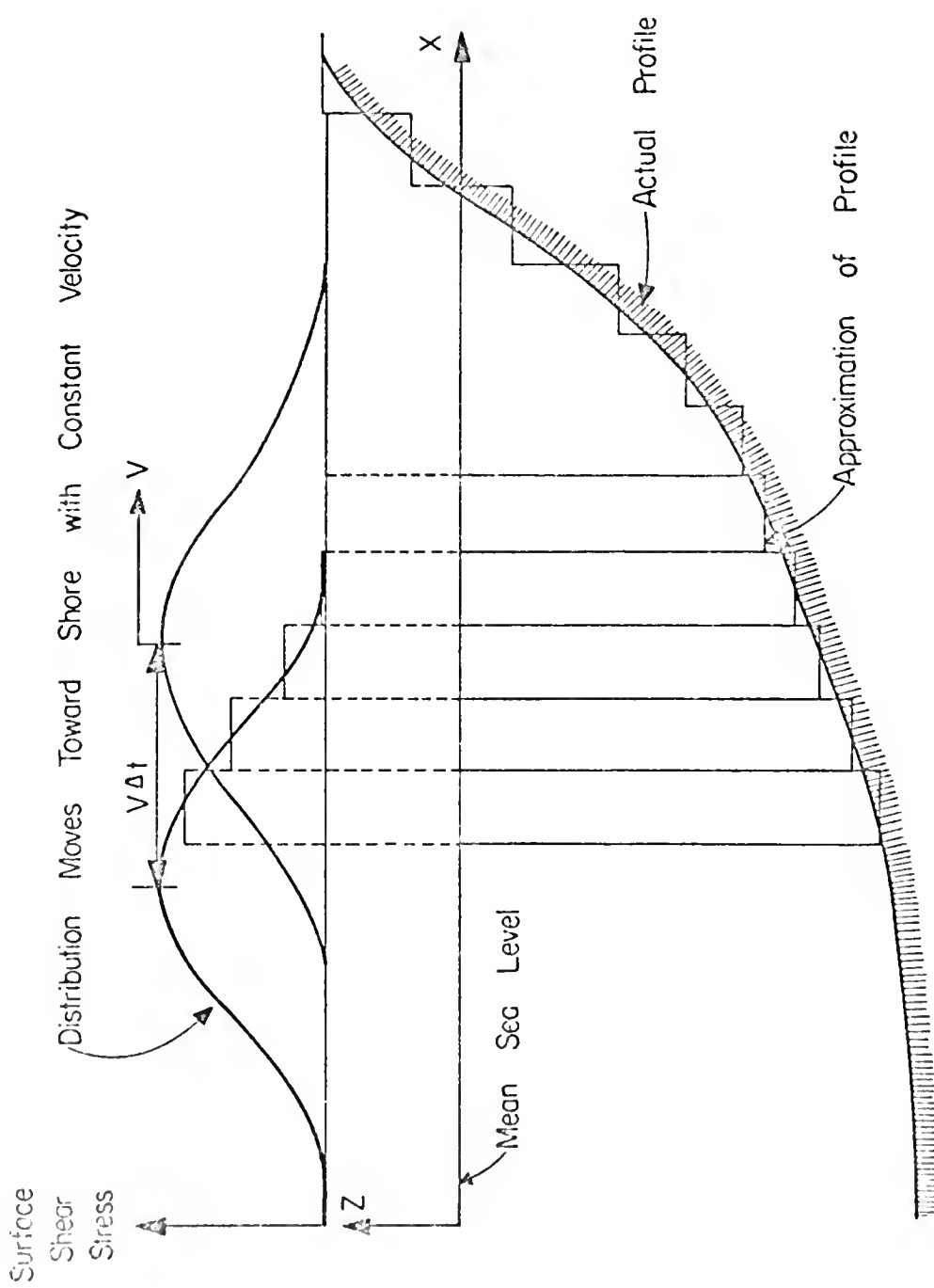
FIGURE 3-2   MOVEMENT OF STORM

Once activated the grid element is constrained to remain activated for a specified number of time steps. Five time steps has been found satisfactory in the present model. In addition to the above, D is set equal to .01 ft. in the just-flooded grid element prior to the calculations for the next time step to prevent zero divide problems. This introduces a small error into the system. Since flooding occurs infrequently with respect to the number of time steps this error is considered acceptable.

To calculate a water velocity u from q_x an average depth over adjacent grids is taken and $u(i,n)$ is approximated as

$$u(i,n) = 2q_x(i,n) [D(i-1,n+1/2) + D(i,n+1/2)]^{-1} \qquad (3-4)$$

Since $u(i,n)$ is not used in the calculations, the approximations in Equation (3-4) are not considered significant. A more accurate value, centered at time n, which must be calculated one time step after the q_x's is given by Equation (3-5).

$$u(i,n) = 4q_x(i,n) [D(i-1,n-1/2) + D(i-1,n+1/2) + D(i,n-1/2)$$

$$+ D(i,n+1/2)]^{-1} \qquad (3-5)$$

It is assumed that the hurricane or pressure and shear stress distributions approach normal to the coast. Numerical stability for the one-dimensional model requires that $\frac{\Delta t}{\Delta x} \leq (gD_{max})^{-1/2}$ where D_{max} is the maximum total depth expected anywhere in the system. Thus given a bottom profile and, shear stress and pressure, as a function of time, the surge can be calculated using this reasonably simple technique. This model is particularly useful in quantifying effects of the numerical model that are not inherent in the equations of motion but result as an effect of dis-

cretization. The model is also easily checked and thus provides a basis for comparison with other models which are not easily checked.

b.   Development in Two Dimensions

The development in two dimensions is analogous to that in one dimension and therefore much of the detail will be omitted. Recalling that the two-dimensional model considers motion in the x and y directions, refer to Equation (2-6), and employing the quadratic bottom friction obtain

$$\frac{\partial q_x}{\partial t} - 2\omega(\sin\phi)q_y + gD\frac{\partial \eta}{\partial x} = -\frac{D}{\rho}\frac{\partial p_n}{\partial x} + \frac{\tau_{n_x}}{\rho} - \frac{f|q|q_x}{8D^2} \qquad (3\text{-}6a)$$

$$\frac{\partial q_y}{\partial t} + 2\omega(\sin\phi)q_x + gD\frac{\partial \eta}{\partial y} = -\frac{D}{\rho}\frac{\partial p_n}{\partial y} + \frac{\tau_{n_y}}{\rho} - \frac{f|q|q_y}{8D^2} \qquad (3\text{-}6b)$$

$$\frac{\partial q_x}{\partial x} + \frac{\partial q_y}{\partial y} + \frac{\partial \eta}{\partial t} = 0 \qquad (3\text{-}6c)$$

These equations are now in forms which can be applied and where no other approximations need be made. Expressing Equation (3-6a) in finite difference form as described in Appendix B leads to the following for the x-equation.

$$q_x(i,j,n+1) = \frac{1}{F_x}\,[q_x(i,j,n) + 2\omega(\sin\phi)\overline{q_y}\,(i,j,n)\Delta t$$

$$+ \frac{\Delta t}{2\rho}\,\{\tau_{n_x}\,(i-1,j,n+1/2) + \tau_{n_x}\,(i,j,n+1/2)\}$$

$$+ \frac{\Delta t}{2\Delta x}\,\{D(i-1,j,n+1/2) + D(i,j,n+1/2)\}\,\{\,\frac{1}{\rho}\,[p_\eta(i-1,j,n+1/2)$$

$$-p_\eta(i,j,n+1/2)] + g\,[\eta(i-1,j,n+1/2) - \eta(i,j,n+1/2)]\}] \qquad (3\text{-}7_1)$$

where

$$F_x = 1 + \frac{f\Delta t}{2} \{ [q_x(i,j,n)]^2 + [q_y(i,j,n)]^2\}^{1/2} \; .$$

$$[D(i-1,j,n+1/2) + D(i,j,n+1/2]^{-2} \qquad\qquad (3\text{-}7b)$$

Equations (3-7a), (3-7b), (3-8a), and (3-8b) are adapted using the form given by Reid and Bodine [10], with changes in notation.

Following the same procedure for the y-equation yields

$$q_y(i,j,n+1) = \frac{1}{F_y} [q_y(i,j,n) - 2\omega(\sin\phi)\, \overline{q}_x(i,j,n)\Delta t$$

$$\frac{\Delta t}{2\rho} \{\tau_{n_y}(i,j,n+1/2) + \tau_{n_y}(i,j-1,n+1/2)\}$$

$$+ \frac{\Delta t}{2\Delta x} \{D(i,j,n+1/2) + D(i,j-1,n+1/2)\} \quad \{\frac{1}{\rho} [p_n(i,j-1,n+1/2)$$

$$- p_n(i,j,n+1/2)] + g[n(i,j-1,n+1/2) - n(i,j,n+1/2)]\}] \qquad (3\text{-}8a)$$

where

$$F_y = 1 + \frac{f\Delta t}{2} \{[\overline{q}_x(i,j,n)]^2 + q_y(i,j,n)]^2\}^{1/2} \; .$$

$$[D(i,j,n+1/2) + D(i,j-1,n+1/2)]^{-2} \qquad\qquad (3\text{-}8b)$$

Here, Δx and Δy are the grid spacings as shown in Figure 3-3. Figure 3-3 also defines the variables in Equation (3-7a) and the sense of operation of a grid element.

The values for the variables, n, p_n, h, D, τ are assumed to be centered in each grid as shown in Figure 3-3. The values are, after that, assumed uniform over the entire grid element for the calculation at that time step.

Since $q_x(i,j,n)$ and $q_y(i,j,n)$ occur at different points it becomes

Time $\equiv n\Delta t$

$\eta(i,j,n)\equiv$ Surge Height at Center of Element (i,j)

$h(i,j)\equiv$ Water Depth at Center of Element (i,j)

$q_x(i,j,n)\equiv$ Volume Transport in X·Direction into Element (i,j)

$q_y(i,j,n)\equiv$ Volume Transport in Y·Direction into Element (i,j)

X

Δx

Δy

$h(i+1,j,n)$
$\eta(i+1,j,n)$

$q_x(i+1,j,n)$

$h(i,j,n)$
$\eta(i,j,n)$

$q_x(i,j,n)$

$q_y(i,j+1,n)$

$q_y(i,j,n)$

$h(i,j+1,n)$
$\eta(i,j+1,n)$

Y
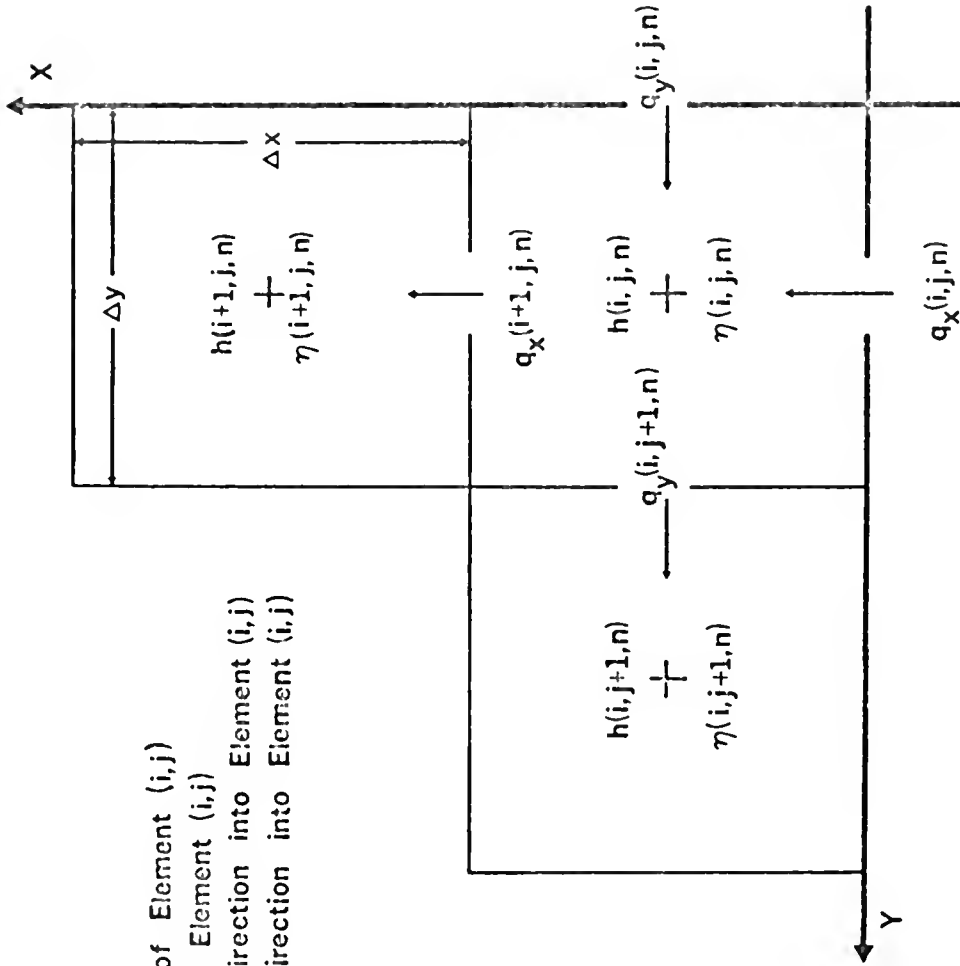
FIGURE 3-3   GRID ELEMENT DESCRIPTION FOR TWO–DIMENSIONAL SCHEME

necessary to obtain spatially averaged values $\bar{q}_x(i,j,n)$ and $\bar{q}_y(i,j,n)$ for use in the Coriolis term and the friction terms F_x, F_y. Thus, $q_y(i,j,n)$ and $\bar{q}_x(i,j,n)$ are considered to be at the same point and $q_x(i,j,n)$ and $\bar{q}_y(i,j,n)$ are considered to be at the same point. This is illustrated more clearly in Figures 3-4a and 3-4b. $\bar{q}_y(i,j,n)$ is defined as

$$\bar{q}_y(i,j,n) = \frac{1}{4} [q_y(i,j,n) + q_y(i-1,j,n) + q_y(i,j+1,n) + q_y(i-1,j+1,n)]$$

and $\bar{q}_x$ is expressed by

$$\bar{q}_x(i,j,n) = \frac{1}{4} [q_x(i,j,n) + q_x(i+1,j,n) + q_x(i+1,j-1,n) + q_x(i,j-1,n)]$$

The equation of continuity, Equation (3-6c), becomes in finite difference form,

$$n(i,j,n+3/2) = n(i,j,n+1/2) + \frac{\Delta t}{\Delta x} [q_x(i-1,j,n+1)-q_x(i,j,n+1)]$$

$$+ \frac{\Delta t}{\Delta y} [q_y(i,j-1,n+1) - q_y(i,j,n+1)] \qquad (3-9a)$$

The total depth D is defined by

$$D(i,j,\xi) = h(i,j) + n(i,j,\xi) \qquad (3-9b)$$

where ξ is an arbitrary time increment.

To carry out an actual computation, a grid network is set up as illustrated in Figure 3-5.

The coordinate convention is the same as Figure 2-1 with x-positive toward shore and y-positive to the left while facing the shoreline. The boundary conditions are illustrated in Figure 3-5 and are described as follows: 1) the fluid flux across any sea-land
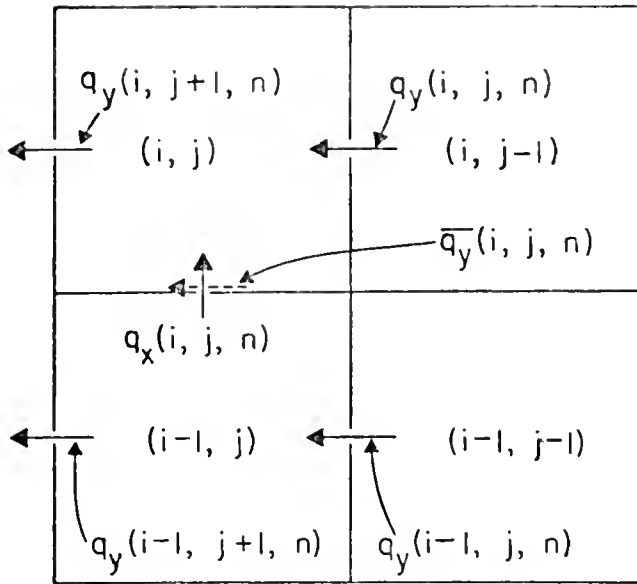
FIGURE 3-4a   COMPONENTS OF $\overline{q_y}(i, j, n)$
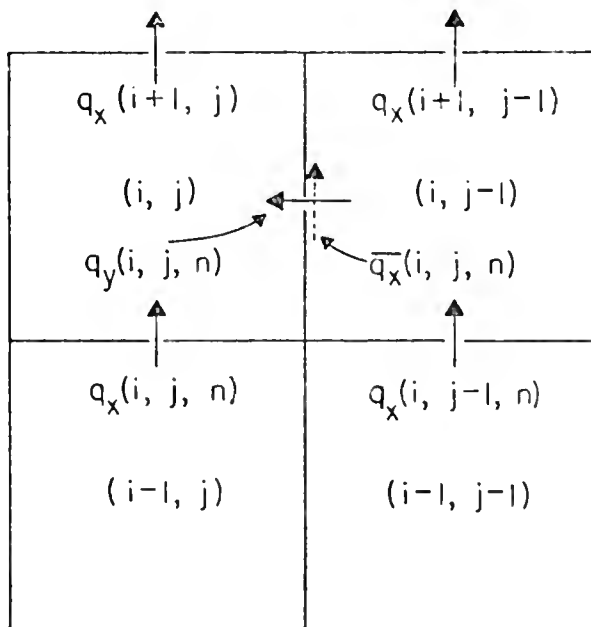
FIGURE 3-4b   COMPONENTS OF $\overline{q_x}(i, j, n)$

η Centered in Seaward and Lateral Boundary Rows is Equated to the Sum of Static Barometric Tide and Astronomical Tide

q_x in Lateral Boundary Column is Equated to Zero

(1,1) .... (1,ny)

$q_x = 0$

Δx Δy

$q_x = 0$ $q_x = 0$

$q_x = 0$

$q_x = 0$

$q_y = 0$ $q_x = 0$ $q_x = 0$ $q_y = 0$

$q_x = 0$

(nx,1) (nx,ny)

Shoreline

Land

q's Normal to Land Boundaries are Equated to Zero

FIGURE 3-5   SCHEMA OF GRID SYSTEM AND BOUNDARY CONDITIONS EMPLOYED IN TWO – DIMENSIONAL CALCULATIONS

boundary is equal to zero; 2) the boundary condition at the seaward

boundary is given as η equal to the barometric tide plus the astro-

nomical tide at that point; 3) at the lateral boundaries $q_x = 0$;

4) also at the lateral boundaries η is set equal to the barometric

tide plus the astronomical tide. Furthermore it will be assumed that

the lateral boundaries are far enough away from the region of interest

that the lateral boundary conditions have little effect. It should be

reemphasized that the lateral conditions are those conditions arrived

at empirically, which allow calculations without instabilities or other

problems with the model. Initially the system is considered quiescent

and in barometric equilibrium. This condition is of little effect

providing the storm begins sufficiently far offshore. In this model

the bathymetry and shoreline are arbitrary and the presence of islands

is allowed.

Currents in the coastal waters are of interest for several

reasons, among them: 1) to aid in making and evaluating future current

and surge calculations, 2) at the coastline hurricane-generated
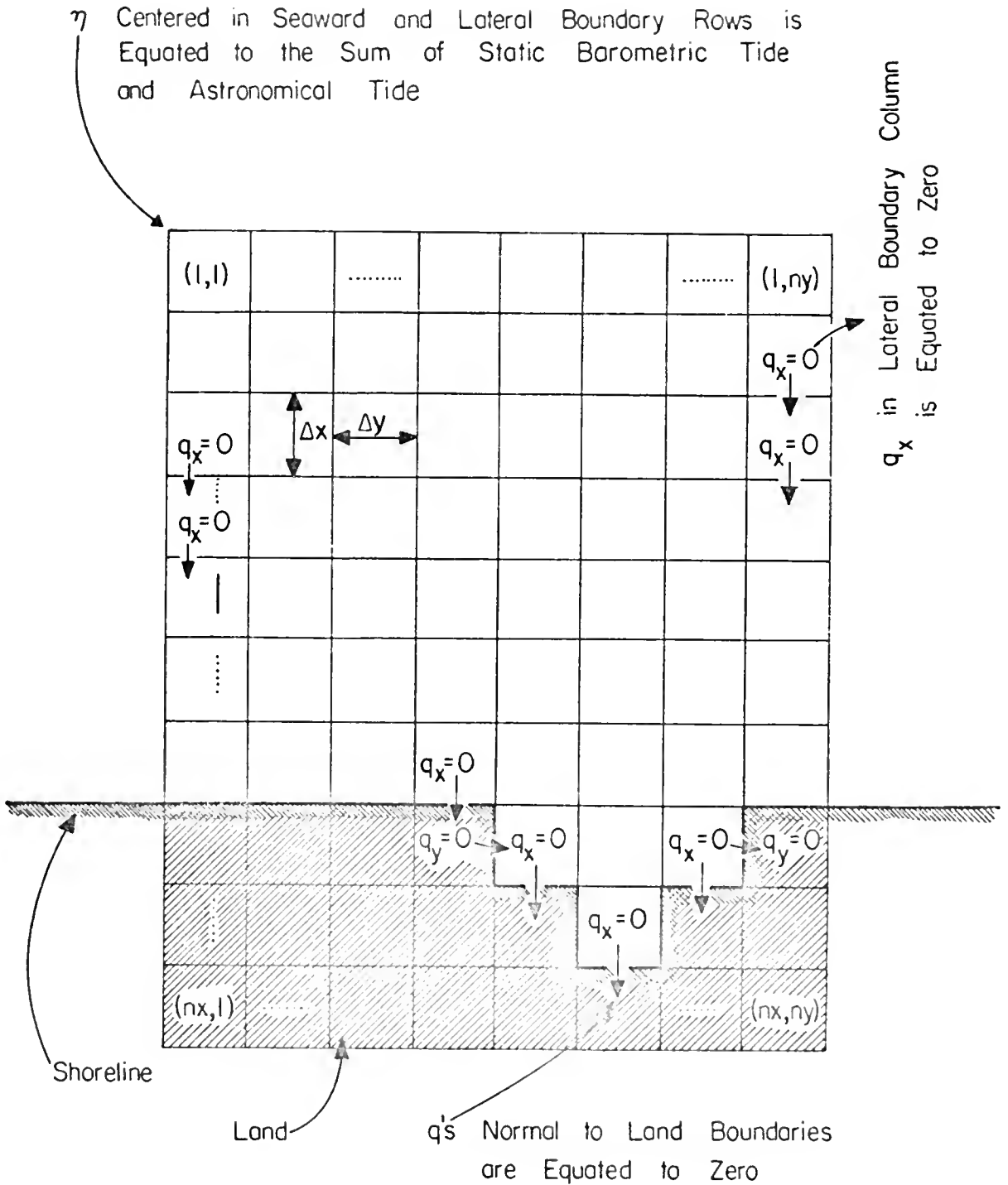
currents are of interest as a cause of beach erosion, 3) hurricane-

generated currents may be instrumental in producing extreme forces on

ocean structures, and 4) currents are instrumental in dispersion and

pollution studies. Thus, it is of further interest to describe the

scheme used to calculate the water velocity at a specified grid

element. As in the one-dimensional case the total depth at time n-1/2

is used to calculate u(i,j,n) and v(i,j,n). In order to maintain a

consistent approach, an average in both the x and y directions is

taken. This leads to the following value of u(i,j,n) and for v(i,j,n)

as described in Figure 3-6.
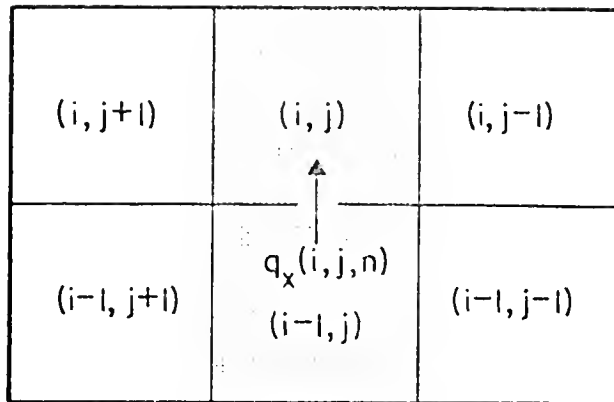
Note:
Shaded Areas
Weighted Twice

Figures Indicate Grid Elements
Involved in Calculating Weighted
Total Depth for Water Velocity
Calculations at Grid (i,j)

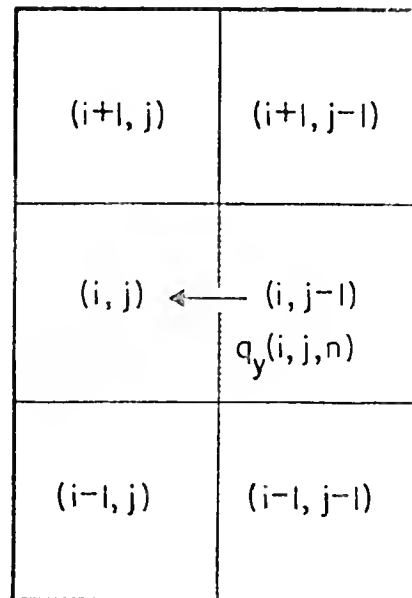FIGURE 3-6   FILTERS USED TO CALCULATE WATER
VELOCITIES

$$u(i,j,n) = 8q_x(i,j,n) \ [2D(i-1,j,n)+2D(i,j,n)+D(i,j+1,n)+D(i-1,j-1,n)$$
$$+D(i,j-1,n)+D(i-1,j+1,n)]^{-1}$$

$$v(i,j,n) = 8q_y(i,j,n) \ [2D(i,j-1,n)+2D(i,j,n)+D(i-1,j,n)+D(i-1,j-1,n)$$
$$+D(i+1,j,n)+D(i+1,j-1,n)]^{-1}$$

Adjacent to the land-sea boundary it is necessary to modify this procedure because of the no flow boundary condition.

c. Effects of Discretization and Checks of the Numerical Model

In any model of this type it is desirable to obtain some estimate of the effects of the grid size, time increments, and lateral boundary conditions on the model output. A check of the programming is also necessary. One way to accomplish this is with a series of two or more programs which although of different concept or design, converge to identical solutions for some limiting case. This does not necessarily prove all are correct but provides confidence in the results.

A one-dimensional time dependent program should give results similar to those of a two-dimensional time dependent program if the radius scale of the hurricane is large enough with respect to some length scale characteristic of the system. A comparison of this type has been carried out for an extremely large storm, with the results and storm characteristics as shown in Figure 3-7. One would, in general, expect the one-dimensional program to over predict water levels far from the coast since a cross-section of the storm is used and this effect extends laterally to infinity, but in the two-dimensional case the pressures and stresses die off with distance from the center line. Near the coast the Coriolis effect and the two-dimensional effects dominate. The one-dimensional plot shown in Figure 3-7a represents a cross section of maximum surge heights. The bottom was a linear slope approximated by a finite difference form.
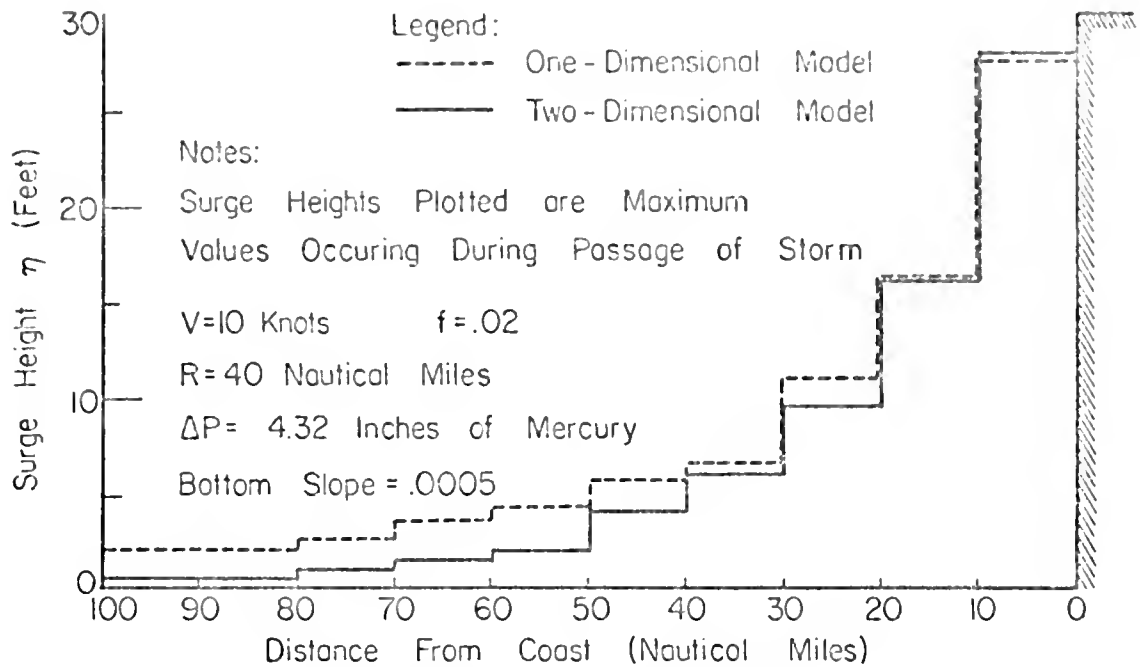
FIGURE 3-7a COMPARISON OF MAXIMUM SURGE HEIGHTS CALCULATED BY THE ONE- AND TWO- DIMENSIONAL MODELS
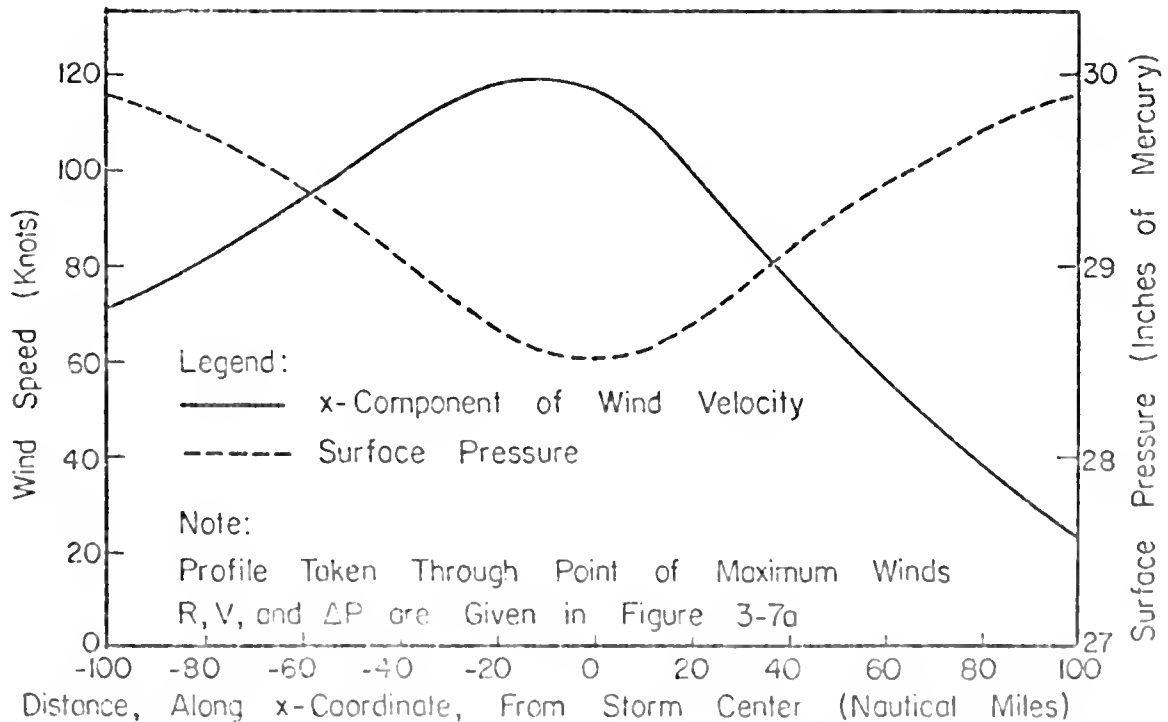

FIGURE 3-7b PROFILES OF STORM CHARACTERISTICS USED IN COMPARISON
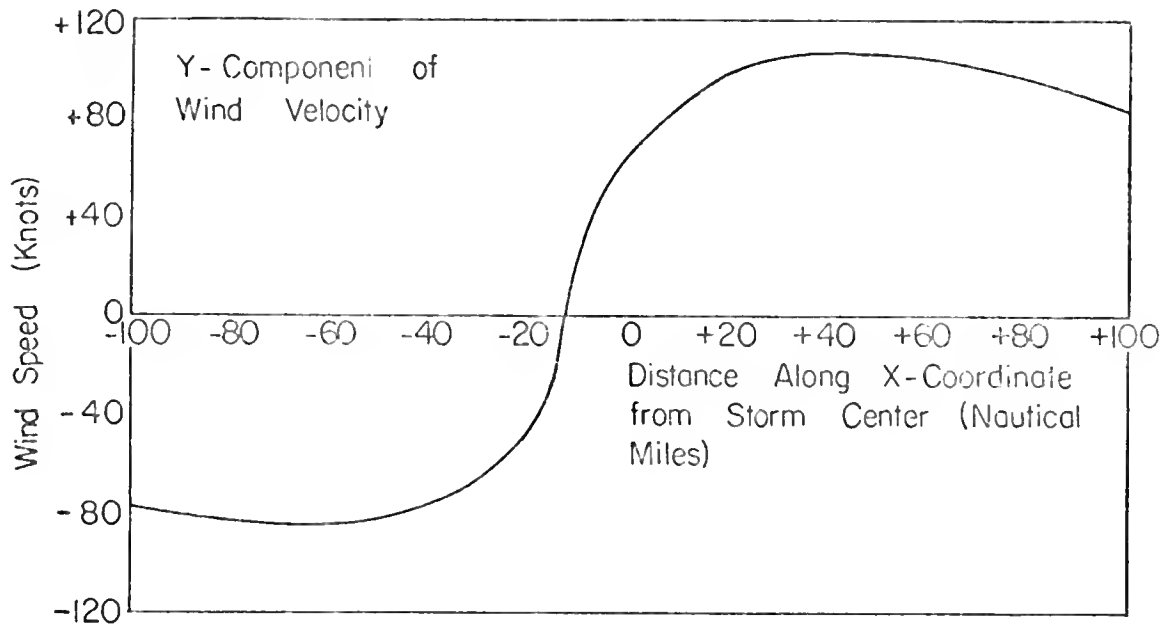
FIGURE 3-7c   Y-COMPONENT OF WIND VELOCITY

As a further comparison, a time independent or steady state model was developed as a further check of the computer modeling. It is one dimensional and time independent in that $\frac{\partial q_x}{\partial t}$ is equal to zero. q_x must then be equal to zero and the bottom friction term is eliminated. The numerical technique consists of a Runge-Kutta starter and Adam's Method predictor [29]. The stepwise bottom profile, with slope .0005 as before, was included and flooding allowed, also as before. The storm characteristics for the one-dimensional time independent case are shown in Figure 3-7b, c, with the storm center placed 10 nautical miles offshore. Note that although the storm is stationary it has the characteristics of a storm traveling with $v = 10$ knots. The numerical results and the steplike bottom profile are illustrated by the dotted line in Figure 3-8.

In order to compare these results with those of the one-dimensional time-dependent routine the time-dependent routine was run with identical storm characteristics and then stopped when the storm center was 10 nautical miles offshore. In this case the bottom friction, f, was set equal to zero and as a result the solution oscillated. The shaded boxes in Figure 3-8 represent the range of oscillations. The stepwise approximation to the uniform slope, .0005, was again used in this case.

How well does the 10 nautical mile step-like bottom profile model a true linear slope? This question can be answered as follows. The time independent model was run with all variables as before, with the single exception of a uniformly sloping bottom. These results are plotted as the solid line in Figure 3-8. In deep water the results are
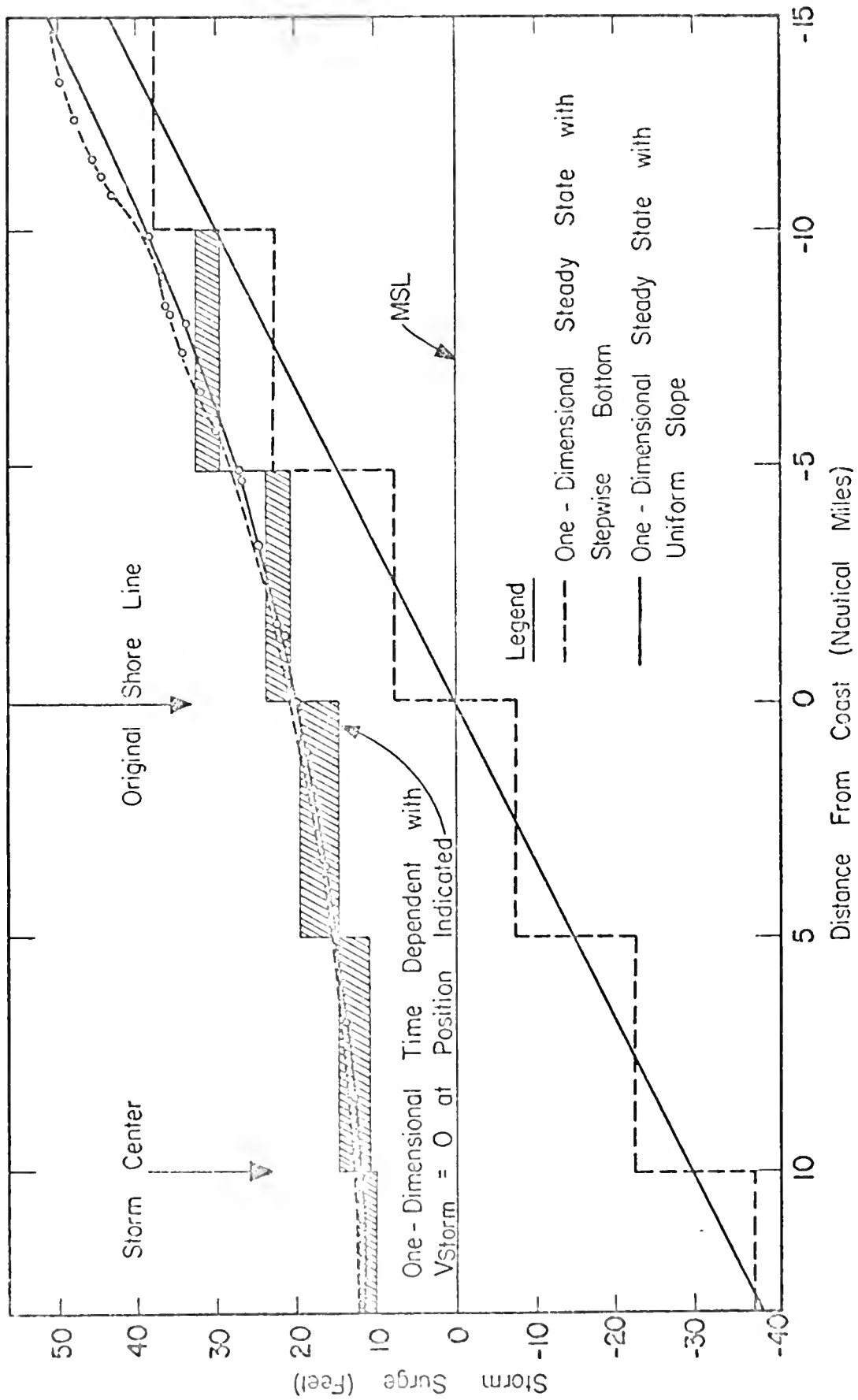
FIGURE 3-8   COMPARISON OF THREE ONE-DIMENSIONAL MODELS

nearly identical. In the shallow region the differences become
noticeable. At the risk of over generalizing, this stepwise grid
network is permissible for values of $D = h + \eta$ greater than 20 feet;
for values less than 20 feet the errors can become significant.

In the two-dimensional problem another "error-dimension"
exists, that of the effect of placement of lateral boundaries. This
is, in addition to, the effects of discretization. The lateral bound-
aries of the model are an artifice and if they are not a sufficient
distance from the zone of high wind stress then their proximity will
influence the calculated storm tides and velocities. In order to
evaluate this effect some basis for comparison must be available. A
two-dimensional analytical treatment of storm tides on continental
shelves is available from Dean and Pearce [21].

Consider the situation illustrated in Figure 3-9 in which a
"strip" wind field is uniform within a total width, w, and zero out-
side of this width. The Coriolis effect is omitted and the bottom
shear stress is expressed as proportional to the transport components
(i.e. linearized). Only shear stresses in the horizontal plane are
considered, i.e. adjacent water columns are considered to be laterally
uncoupled by stress terms; it may be anticipated that this will result
in a discontinuity in q_x, the transport component in the x-direction.
The windstress in the region $|y| < w/2$ drives the water onshore and
results in a storm tide field which is a maximum at $(x' \equiv x/\ell = 1.0,$
$y' \equiv y/\ell = 0)$. The q_x field in this region is a maximum at the
shelf break and decreases to zero at the coastline. It is clear, on an
intuitive basis, that the narrower the wind field relative to the
shelf width, the smaller the storm tide will be. For a very
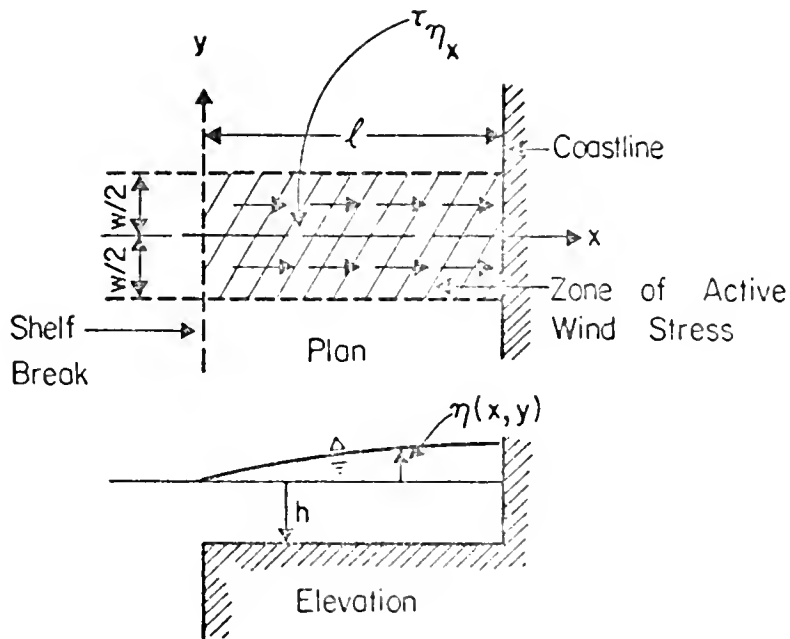
FIGURE 3-9 IDEALIZED SHELF RESPONSE PROBLEM
WITH UNIFORM DEPTH

broad wind field, the storm tide at the shelf should approach the value

corresponding to a one-dimensional condition. For wind fields which

are laterally limited, there will be a gradient in the storm tide

field such that the storm tide approaches zero as $|y'| \to \infty$. The

surface gradient and wind stress fields will cause an onshore transport

in the wind stress region, an offshore transport outside of this

region and a y component of transport (" longshore transport") which

is directed outward from the region of onshore wind stress. Response

in terms of dimensionless n, q_x and q_y are presented in Figures

3-10a, b, c.

If the (artificial) lateral boundaries in the numerical model are

not a sufficient distance from the zone of high wind stress, the

proximity of the model boundaries will influence the calculated storm

tides and velocities. In order to evaluate this proximity effect,

numerical model computations were carried out for the shelf geometry

shown in Figure 3-11. The friction and total water depth terms in

the numerical model were linearized in order that the differences in

quantities calculated by the numerical model and the analytical

solution should be indicative only of artificial effects introduced

by the numerical model. The results of these calculations are de-

scribed in the following paragraphs.

The first set of calculations was carried out for a ratio of

shelf width to one-half the wind field breadth ($\alpha \equiv \ell/(w/2)$) of 1.83

and a grid size, Δx, which is variable. The lateral extent of the

shelf, incorporated into the model is denoted w^* and the ratio of

wind field width to shelf extent, α^* (i.e. $\alpha^* = w/w^*$). The parameter
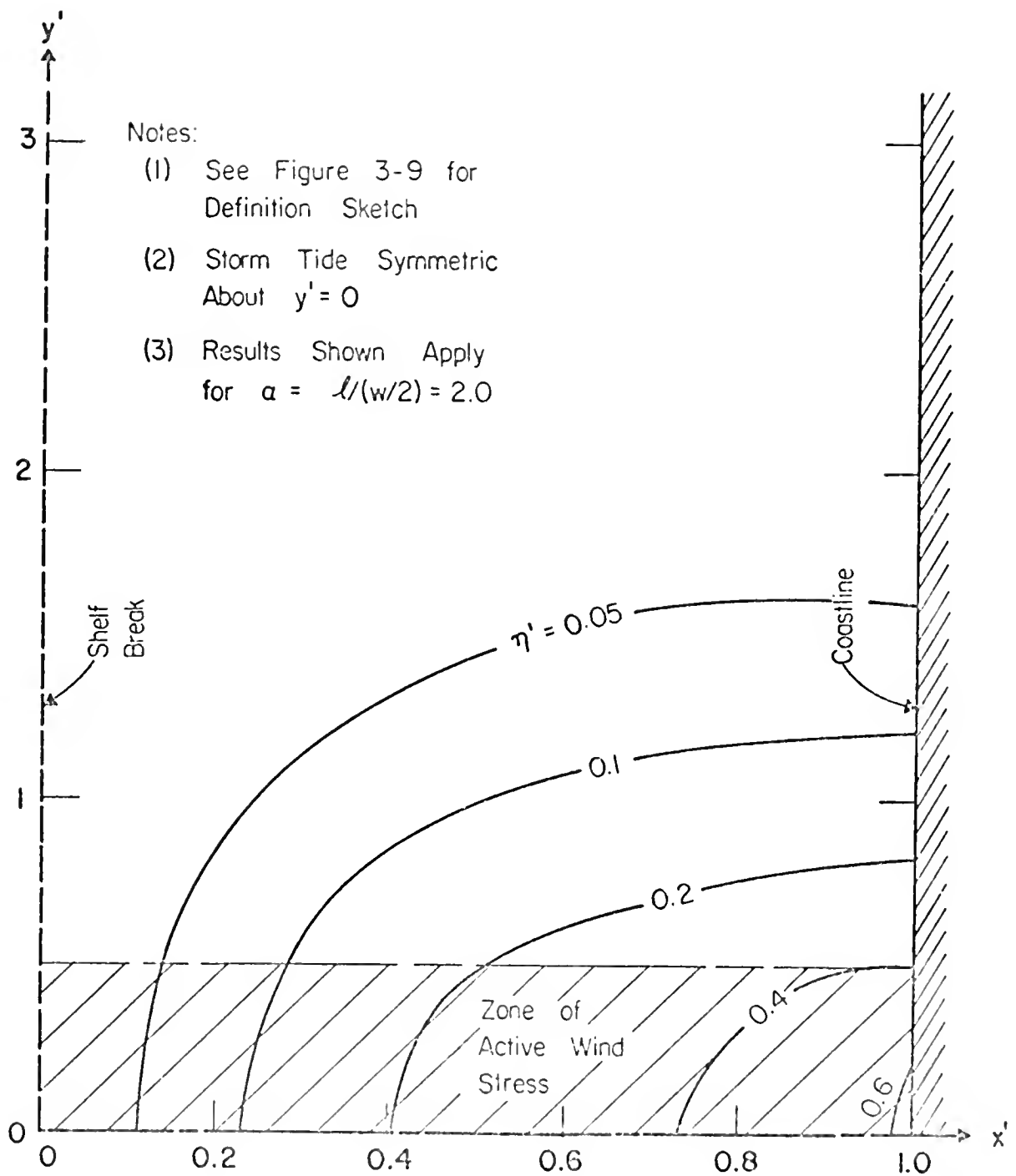
FIGURE 3-10a ISOLINES OF DIMENSIONLESS STORM
TIDE, ANALYTICAL SOLUTION
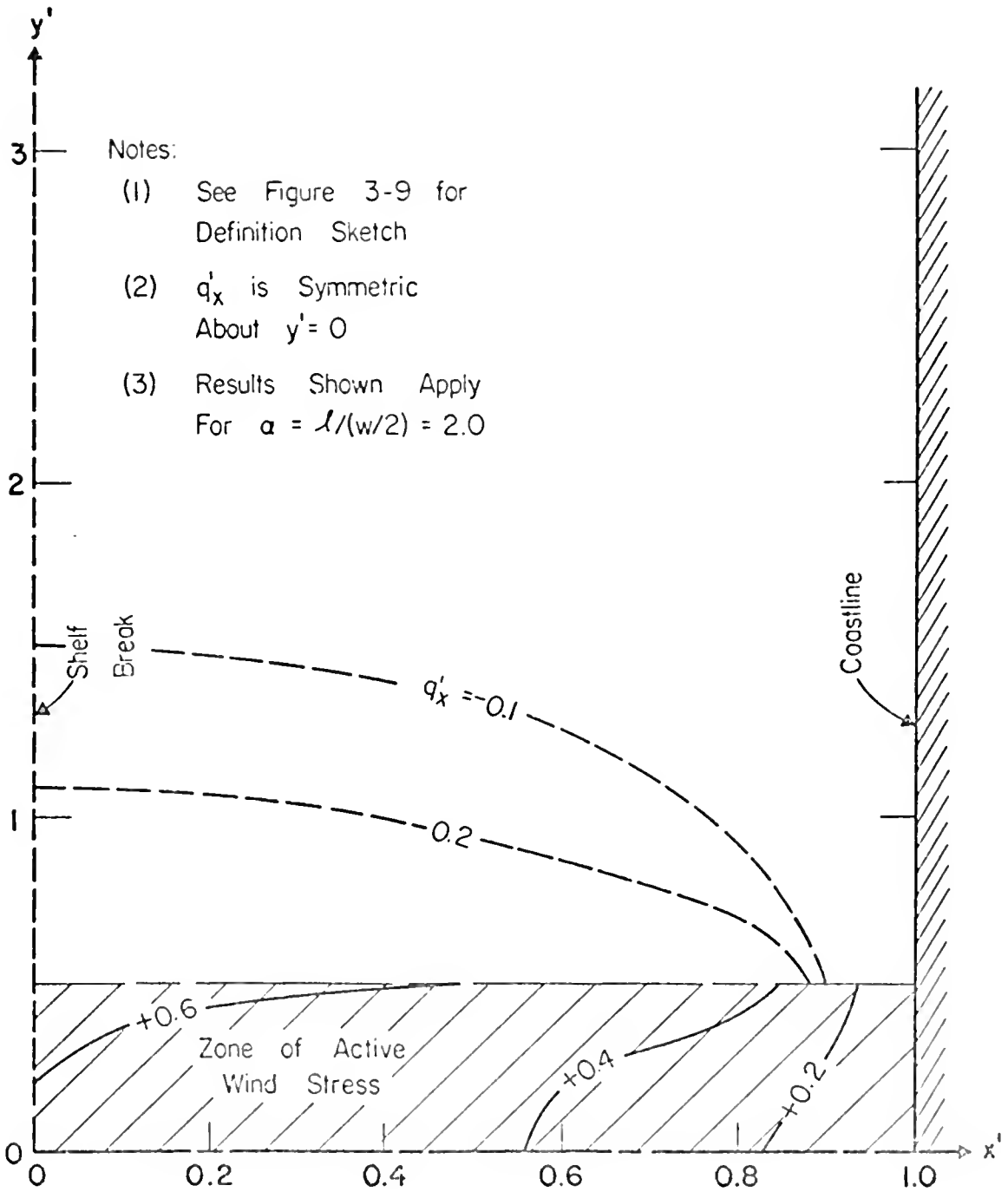
FIGURE 3-10b   ISOLINES   OF   DIMENSIONLESS   TRANSPORT
IN   x—DIRECTION,   ANALYTICAL   SOLUTION
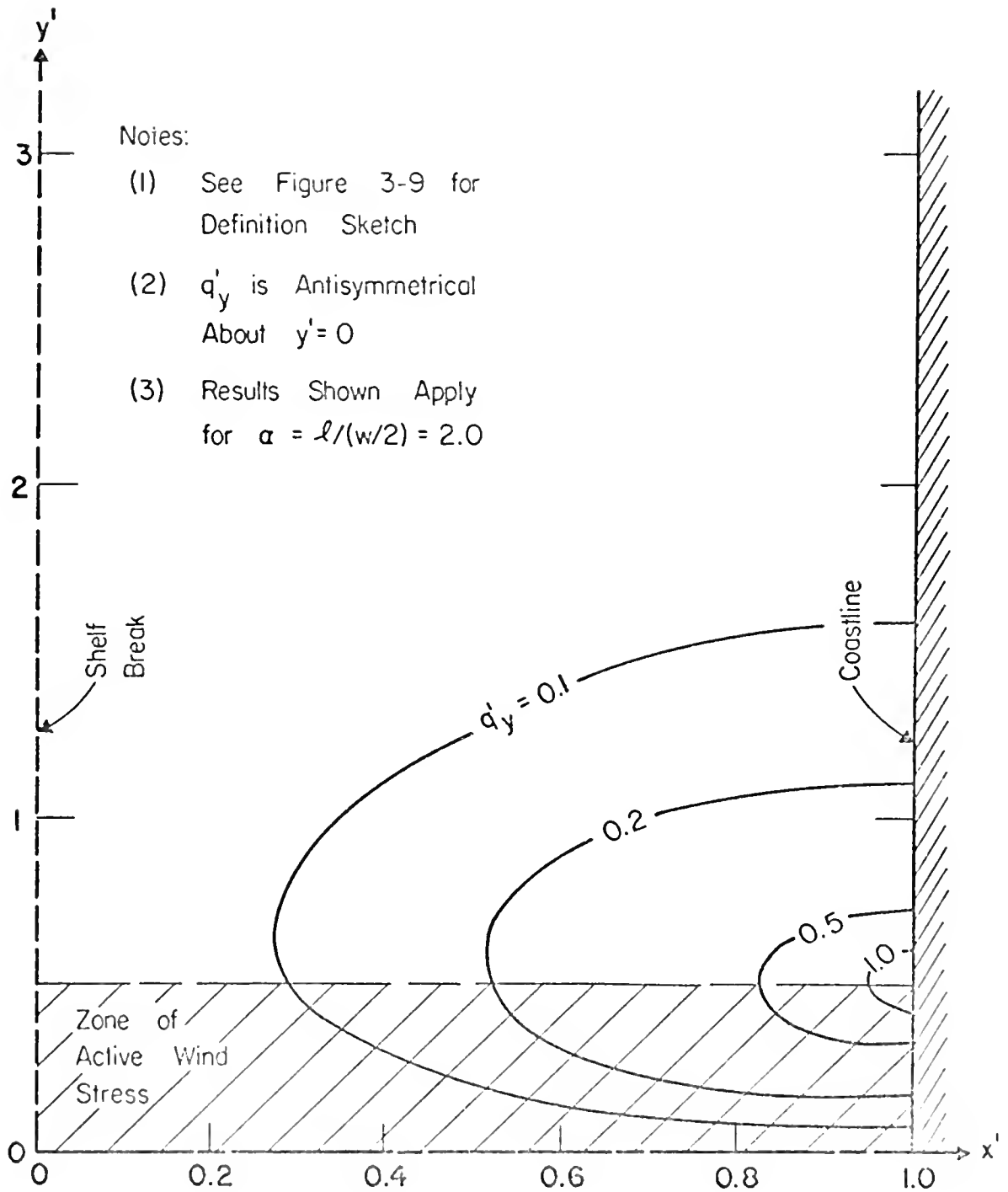
FIGURE 3-10c ISOLINES OF DIMENSIONLESS TRANSPORT IN y—DIRECTION, ANALYTICAL SOLUTION
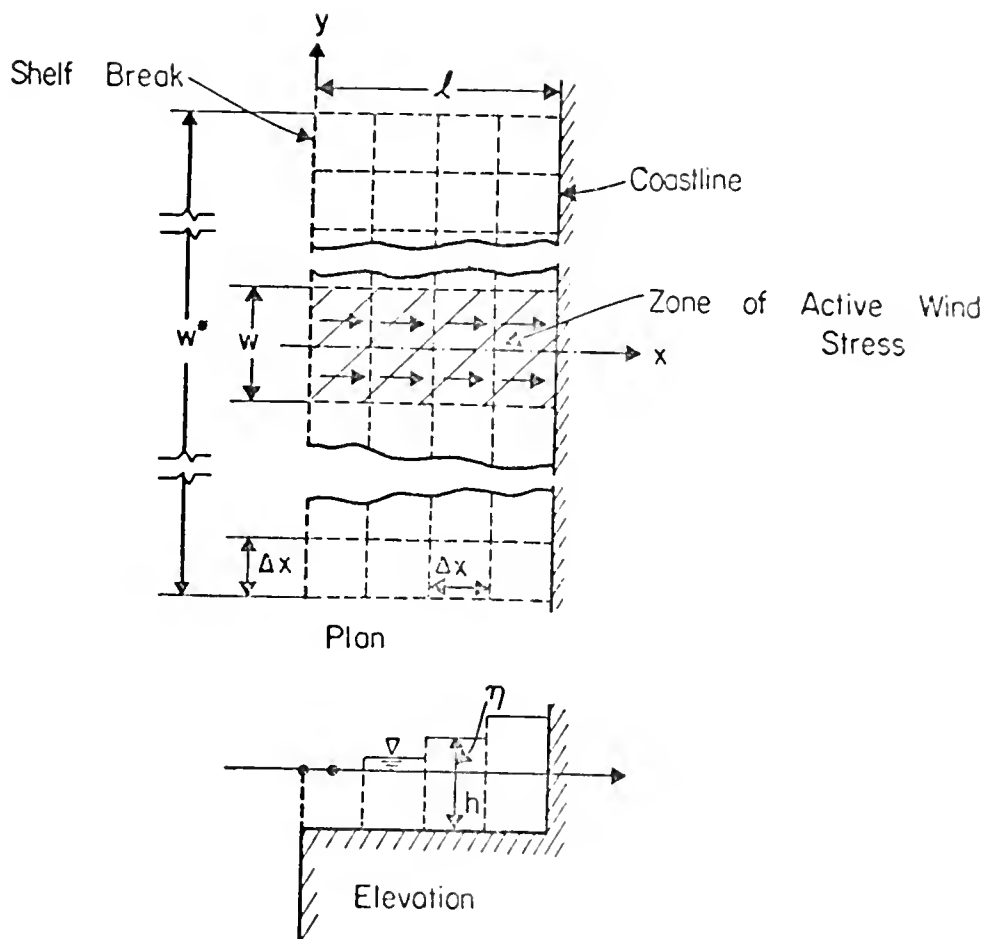
FIGURE 3-11   DEFINITION   SKETCH   FOR   NUMERICAL
MODEL

α^* was varied over the range $0.24 < \alpha^* < 0.73$. The results [30]
are presented in Figure 3-12, where the ordinate represents the
maximum storm tide ratio as determined by the numerical and analytical
solutions. Perfect agreement is indicated by a value of 1.0.
From this figure, if $\alpha^* < 0.5$, the resulting errors in η_{max} will be
less than 10%. As indicated in Figure 3-12, various ratios of
shelf length, ℓ, to grid size were employed, however there does not
appear to be any significant differences in the results for $\ell/\Delta x$
values as low as 3-1/2. It is noted that these calculations were
conducted for $\alpha = 1.83$ and that for a very wide shelf, the parameter
$\alpha^{**} \equiv \ell/w^*$; may also be of importance.
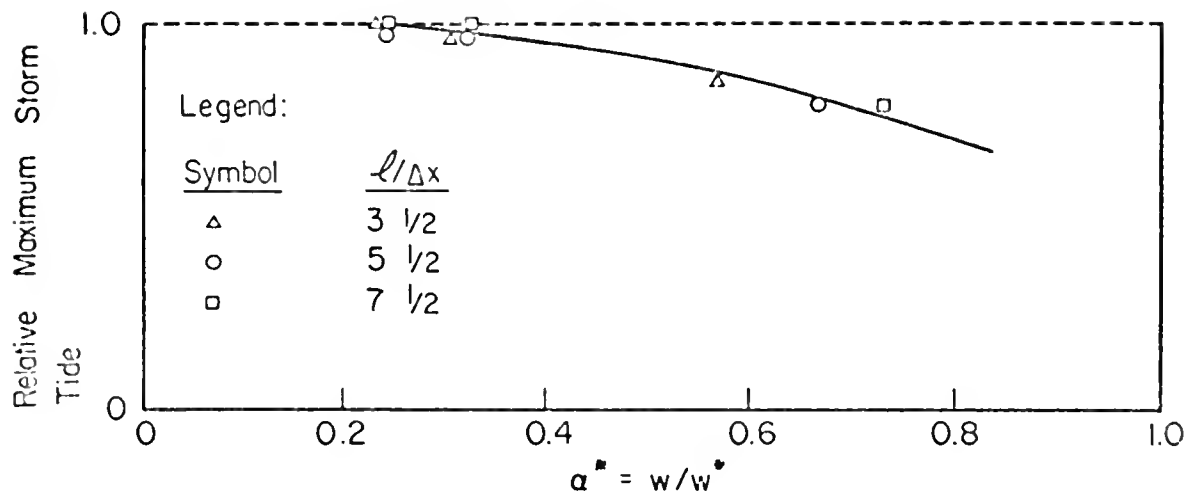
FIGURE 3-12   EFFECT OF LATERAL BOUNDARY
              PROXIMITY AND RELATIVE GRID SIZE
              ON MODEL RESPONSE

CHAPTER 4
RESULTS OF NUMERICAL CALCULATIONS
a. Introduction

The surges and currents produced by Hurricane Camille were chosen for analysis in this study. The severity of the storm and the extensive damage resulting from it crystallized concern about storm surge calculations. The only available open-coast current data taken during a hurricane were by Murray [16,17] during Hurricane Camille. The surge data available for hurricane Camille, consisting primarily of high water marks [31,32] while by no means extensive, are significant when compared to data from other storms. Affected by the storm, is the section of the U. S. Gulf Coast ranging from Barataria Bay, Louisiana to Panama City, Florida. This region is shown in Figure 4-1, where the water depth contours are in fathoms. For the purposes of the numerical calculation the region is divided into a grid element network as in Figure 3-5. Two grid dimensions were used, one with a 16.16 nautical mile grid width, the other 5.99 nautical miles. Square grid elements are used in both cases. The large (16.16 n.m.) grid array is shown in Figure 4-2a superimposed on a map of the region, the grid indexes i, j are given along the right hand side and bottom of the figure, respectively. The depths are shown in Figure 4-2b where dry land is indicated by a minus number and the location of the decimal point represents the center of a grid element. The depth shown indicates an average depth for the grid element and is assumed to be located at the center of the grid element.
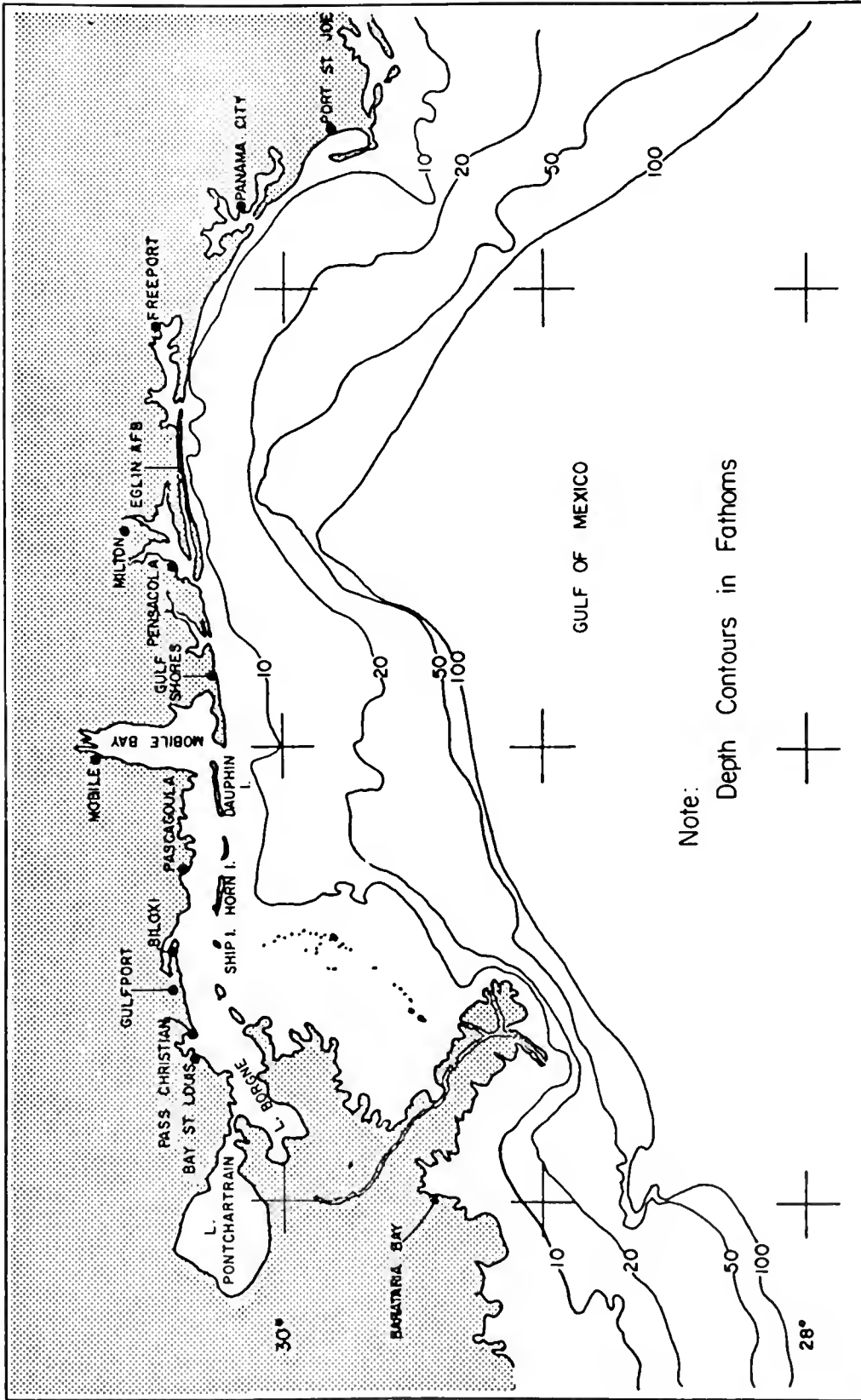
FIGURE 4-1 COASTAL REGION MODELED

FIGURE 4-2a   LARGE GRID MODEL

j \ i	10	9	8	7	6	5	4	3	2	i=1
1	-99.	-99.	-99.	-99.	-99.	30.	60.	100.	180.	240.
2	-99.	-99.	-99.	-99.	-99.	30.	70.	100.	250.	350.
3	-99.	-99.	-99.	40.	90.	90.	120.	200.	400.	600.
4	-99.	-99.	-99.	90.	120.	180.	240.	500.	600.	600.
5	-99.	-99.	60.	120.	180.	300.	600.	600.	600.	600.
6	-99.	-99.	80.	200.	300.	600.	600.	600.	600.	600.
7	-99.	-99.	80.	300.	600.	600.	600.	600.	600.	600.
8	-99.	-99.	60.	200.	600.	600.	600.	600.	600.	600.
9	-99.	-99.	60.	90.	250.	600.	600.	600.	600.	600.
10	-99.	-99.	50.	90.	200.	600.	600.	600.	600.	600.
11	-99.	30.	60.	90.	200.	600.	600.	600.	600.	600.
12	-99.	30.	60.	90.	180.	500.	600.	600.	600.	600.
13	-99.	25.	50.	60.	120.	250.	600.	600.	600.	600.
14	-99.	18.	9.	16.	45.	180.	600.	600.	600.	600.
15	-99.	10.	-10.	14.	25.	-10.	300.	600.	600.	600.
16	-99.	9.	-99.	10.	-99.	35.	240.	600.	600.	600.
17	-99.	-99.	-99.	-99.	24.	90.	180.	600.	600.	600.
18	-99.	-99.	-99.	-99.	-99.	60.	180.	600.	600.	600.
19	-99.	-99.	-99.	-99.	-99.	50.	100.	150.	600.	600.
20	-99.	-99.	-99.	-99.	-99.	50.	60.	180.	600.	600.

x
y

Notes:
(1) Decimal Point Location Represents Center of Grid Element
     Grid Element Width = 16 16 Nautical Miles
(2) Minus Sign Indicates Land
(3) Depths are Feet Below MSL

FIGURE 4-2b   DEPTHS USED IN LARGE GRID MODEL

Figure 4-2c shows the small grid model and Figure 4-2d the depths used in the small grid model. The grid size and arrangements were chosen heuristically to approximate the land mass as closely as possible. The storm is idealized by the storm model discussed in Section 2-c. The storm parameters are assumed constant during the traverse over the shelf. Therefore, a grid network o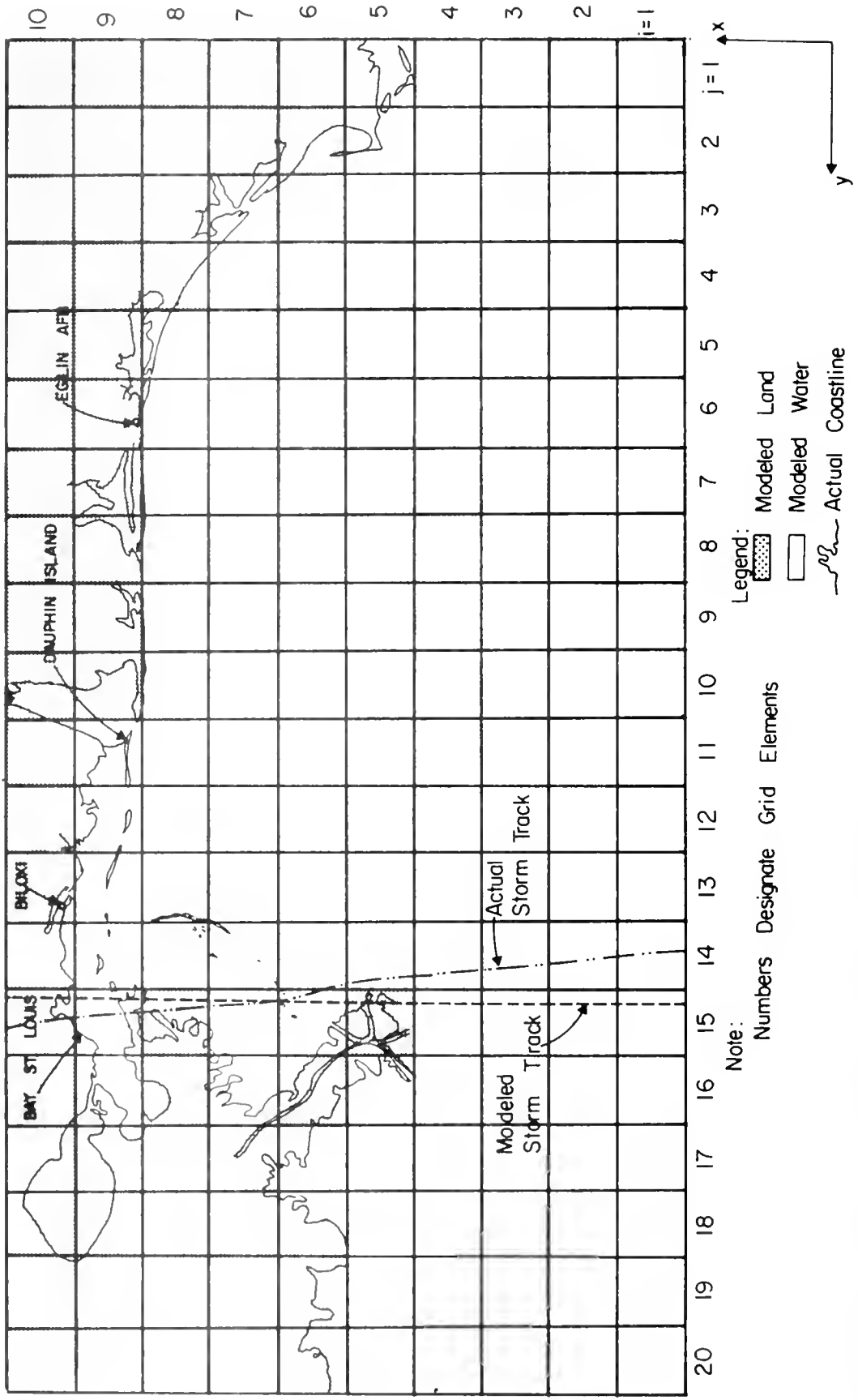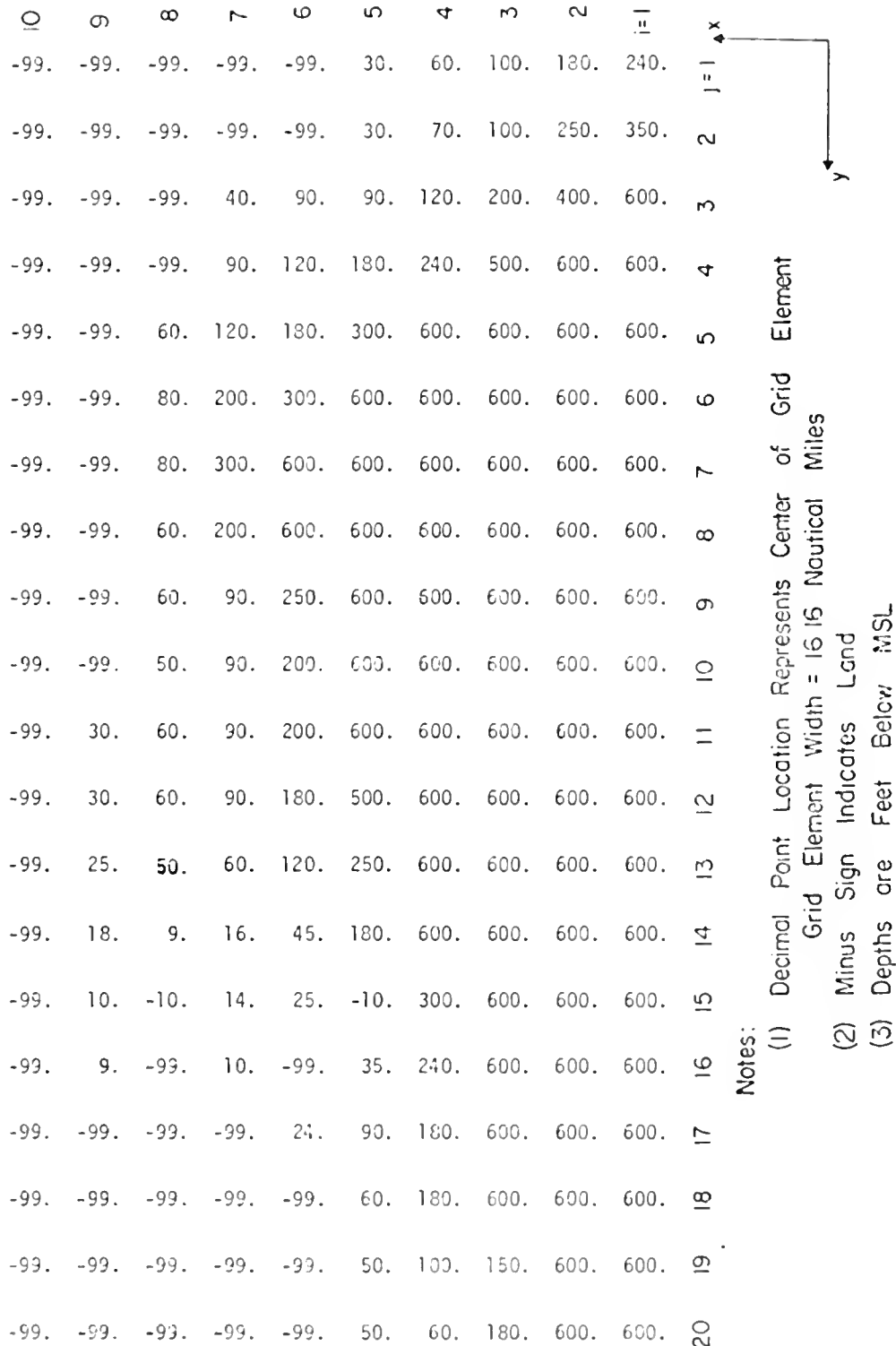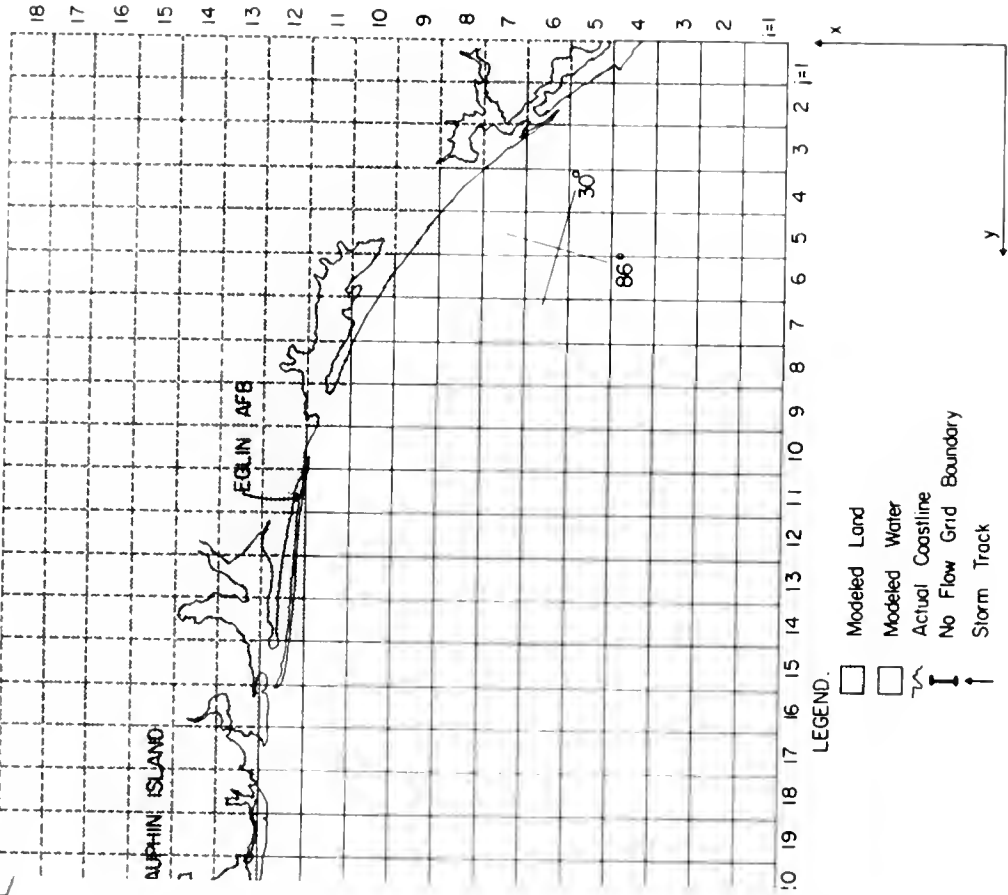f storm parameters is set up and superimposed on the existing grid network. This network of storm parameters is then moved ashore at constant velocity with the values of surface pressure and shear stress interpolated to the centers of the stationary grid elements. Hurricane Camille is assumed to travel at 13 knots and to be in the vicinity of Pass Christian, Mississippi at 1130 hours CDT August 17, 1969. Also, for the purpose of computations it is assumed that the storm motion is parallel to the grid lines crossing the coast. The idealized and actual storm tracks are shown in Figure 4-2a.

LEGEND.

□	Modeled Land
□	Modeled Water
⌒	Actual Coastline
⊥	No Flow Grid Boundary
↓	Storm Track

FIGURE 4-2c SMALL GRID MODEL

NOTE
Numbers Designate Grid Elements

LEGEND

☐ Modeled Land
☐ Modeled Water
〜 Actual Coastline
I No Flow Grid Boundary
↑ Storm Track

NOTES:
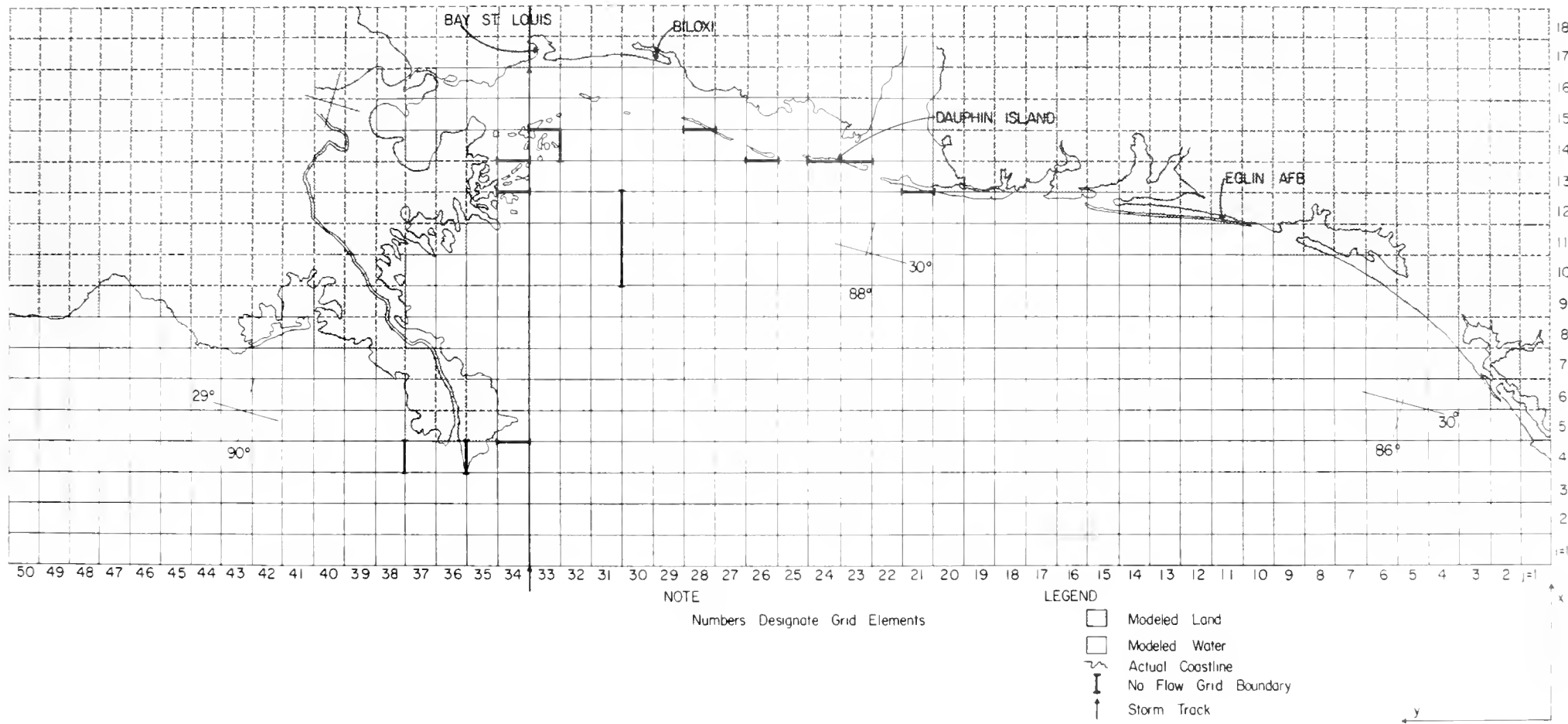(1) Decimal Point Location Represents Center of Grid Element
    Grid Element Width = 5.99 Nautical Miles
(2) Minus Sign Indicates Land
(3) Depths are Feet Below MSL

FIGURE 4-2d   DEPTHS USED IN SMALL GRID MODEL

b.   Numerical Calculations and Comparison
      with Available Data

Figures 4-3a-e depict the calculated surge heights at different times, using the large grid model and storm characteristics for Hurricane Camille. Although Figures 4-3a-e provide output from the model in an interesting form, unfortunately two-dimensional arrays of measured surge height elevation are not available for comparison. In order to gain some idea of the effectiveness of the model, comparisons must be made with measured data. This section will emphasize these comparisons and interpretations to be made from them.

Figure 4-4 depicts the measured maximum surge that occurred along the Gulf Coast during Hurricane Camille. These data are from high water marks [31] and it should be noted that a maximum high water mark of 24.6' was determined at Pass Christian, Mississippi from a "debris line". Superimposed on Figure 4-4 are the numerical calculations using the previously stated assumptions. The values shown represent maximum surges at all locations. A bottom friction coefficient of $f = .005$ was used for the calculations shown in Figure 4-4. It can be seen in Figure 4-5 however, that the calculated surge is not sensitive to f. The model used to obtain Figure 4-5 was an earlier version than the present model, and did not include grid elements (15,9), (16,9), (15,7), (16,7), and (15,6). The sensitivity of the model is, however, clearly illustrated.

In general the locations of calculated surges, centered at the
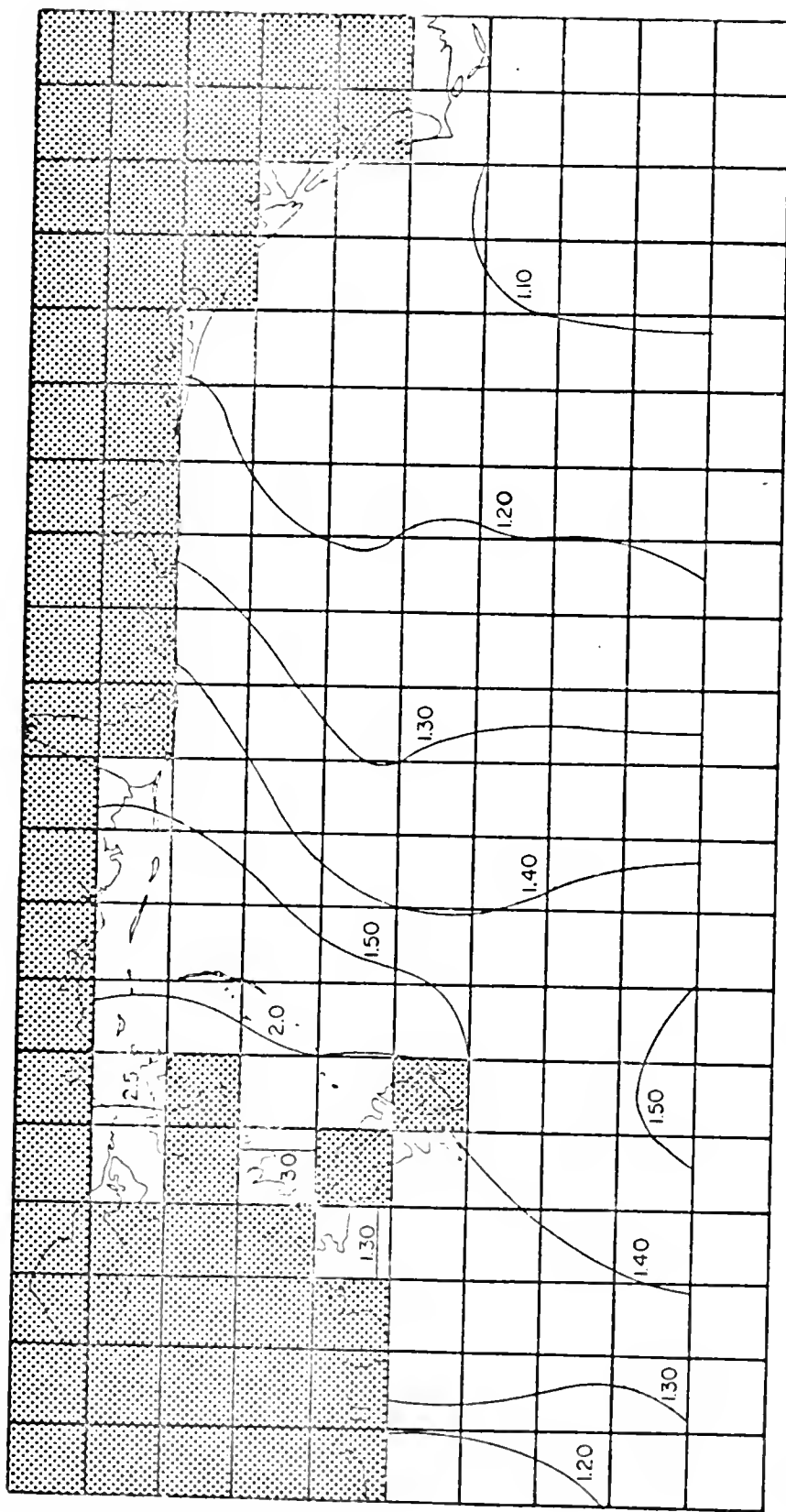
NOTE: 1) 0920 Hours CDT August 17, 1969

2) Superimposed 0.8 Foot Astronomical Tide

3) $f = .005$, $\Delta p = 3.19$ Inches of Mercury, $V = 13$ Knots, $R = 14$ Nautical Miles

4) Surge Elevations in Feet Above MSL

5) Starting Point of Storm Center as Distance From Landfall, $X_s = 300$ Nautical Miles

FIGURE 4-3a   CALCULATED STORM SURGE ELEVATIONS - 8/17/0920
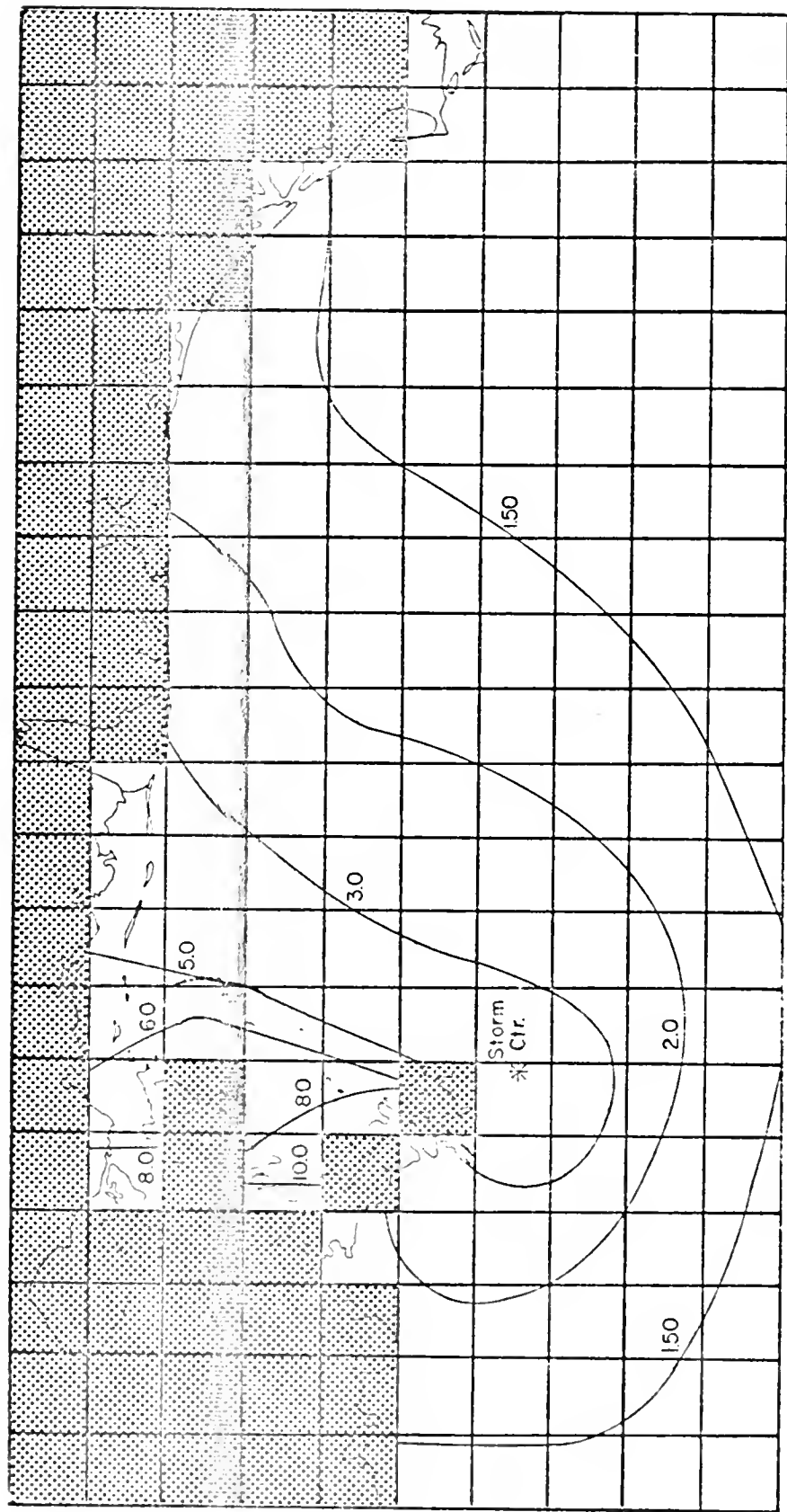
NOTE: 1) 1640 Hours CDT August 17, 1969

2) Superimposed 0.8 Foot Astronomical Tide

3) f = .005, Δp = 3.19 Inches of Mercury, V = 13 Knots, R = 14 Nautical Miles

4) Surge Elevations in Feet Above MSL

5) Starting Point of Storm Center as Distance From Landfall, X_s = 300 Nautical Miles

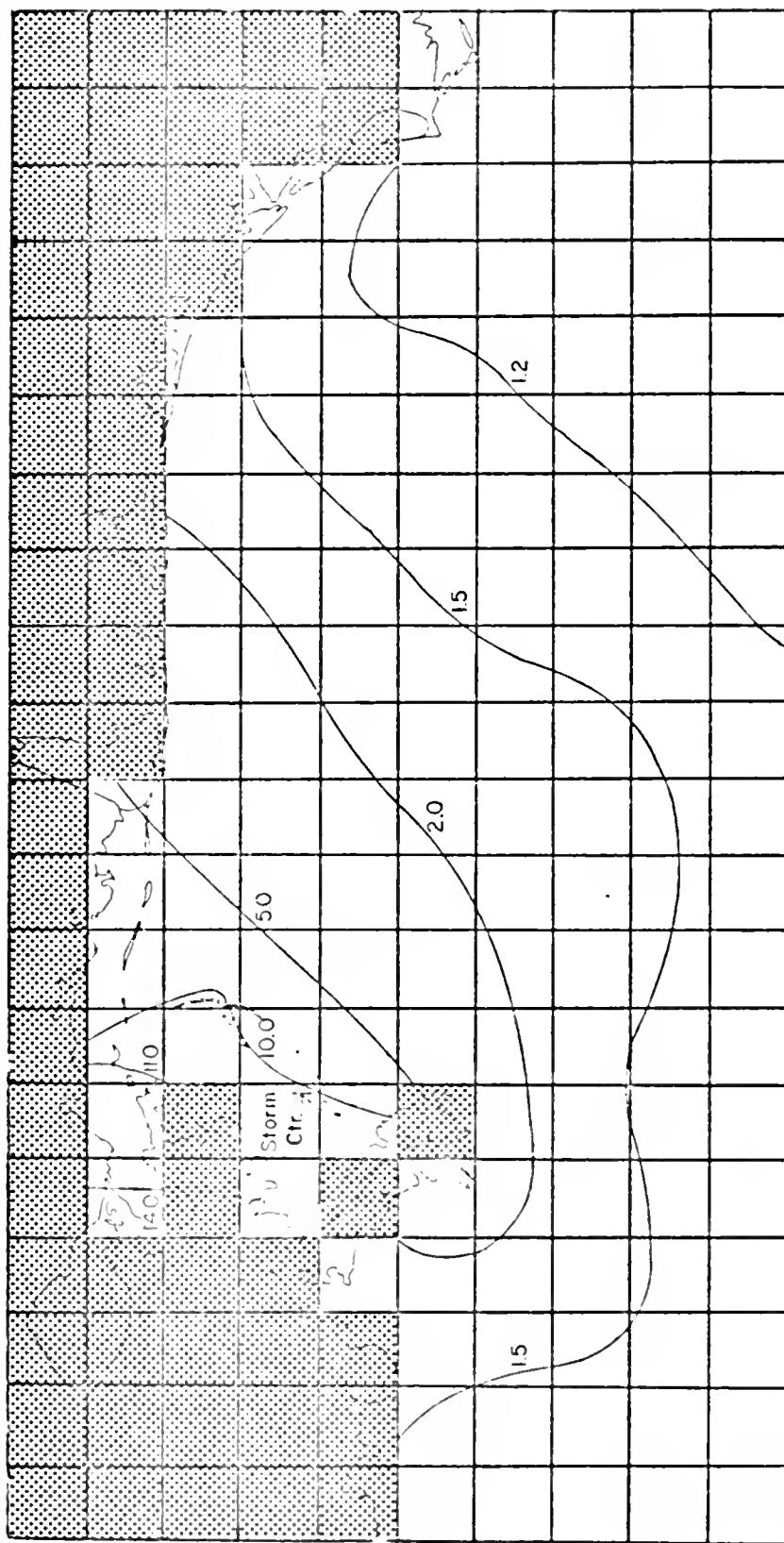FIGURE 4-3b CALCULATED STORM SURGE ELEVATIONS - 8/17/1640

NOTE: 1) 2000 Hours CDT August 17, 1969

2) Superimposed 0.8 Foot Astronomical Tide

3) $f = .005$, $\Delta p = 3.19$ Inches of Mercury, $V = 13$ Knots, $R = 14$ Nautical Miles

4) Surge Elevations in Feet Above MSL

5) Starting Point of Storm Center as Distance From Landfall, $X_s = 300$ Nautical Miles

FIGURE 4-3c   CALCULATED STORM SURGE ELEVATIONS - 8/17/2000
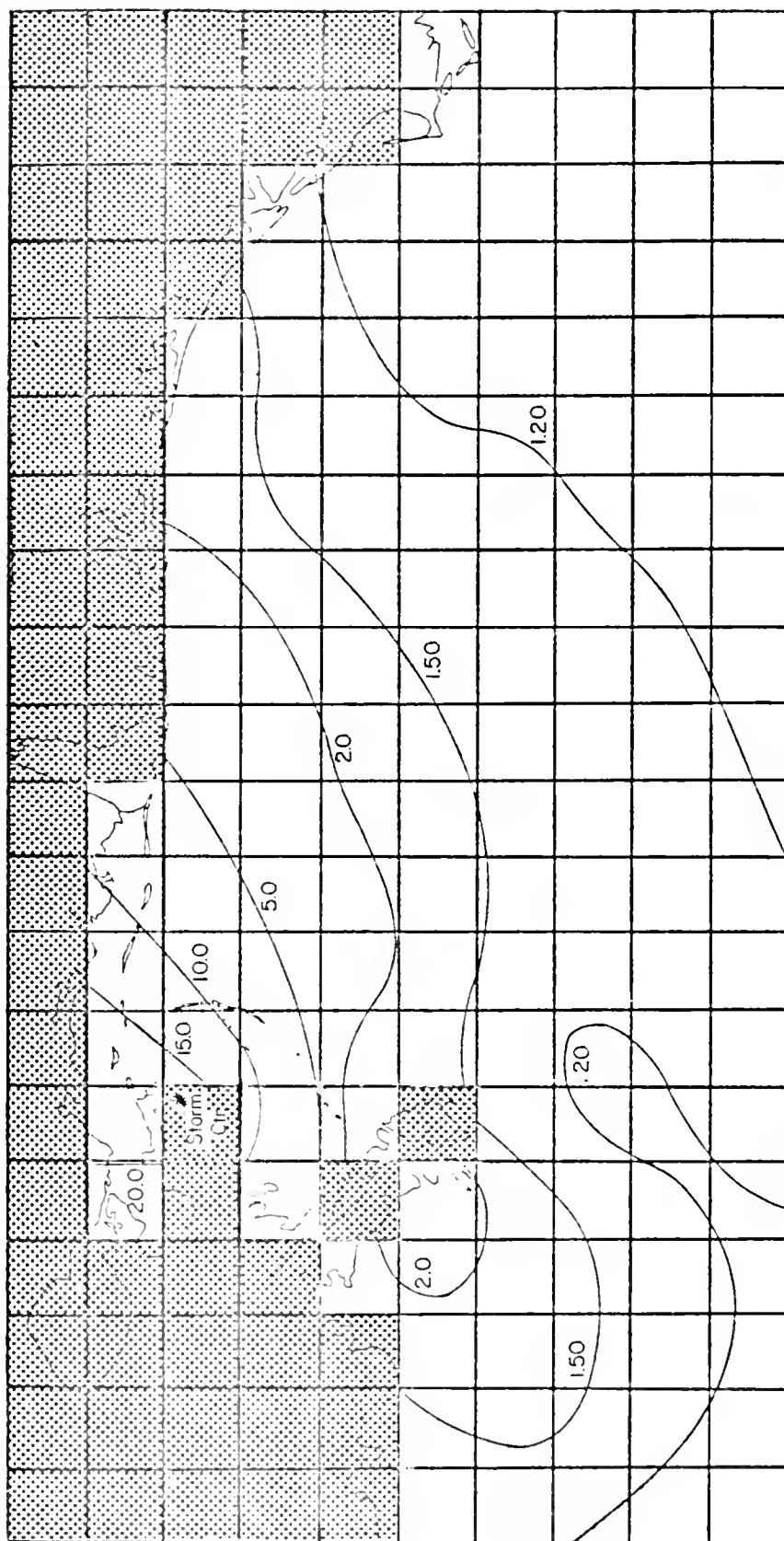
NOTE: 1) 2200 Hours CDT August 17, 1969

2) Superimposed 0.8 Foot Astronomical Tide

3) f = .005, Δp = 3.19 Inches of Mercury, V = 13 Knots, R = 14 Nautical Miles

4) Surge Elevations in Feet Above MSL

5) Starting Point of Storm Center as Distance From Landfall, X_s = 300 Nautical Miles

FIGURE 4-3d CALCULATED STORM SURGE ELEVATIONS - 8/17/2200

NOTE: 1) 2340 Hours CDT August 17, 1969

2) Superimposed 0.8 Foot Astronomical Tide

3) f = .005, Δp = 3.19 Inches of Mercury, V = 13 Knots, R = 14 Nautical Miles

4) Surge Elevations in Feet Above MSL

5) Starting Point of Storm Center as Distance From Landfall, X_s = 300 Nautical Miles

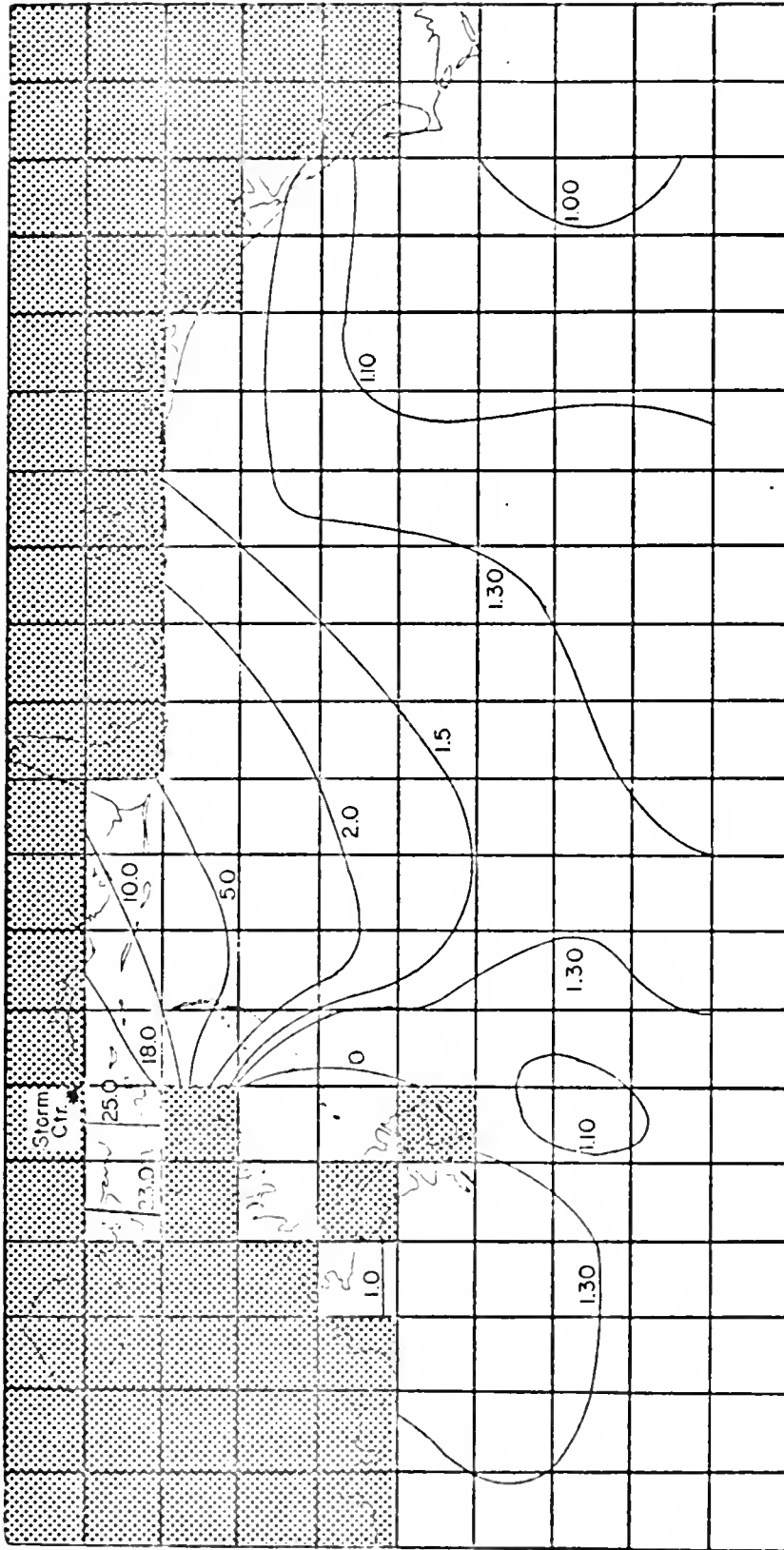FIGURE 4-3e CALCULATED STORM SURGE ELEVATIONS - 8/17/2340
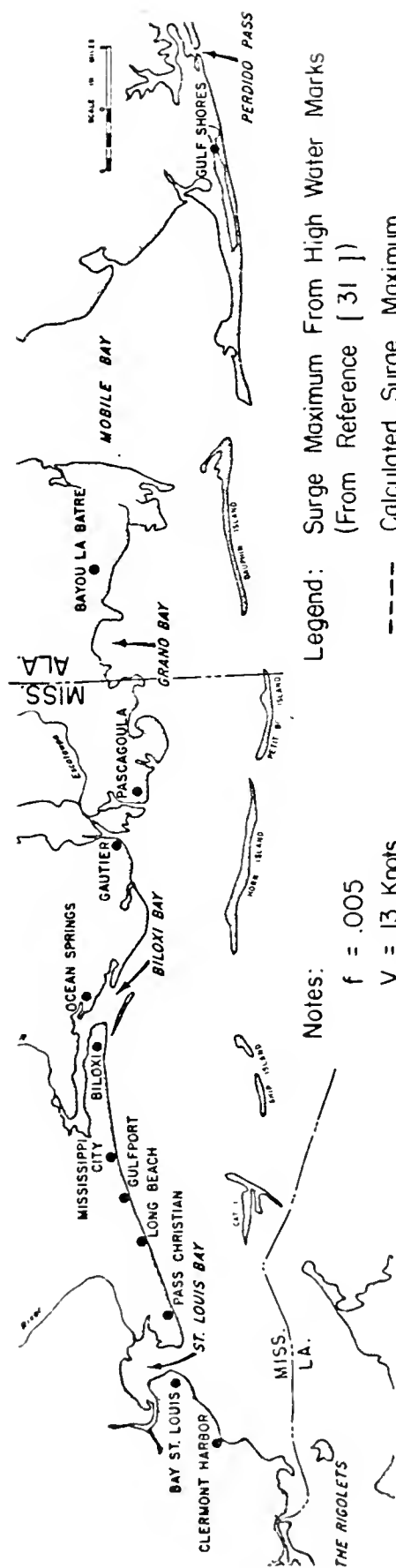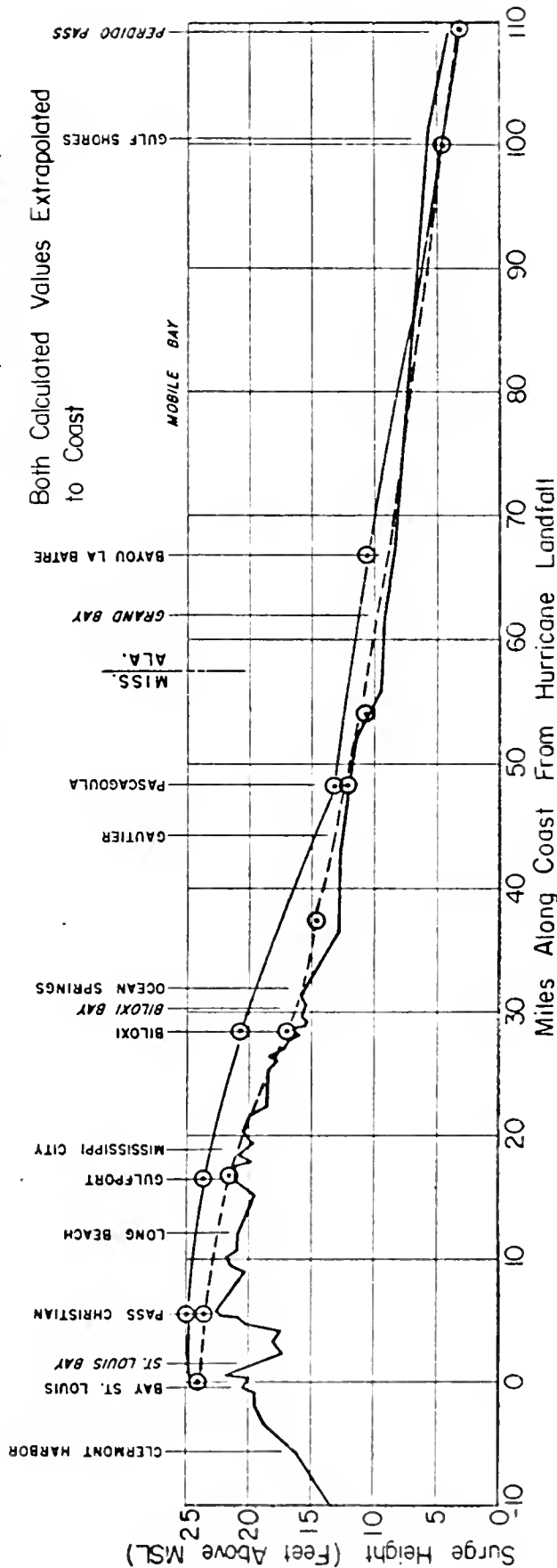
FIGURE 4-4 COMPARISON OF OBSERVED AND CALCULATED SURGE HEIGHT MAXIMA
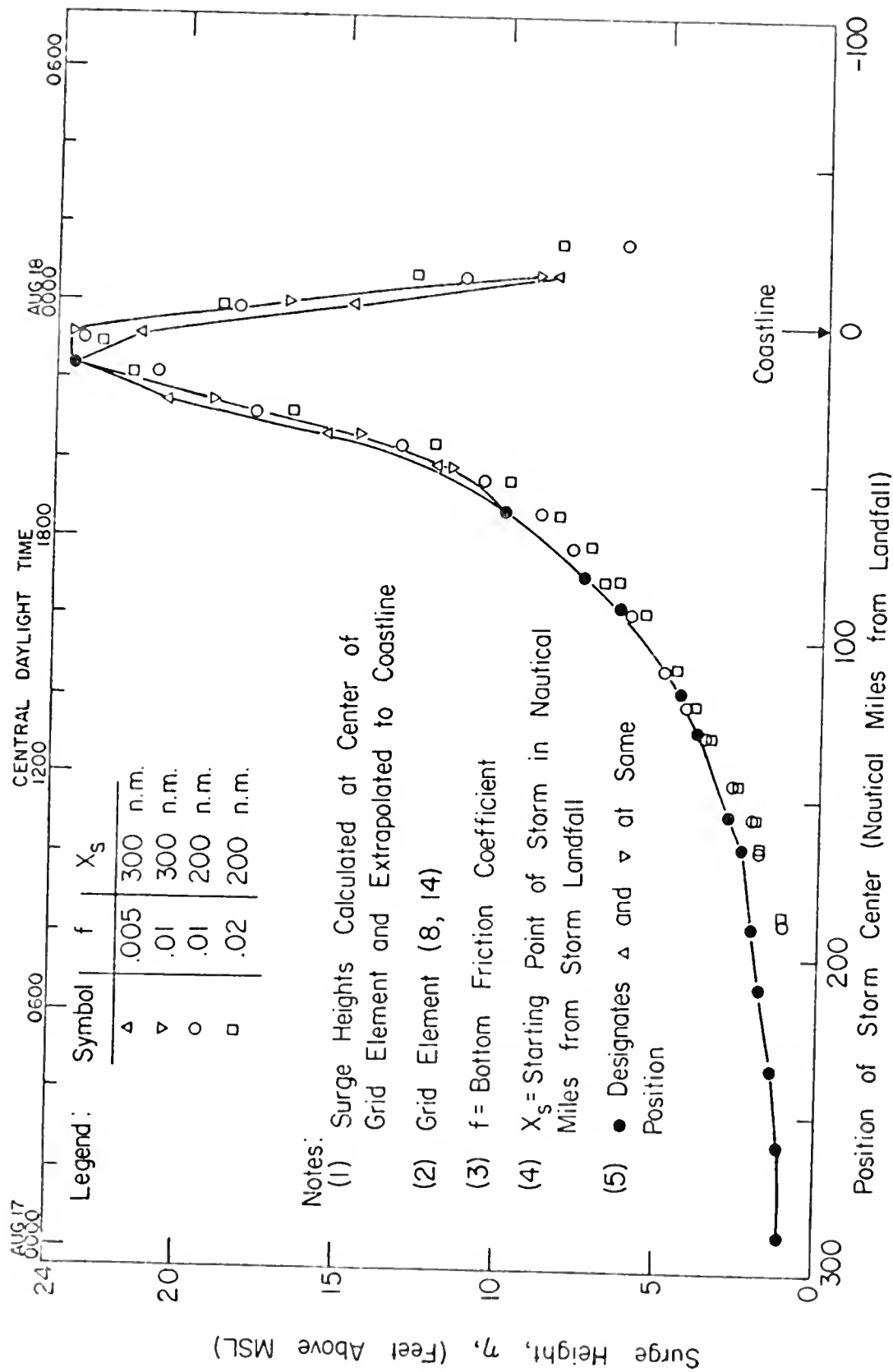
FIGURE 4-5 SENSITIVITY OF SURGE CALCULATIONS TO VARIATIONS IN f AND X_s

grid elements, will not coincide with actual coastline locations or other locations of interest. In order to establish surge elevations at locations other than at those calculated, two techniques were used. To obtain the surge at a location not on the coast, such as an island, a direct correspondence between model and prototype was assumed, as shown in Figures 4-2a and 4-2c. To obtain the surge at the location in question, the values at the surrounding grid centers are used to find a value at the desired point by linear interpolation.

Since the effects of the boundary may be important, a different scheme is used to correlate between points on the model coastline and the prototype coastline. If the grid boundaries and the coastline coincide there is no problem. When the coastline and grid boundary do not exactly coincide then the point on the model coastline nearest the point on the prototype coastline is chosen as the point at which to obtain the surges and currents. This technique, could lead to inconsistencies; however, all calculations for a particular comparison are done in the same manner. In general since the available data are from high water marks it is necessary to extrapolate to the coast as shown in Figure 4-6.

$$\eta_{COAST} = \eta(i+1,\ j) + \frac{\eta(i+1,\ j) - \eta(i,\ j)}{2}$$

FIGURE 4-6   SCHEME USED TO EXTRAPOLATE SURGE HEIGHTS TO COAST

Because the storm surge is not linear with distance, linear extrapo-
lation produces an error. Since the model is discrete with a varying
forcing function, it is unreasonable to extrapolate over many grid ele-
ments; for this reason, and also because of its simplicity, linear extra-
polation is used. Figure 4-7 compares the calculated tidal heights at
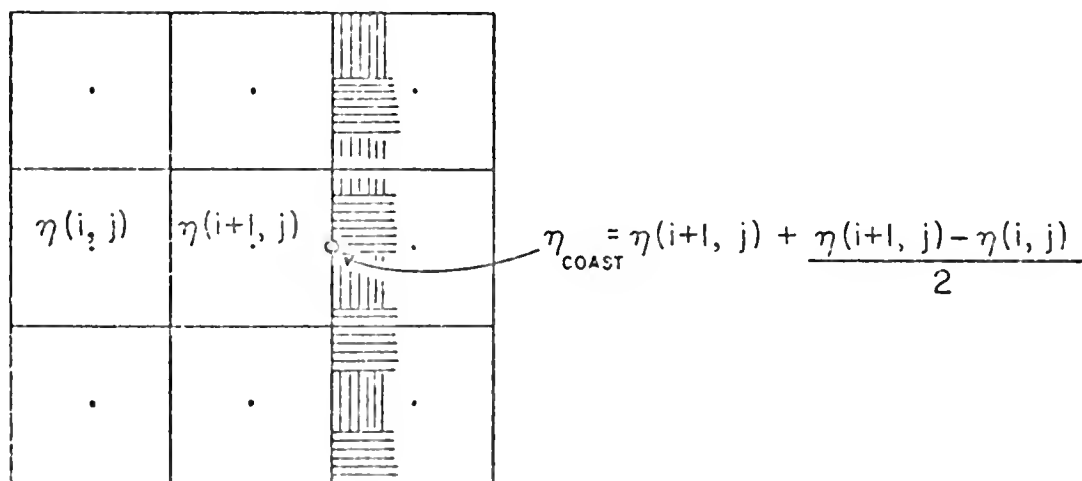the mouth of Biloxi Bay, Mississippi for both the extrapolated and not
extrapolated cases. Grid elements (8, 13) and (9, 13) are used to
extrapolate to the coast.

The grid size of the model is too large to appropriately handle
small bays and estuaries. The barrier islands in the region, such as
Dauphine Island, Alabama, have a characteristic long thin shape which
presents a problem in modeling them. Their area is small compared to a
grid element, making it unreasonable to use whole grid elements for the
island, yet they may provide an effective flow barrier over the width of
one or more grid elements. Bearing in mind that these islands were in
general flooded during the hurricane passage the problem was approached
as follows: For the large grid model the islands were ignored. For the
small grid model the flows at appropriate grid boundaries were constrain-
ed to be zero and for comparison the small grid model was also run with
no flow restrictions. In all of these cases a bottom friction coeffi-
cient of $f = .005$ was used.

Figure 4-8a depicts the measured water level at the Dauphine
Island, Alabama Marine Laboratory [31] compared to the surge calculated
by the large grid model and interpolated to the appropriate location.
There are very little tide data available and the Dauphine Island data
are unique in being close to the open Gulf. Most tide data are taken in
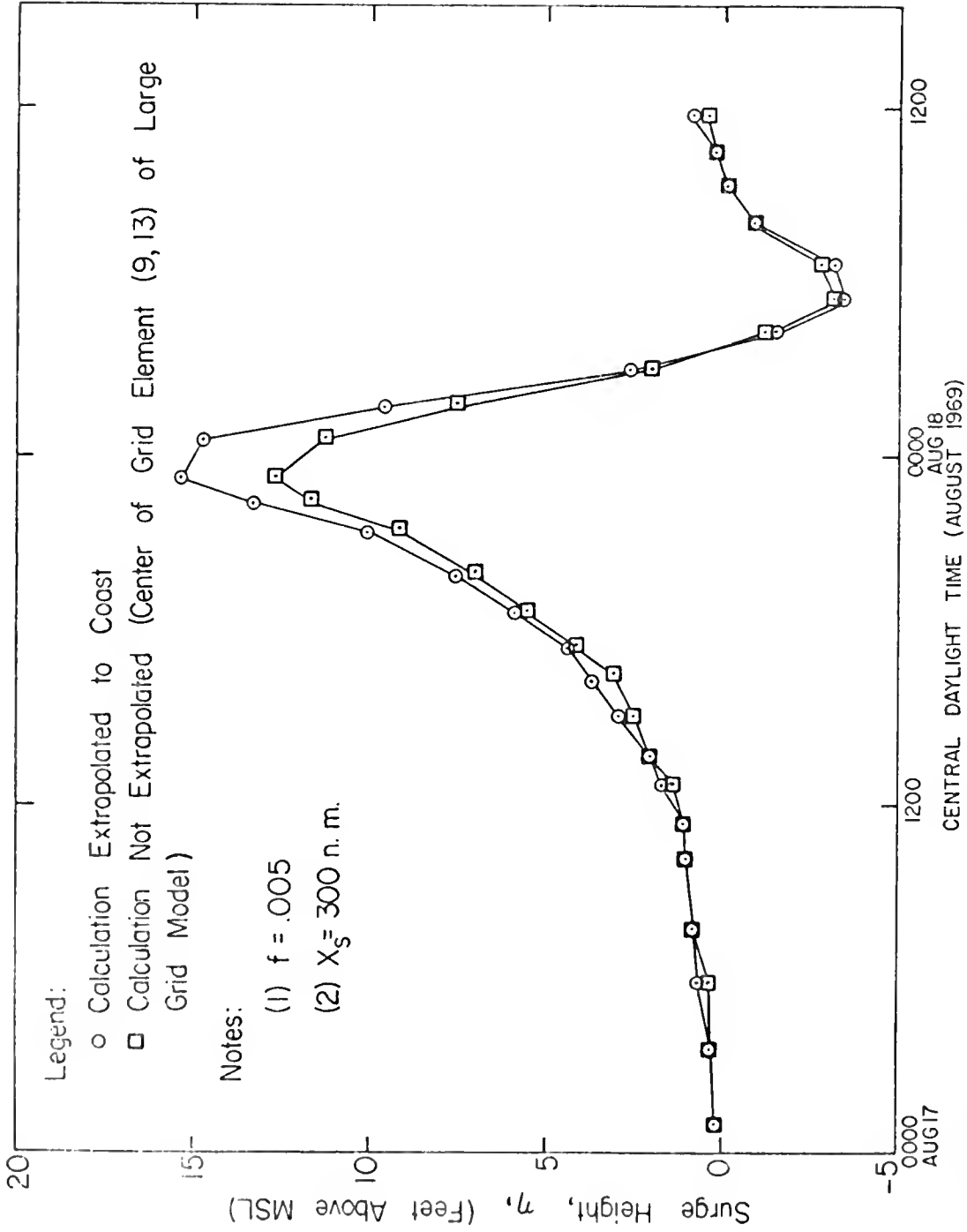rivers and estuaries where the tidal conditions are different from those

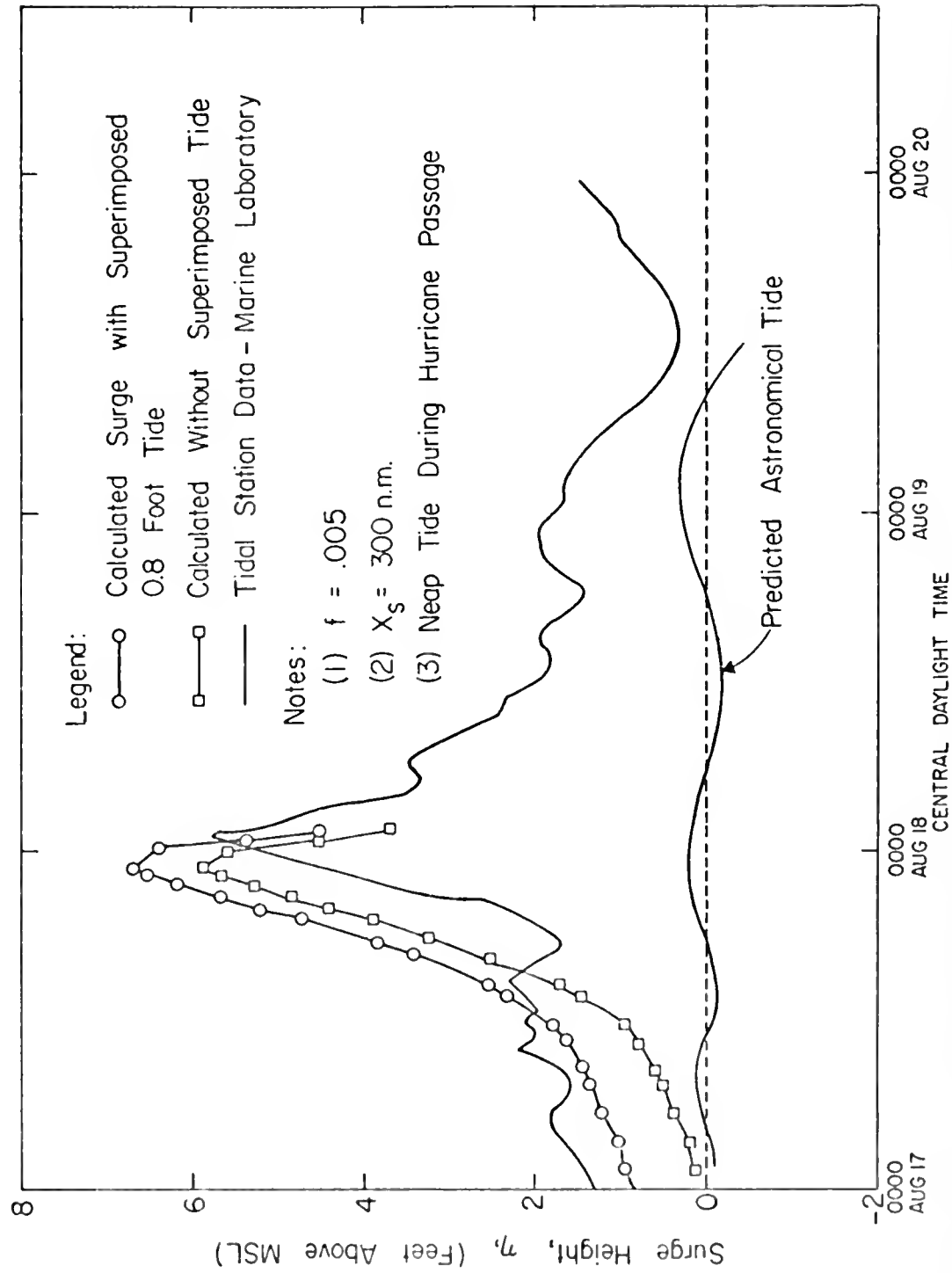FIGURE 4-7 COMPARISON OF EXTRAPOLATED AND NON-EXTRAPOLATED SURGE CALCULATIONS AT BILOXI BAY, MISSISSIPPI

FIGURE 4-8a   COMPARISON OF OBSERVED AND PREDICTED SURGE AT DAUPHIN ISLAND, ALABAMA – LARGE GRID MODEL

in the Gulf of Mexico. Also superimposed on these data is the predicted astronomical tide [33].

Figure 4-8b depicts the measured tide at Dauphin Island compared to results of the small grid model with and without the flow restriction representing the island. Note the difference between the Gulf side and the Mississippi Sound side of the island for the calculations with flow restriction. Note also the increased phase difference. A weighted average of the elements (23,14), (23,13), (22,14), and (22,13) of the small grid model was used to locate the calculations at Dauphine Island. The effect of Mobile Bay which is included in the small grid model may produce the discrepancies noted above. The assumption of constant storm characteristics may also be responsible for the phase difference of measured and predicted surge height.

Average water currents were also calculated. The current measurements by Murray [16,17] are plotted along with direction and wind measurements in Figure 4-9a. Figure 4-9b shows the coastal topography in the immediate vicinity of the current measurements. Notice that the beach is oriented East-West and that at the time of maximum currents the flow direction is offshore. The meter was installed 1.4 meters above the bottom, in 6.3 meters of water and about 360 meters offshore.

Figure 4-10 depicts the observed current magnitude from Reference [16] as compared to four cases of f and X_s for the large grid model and one case for the small grid model. The most important point here is the sensitivity of the model to changes of both bottom friction f and the starting point of the storm X_s, in nautical miles from storm landfall.

Recent longshore current measurements [34] were made approximately fifteen hours after the passage of Hurricane Agnes (1972). These

Legend:

——— Measured Tide Dauphin Island
—□— Grid (14, 23) Bay Side With Flow Restriction
—△— Grid (13, 23) Gulf Side With Flow Restriction
—○— Interpolated Without Flow Restriction

Notes:

(1) Numerical Results for Small Grid Model
  (a) f = .005
  (b) x_s = 300 n.m.

(2) Tide Gage Installed on Bay Side of Island

Surge Height, η, (Feet Above MSL)

CENTRAL DAYLIGHT TIME

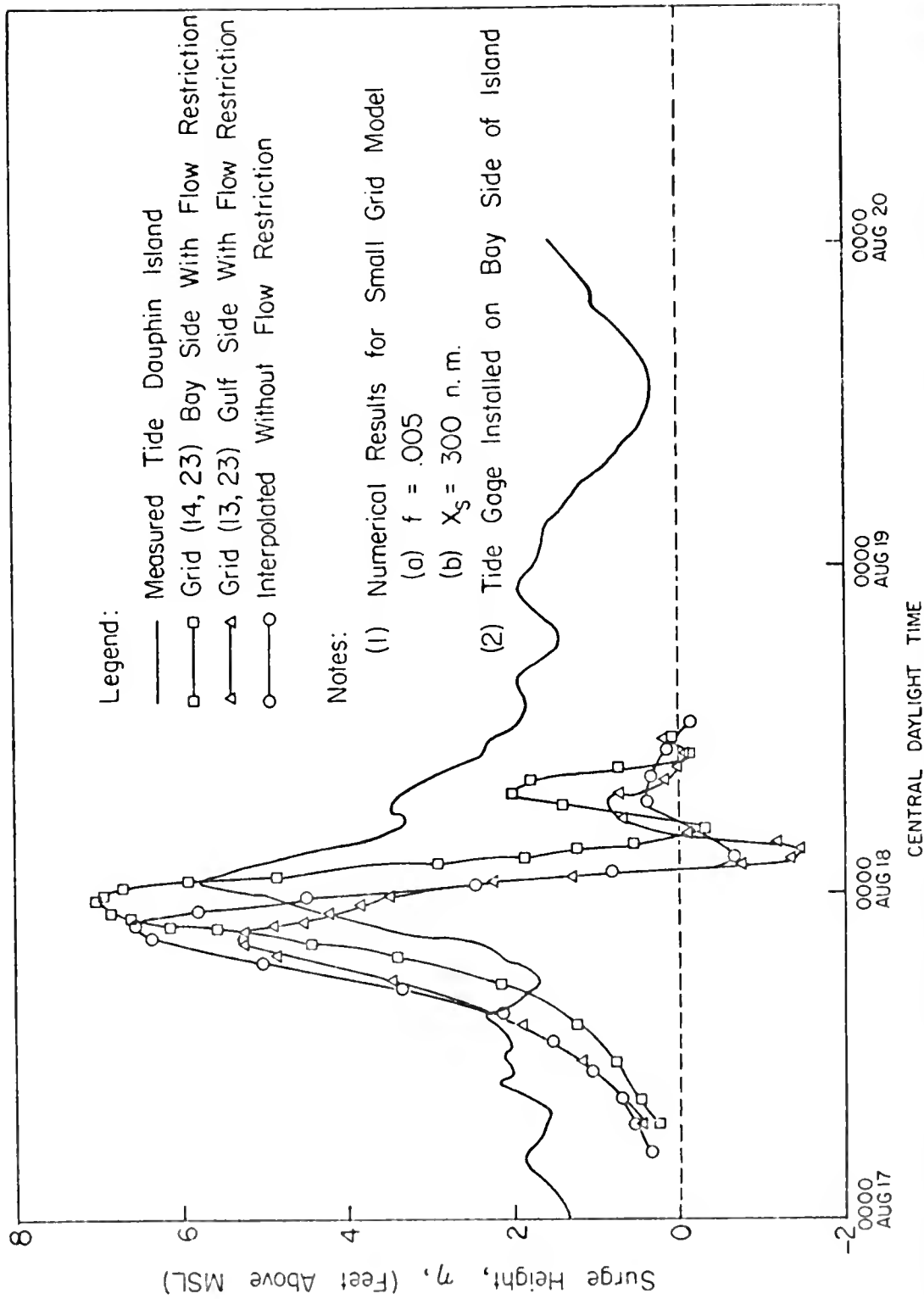0000 AUG 17 0000 AUG 18 0000 AUG 19 0000 AUG 20

FIGURE 4-8b COMPARISON OF OBSERVED AND PREDICTED SURGE AT DAUPHIN ISLAND, ALABAMA — SMALL GRID MODEL
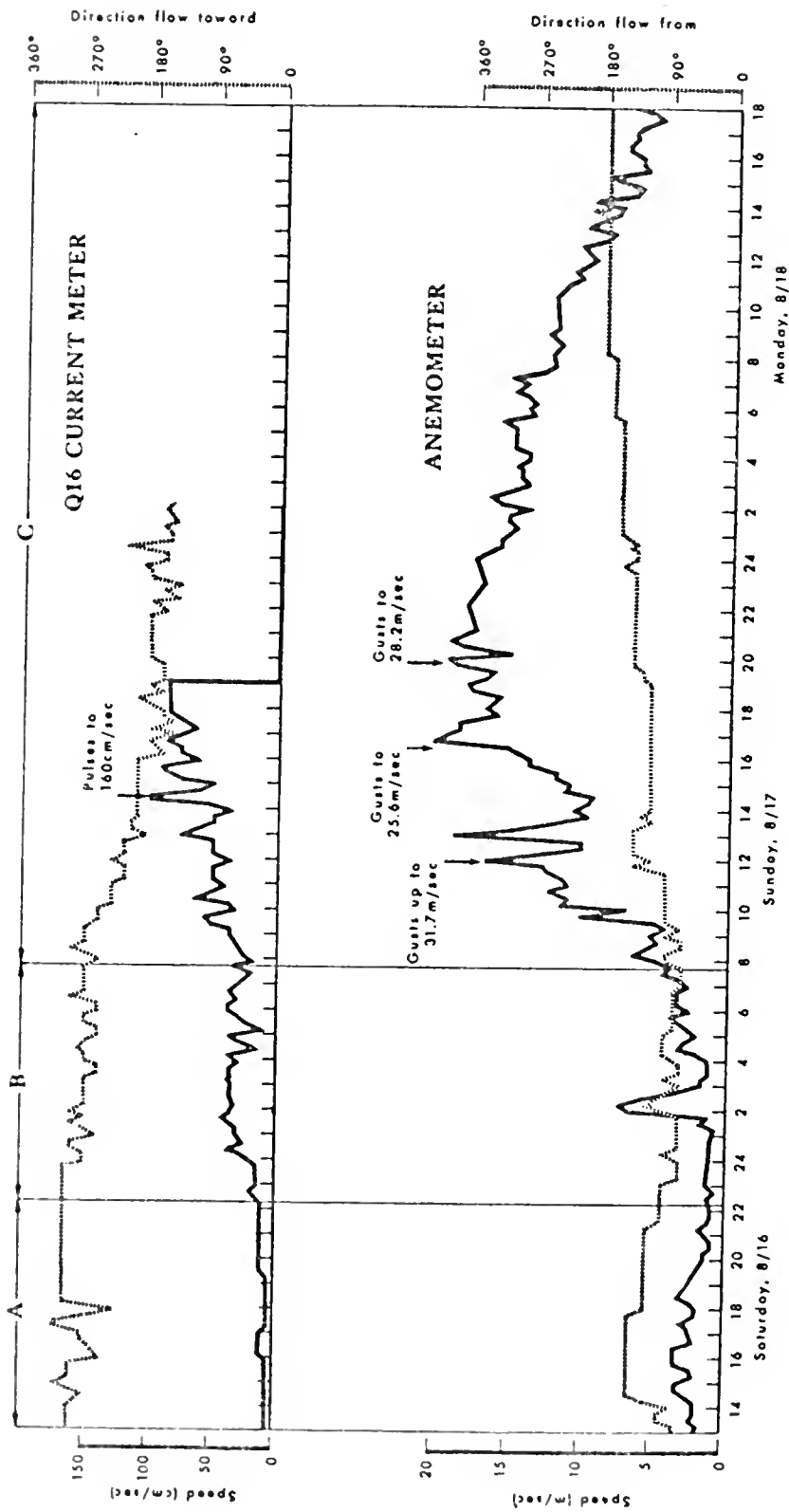
FIGURE 4-9a WATER AND WIND VELOCITY RECORDS FOR HURRICANE CAMILLE AT EGLIN AFB, FLORIDA (FROM REFERENCE [16])
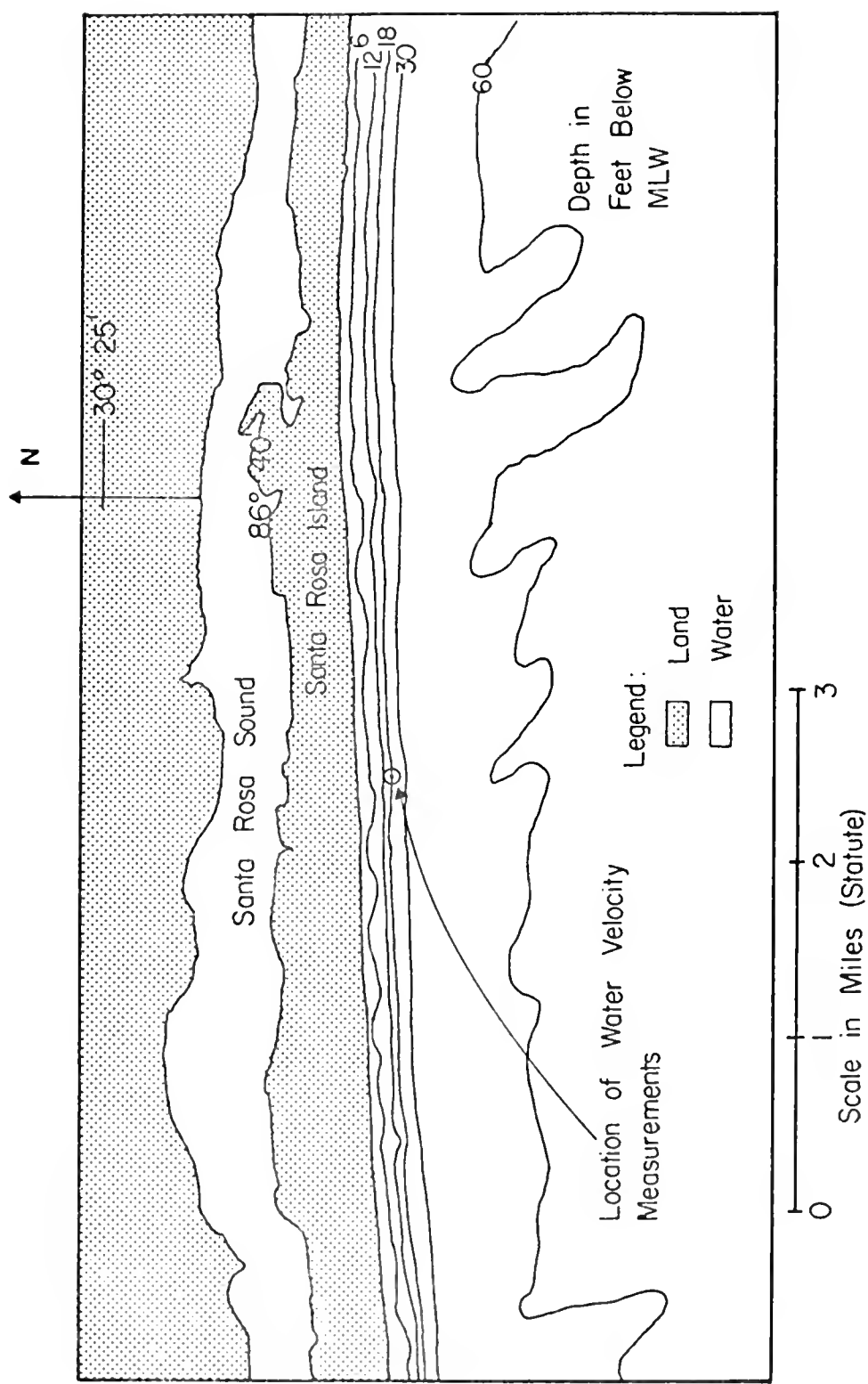
FIGURE 4-9b   COASTAL TOPOGRAPHY AT SITE OF WATER VELOCITY MEASUREMENTS
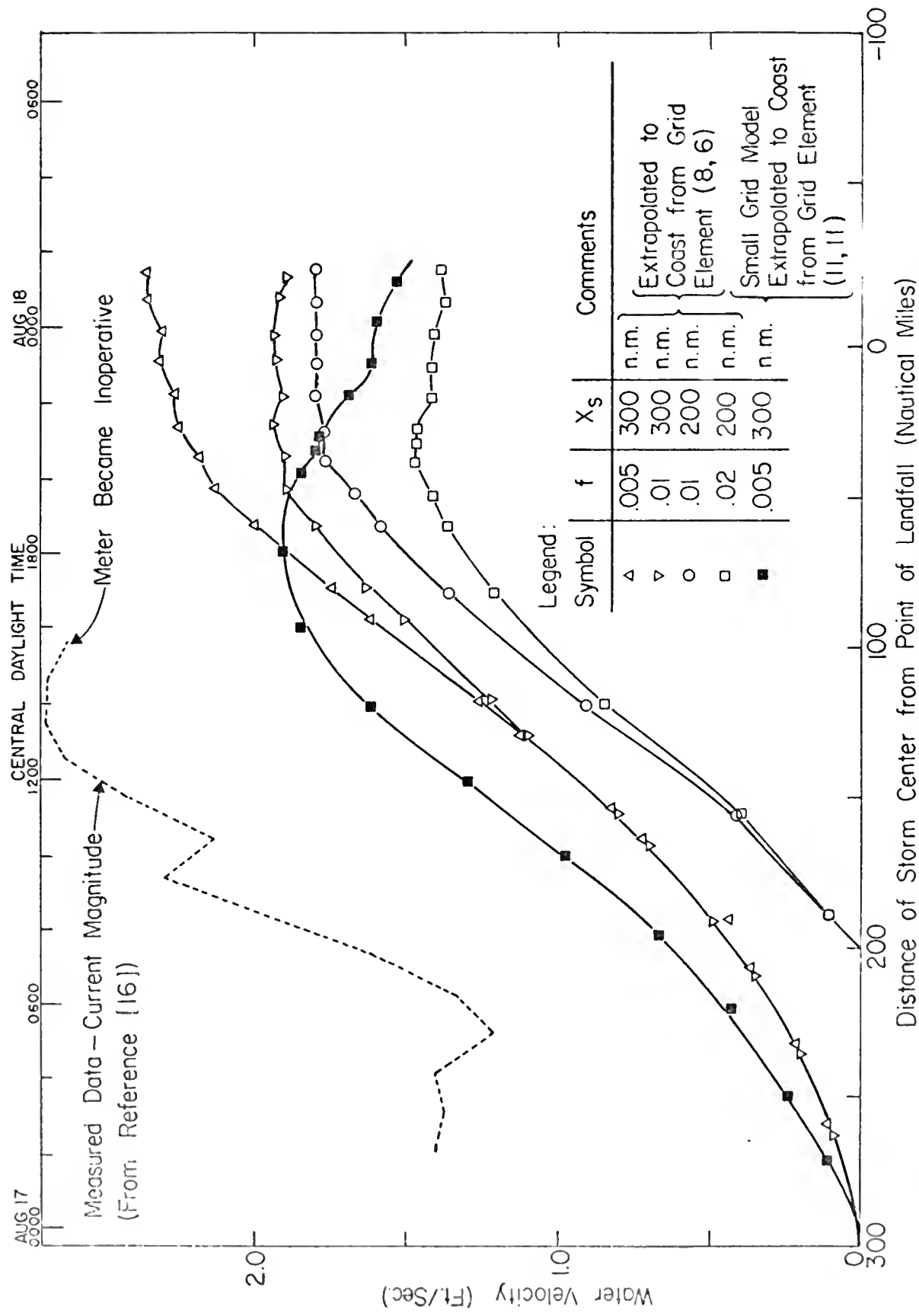
FIGURE 4-10 COMPARISON OF CALCULATED AND MEASURED WATER VELOCITIES

results, presented in Figure 4-11, show that longshore currents of 2-3 ft/sec. are entirely reasonable. The beach slope of m = .02 is the same as for the condition at Eglin AFB and the wave period of 8 sec. slightly less than the 10 sec. maximum observed by Sonu [35]. Of interest is the magnitude of the calculated winds for Camille and a comparison with measured data in Figure 4-12.

In examining Murray's data, one is tempted to postulate the existence or even predominance of longshore currents, however it is not reasonable to explain the current normal to shore as a longshore current. The numerical model predicts essentially zero normal current that close to shore since the normal flux through the boundary is constrained to zero. Since the wind direction is approximately south preceding the offshore current a quasi-steady-state circulation cell with onshore flow at the surface and offshore flow at the bottom could explain the observed phenomena. The important point is that the assumptions made in the present numerical model preclude the representation of a flow variation over depth. An obvious conclusion is that more extensive data are needed to better explain the processes involved in nearshore circulation.

Damage to low-lying coastal areas is caused primarily by flooding and the ensuing wave action and beach erosion. To a "user" of a storm surge prediction scheme, frequently the only result of importance is whether or not a particular area will be flooded. For the case of a storm approaching the coast, the latest available storm parameters would be used in predicting flooding to warn local residents. Design of various coastal structures relies on surge and flooding calculated for a statistically appropriate storm, frequently the Standard Project Hurricane, SPH. A detailed study of flooding is not within the scope of this project.
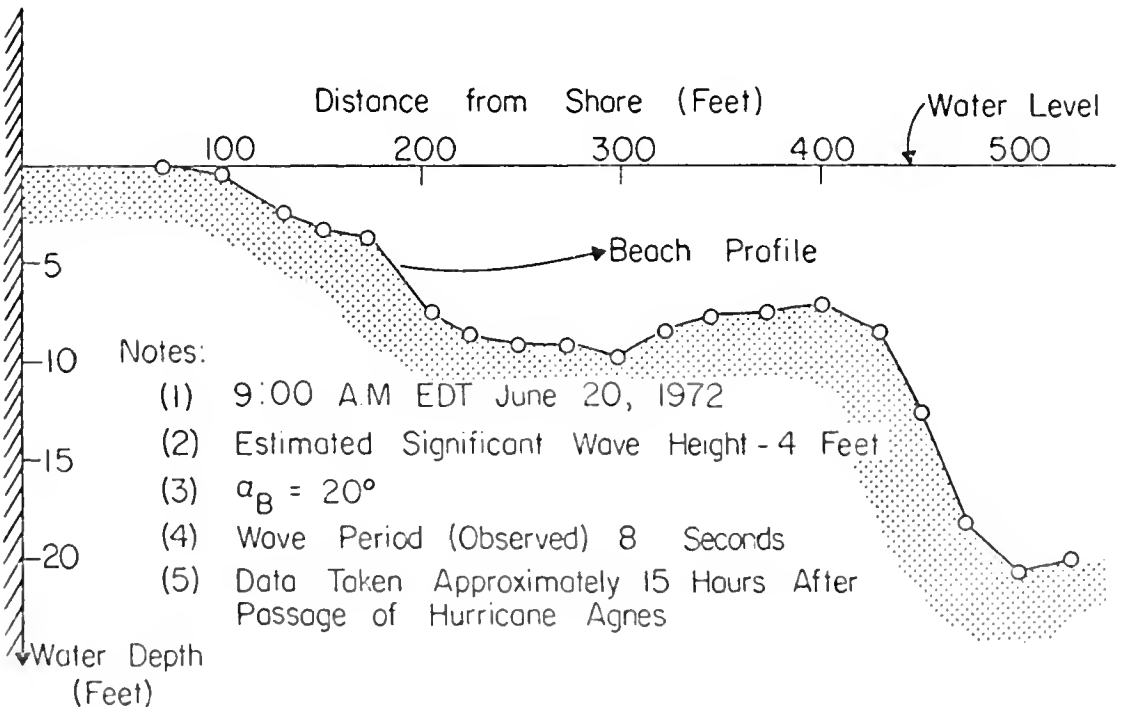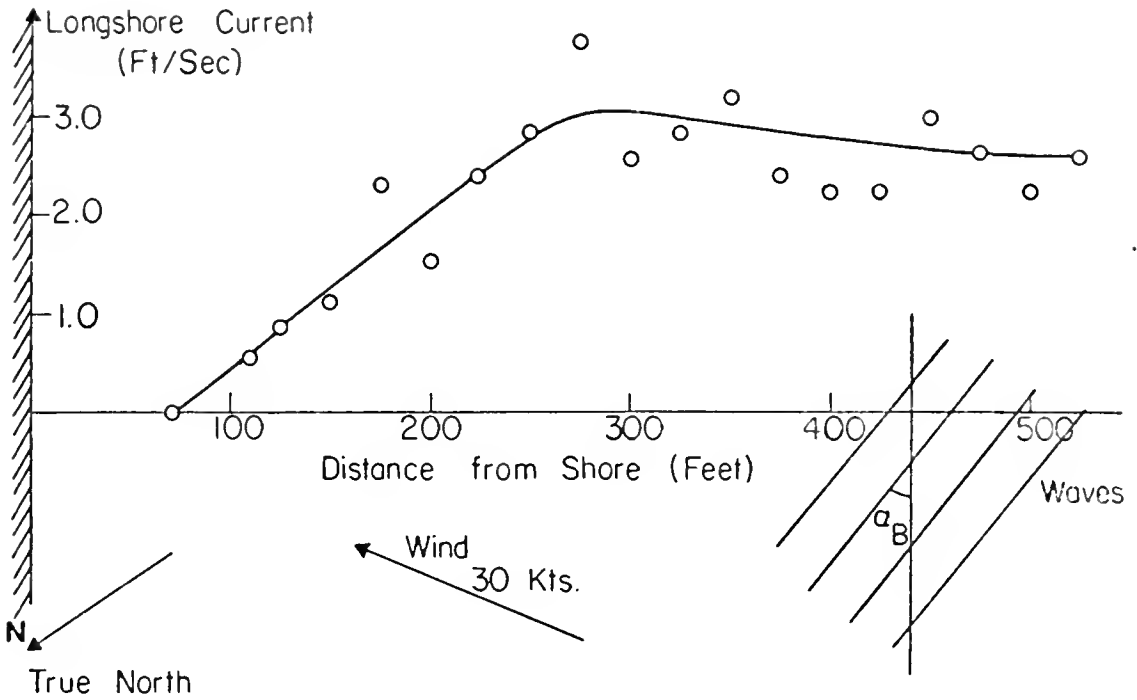
FIGURE 4-11 LONGSHORE CURRENT AND BEACH PROFILE
MEASURED AT MUNICIPAL PIER, PANAMA
CITY, FLORIDA
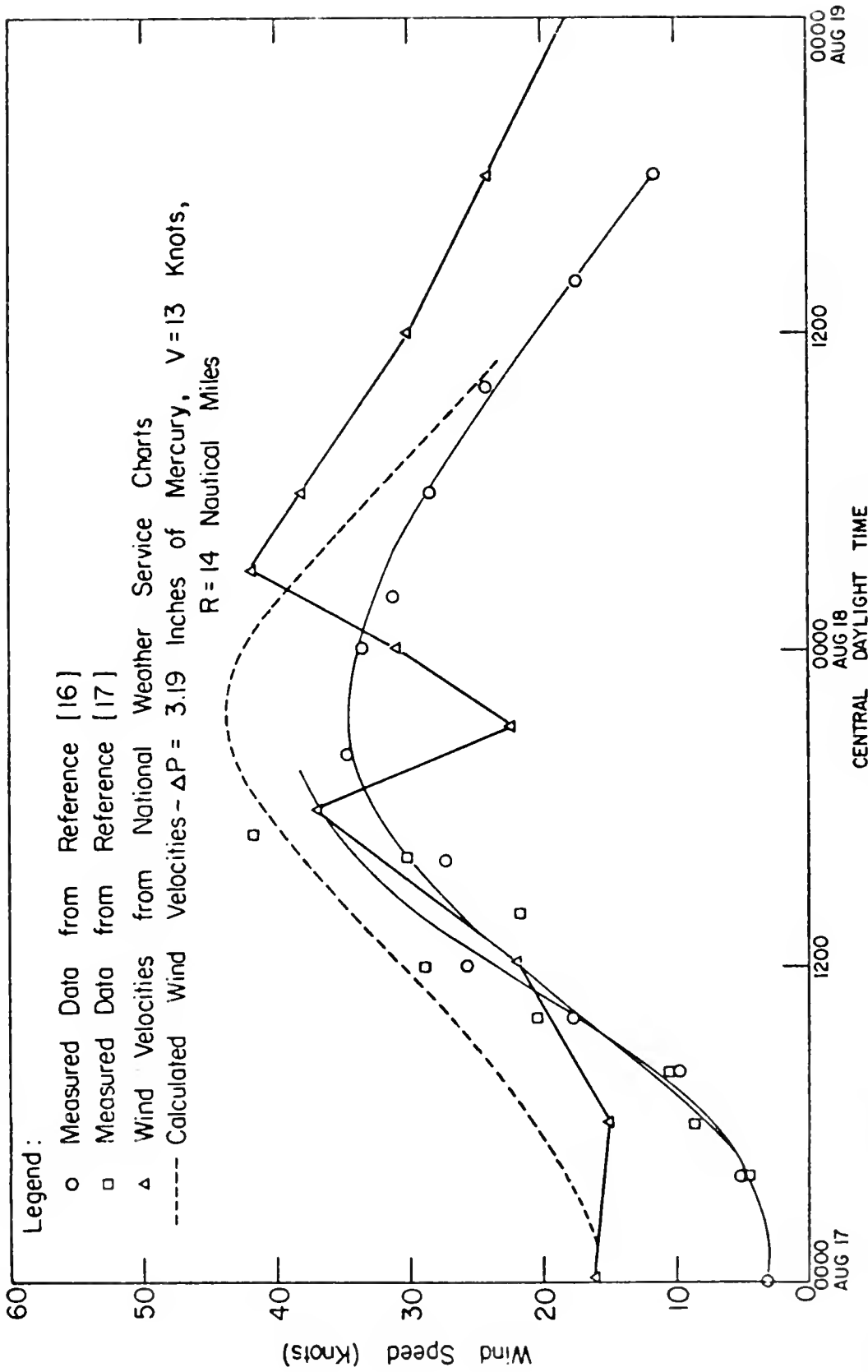
FIGURE 4-12   COMPARISON OF MEASURED AND CALCULATED WIND SPEEDS AT SITE
OF WATER VELOCITY MEASUREMENTS

However, a first approximation of the flooding and the comparison of measured and predicted flooding provides a suitable conclusion to this stage of the study.

The flooded region is predicted using the simple assumption that the water level inland near the coast will be at the predicted surge elevation. Thus the water is assumed to extend inland horizontally from the elevation predicted at the coast. For example, if a surge 10 feet above MSL were predicted for a region, then the predicted flooded area for that region would extend from the normal coastline to the 10 foot (above MSL) contours on a topographical map. The predicted surge in this case is that from the large grid model as shown in Figure 4-4, with the surge elevation extrapolated to the coastline. A typical comparison of these predictions and the actual flooding as documented by the U. S. Army Corps of Engineers [31] is given in Figure 4-13.

If the results of the type in Figure 4-13 are to be evaluated, some quantitative measure of the "goodness" of the fit to the data is necessary. Because of the convoluted nature of the flooded region comparisons based on a flooded length would, in general, have little significance. For this reason it was decided to compare actual and predicted flooded areas per unit length of coastline. In practice this consisted of taking an approximately 3 mile wide strip running north from the coast, and, for that strip, calculating the measured and predicted flooded areas as determined using a planimeter. As a consistent measure these areas were divided by the width of the strip to obtain area per unit length. Whenever possible the areas were taken to the northern extent of the flooding. In several cases this was impossible and an arbitrary boundary was drawn about 8 statute miles from the coast.
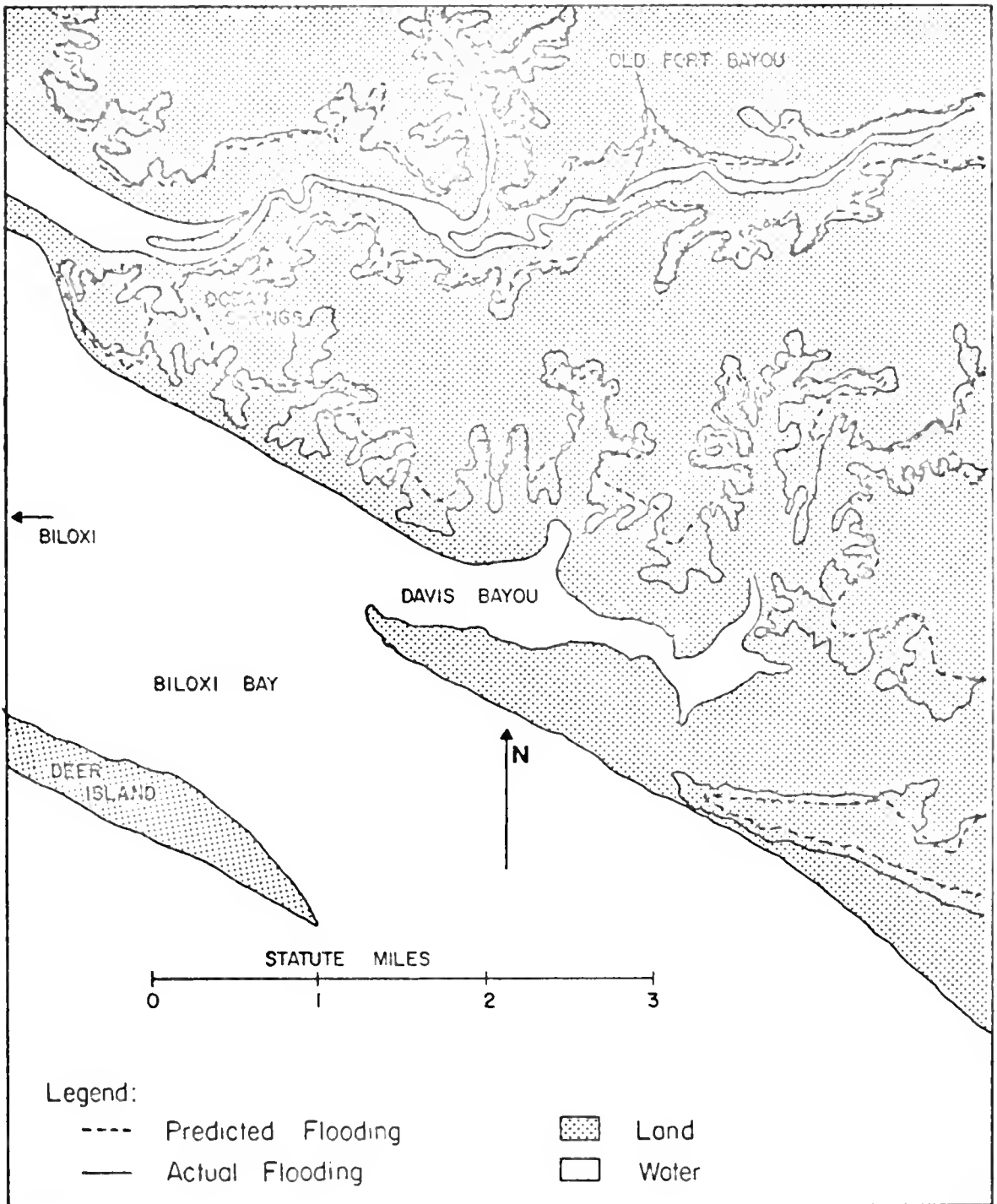
FIGURE 4-13 COMPARISON OF PREDICTED AND ACTUAL
FLOODING ON MISSISSIPPI COAST

The plot in Figure 4-14 runs from Edgewater Park, Mississippi eastward to Bayou La Batre, Mississippi. In general this scheme over-predicts the flooded area. There are two apparent reasons for this: 1) the model predicts surges slightly too large in that region, 2) friction and inertia prevent the surge from reaching points far inland even though they are at a low elevation.
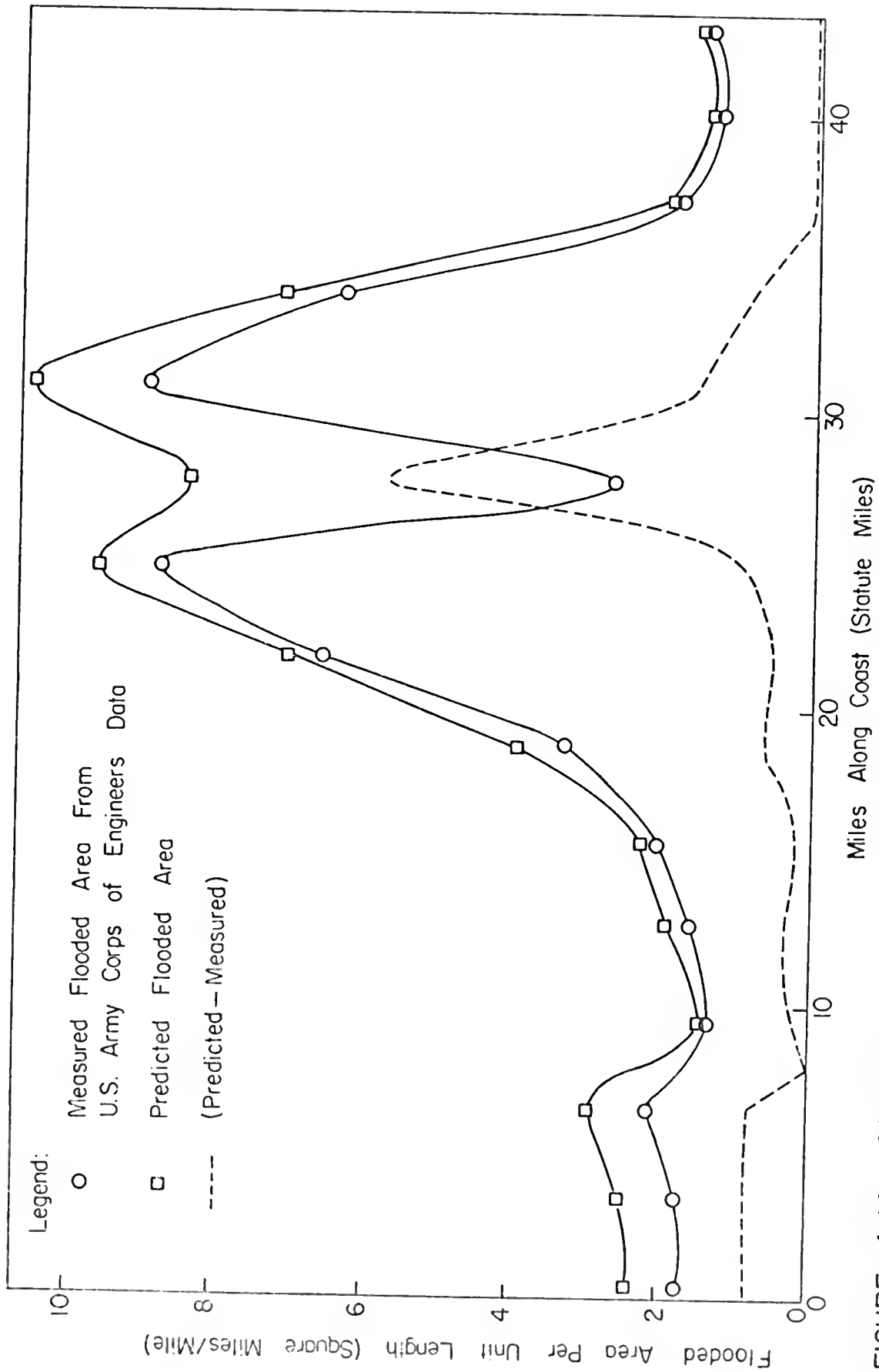
FIGURE 4-14   COMPARISON OF PREDICTED AND MEASURED FLOODED AREAS PER UNIT LENGTH ALONG COAST

Legend:
○   Measured Flooded Area From U.S. Army Corps of Engineers Data
□   Predicted Flooded Area
----   (Predicted – Measured)

Flooded Area Per Unit Length (Square Miles/Mile)

Miles Along Coast (Statute Miles)

CHAPTER 5

FIELD DATA AND INSTRUMENTATION

The measurement of storm surges and currents is difficult
because of the extreme weather conditions prevailing at the time
observations are to be made. There exist two basic methods for
approaching this problem, excluding that of the observer being present
during the storm. One may have a permanent installation or install-
ations and wait for a significant storm, or one may "run before the
storm" and position equipment to record the necessary phenomena.
The latter appears the best choice but the logistics of implementation
and recovery are great, and seas may be quite rough preceding the
storm due to the presence of forerunners. Sonu [35] taking obser-
vations at Santa Rosa Island, Florida observed a period of wave
action dominated by forerunners originating in Hurricane Camille. This
period lasted for 28 hours from 1200 hours Central Daylight Time, (CDT)
August 16 to 1600 hours CDT August 17 and ended with the arrival of
gale-force winds and locally generated windwaves. The period of
forerunners was characterized at this location by a maximum breaking
wave height of approximately 3 meters. At the closest point of
approach Hurricane Camille was 200 miles from the point of observation.

The considerations for the predictions of hurricane movement are
not within the scope of this report. The predictions are, however,

an important consideration for successful completion of any field measurement program. To acquire insight into the problems involved in gathering field data, observe the hurricane advisories issued by the National Weather Service as presented in Figure 5-1 and also observe that storm landfall near Bay St. Louis, Mississippi between 2300 and 2400 hours, CDT, on August 17, 1969. Using this information, a Gedanken* field measurement can be carried out. At 1900 hours CDT the storm was over the western tip of Cuba, traveling to the north-west. At that time the field crew readied all instrumentation and equipment. The point of landfall is unknown, assuming the crew to be in New Orleans, they remain since the probability of intercepting the storm does not increase by moving at this time. At 2300 hours CDT August 15 the National Weather Service advised that a hurricane watch would probably be established for the northeast Gulf region prior to 1100 hours CDT August 16. At this time the crew begins traveling east and at 0800 hours CDT receive the bulletin from the National Weather Service extending a hurricane watch from Biloxi, Mississippi to St. Marks, Florida (Figure 4-1). It is decided to install the instrumentation at the midpoint of the 0800 watch area near Ft. Walton Beach, Florida. Three hours later at 1100 hours Advisory 10 is issued posting hurricane warnings from Ft. Walton to St. Marks. By this time the instrumentation has been installed and the further success is left to chance. The hurricane actually went ashore at Bay St. Louis, Mississippi and the field crew missed by

---

*Gedanken - To carry out by proposing a hypothesis in thought only.

Advisory Number 5, 1100 CDT, Friday August 15.
Cuba warned of tides up to 8 ft. and 5 to 10 inches of rain.

Advisory Number 6, 1700 CDT, Friday August 15.
Gale warnings issued for Marquesas Keys and Dry Tortugas.

Advisory Number 7, 2300 CDT, Friday August 15.
Stated Camille a dangerous hurricane and poses a great threat to
the U.S. mainland. Advised that a hurricane watch would probably
be issued for a portion of the coastal area of the northeast
Gulf prior to 1100 CDT, Saturday August 16.

Advisory Number 8, 0500 CDT, Saturday August 16.
Small craft along the northwest Florida coast and as far west
as Mobile urged to seek safe harbor. Repeated that a hurricane
watch would be issued later in morning.

Advisory Number 9, 0800 CDT, Saturday August 16.
Hurricane watch issued extending from Biloxi, Mississippi, to
St. Marks, Florida. Advised that a hurricane warning would be
issued at 1100 hours.

Advisory Number 10, 1100 CDT, Saturday August 16.
Hurricane warning issued extending from Ft. Walton to St. Marks.
Gale warnings elsewhere from Pensacola to Cedar Key.

Advisory Number 11, 1700 CDT, Saturday August 16.
Highest winds raised from 115 MPH to 150 MPH. 5 to 12 feet
tides forecast.

Advisory Number 12, 2300 CDT, Saturday August 16.
Tides of 15 feet forecast.

Advisory Number 13, 0500 CDT, Sunday August 17.
Hurricane warnings extended westward to Biloxi. Hurricane
watch extended westward to New Orleans and Grand Isle.

Bulletin, 0500 CDT, Sunday August 17.
Advised that if present movement toward the mouth of the
Mississippi continued for a few more hours, hurricane warnings
would be extended westward to New Orleans and Grand Isle.

Advisory Number 14, 0900 CDT, Sunday August 17.
Hurricane warnings extended westward to New Orleans and Grand Isle.

Advisory Number 16, 1500 CDT, Sunday August 17.
Highest winds raised to 190 MPH and tides 15 to 20 feet.
Predicted landfall near Gulfport, Mississippi.

FIGURE 5-1   SUMMARY OF CRITICAL WARNINGS
(FROM REFERENCE [36])

200 miles. They did, however, recover some current data, which turned out to be the only data in existence for wind-generated currents during a hurricane.

It should be noted that this is in no way related to the data of Sonu [35] and Murray [16]; Murray's instrumentation was in place for another study and fortunately current, wind data, and wave height observations were obtained.

This hypothetical deployment of equipment in anticipation of a hurricane points out that this type of operation involves a certain amount of risk, since, by observation the storm forerunners were beginning to arrive during the installation procedure (see Figure 5-2). A problem postponing the operation a few hours may postpone it completely. Thus, matters such as method of equipment deployment are very important and in fact critical since the operating environmental conditions will be extreme. The probability of loss of equipment is impossible to determine but certainly high. Murray [16] employed three current meters, two in the nearshore zone which did not function and one in about 21 feet of water seaward of the "outer bar" which functioned for about one half the storm. If the storm had passed directly over the instrumentation further conse-quences could have been expected. A system that is 100% reliable is desired in view of the long waiting time involved and in view of the need for data to improve surge and current predictions.

The author feels that the technique discussed in the Gedanken measurement is not reliable enough. A system that is deployable from an airplane or helicopter would be very desirable. Also desirable would be a series of permanent field stations located in
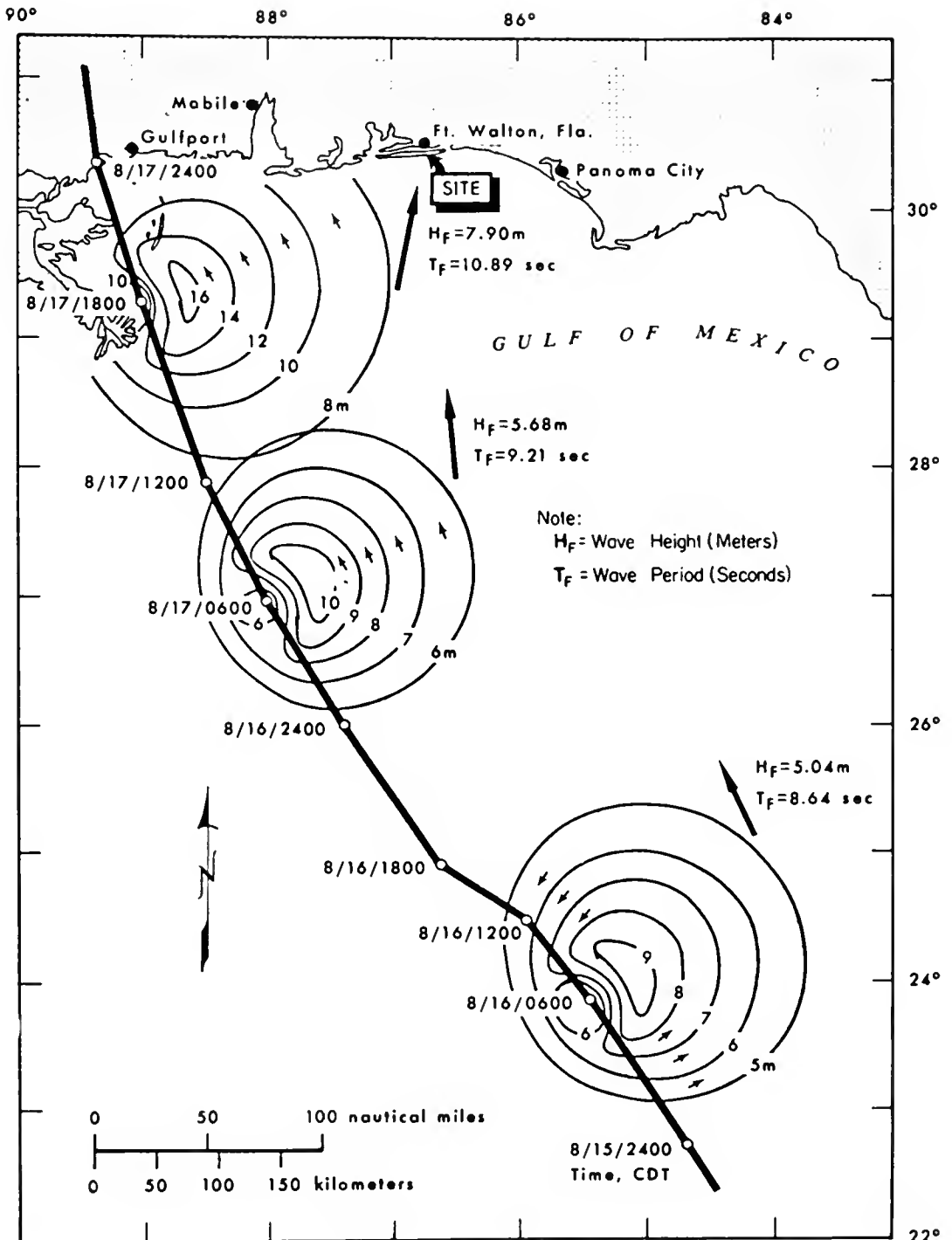
FIGURE 5-2 HINDCAST WAVE FIELDS FOR HURRICANE CAMILLE (AFTER REFERENCE [35])

areas of high hurricane probability. Harris [37] provides in Figure 5-3 a chart of absolute number of destructive storms reaching a given location in a 54-year period. Using this and other data including accessibility of the area in question it would be desirable to establish a network of five permanent underwater surge and current monitoring stations around the State of Florida in the configuration shown in Figure 5-4; these installations would be activated only during the hurricane season. This network in conjunction with a single "run before the storm" installation, when practical, should provide the necessary redundancy.

The fixed sites should have a recording capability of 30 days or more. This would then require three or four servicings of the equipment between installation at the beginning of the hurricane season and recovery at the end.

The development of inexpensive but effective equipment is always desirable, especially where a high probability of loss is involved. The instrument shown in Figure 5-5 and Figure 5-6 is a recording underwater tide or pressure gauge and was developed from items easily available commercially. It could be deployed very economically in quantities of 5-10 or more. At the present time the response time is of the order of one second. For the prototype situation this would be increased to about 30 seconds because of the desirability of suppressing long period wave action present during a storm. A prototype instrument has been tested at Angelfish Creek at the northern tip of Key Largo with the results presented in Figure 5-7 and compared to a nearby conventional tide gauge recorder.
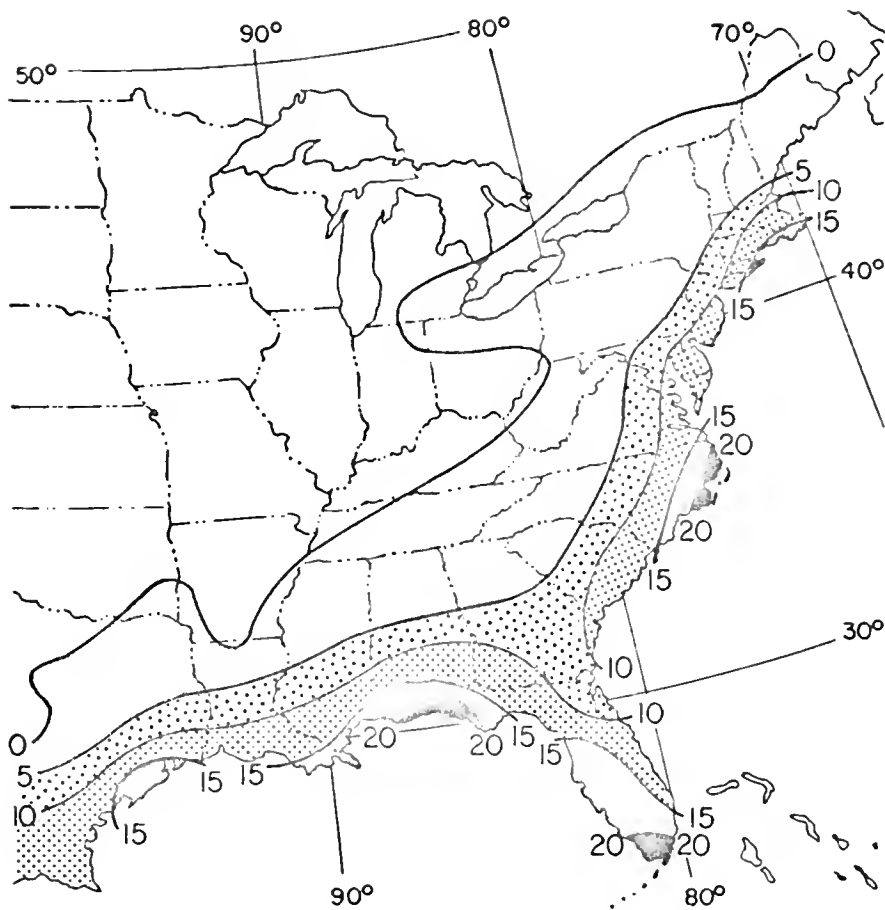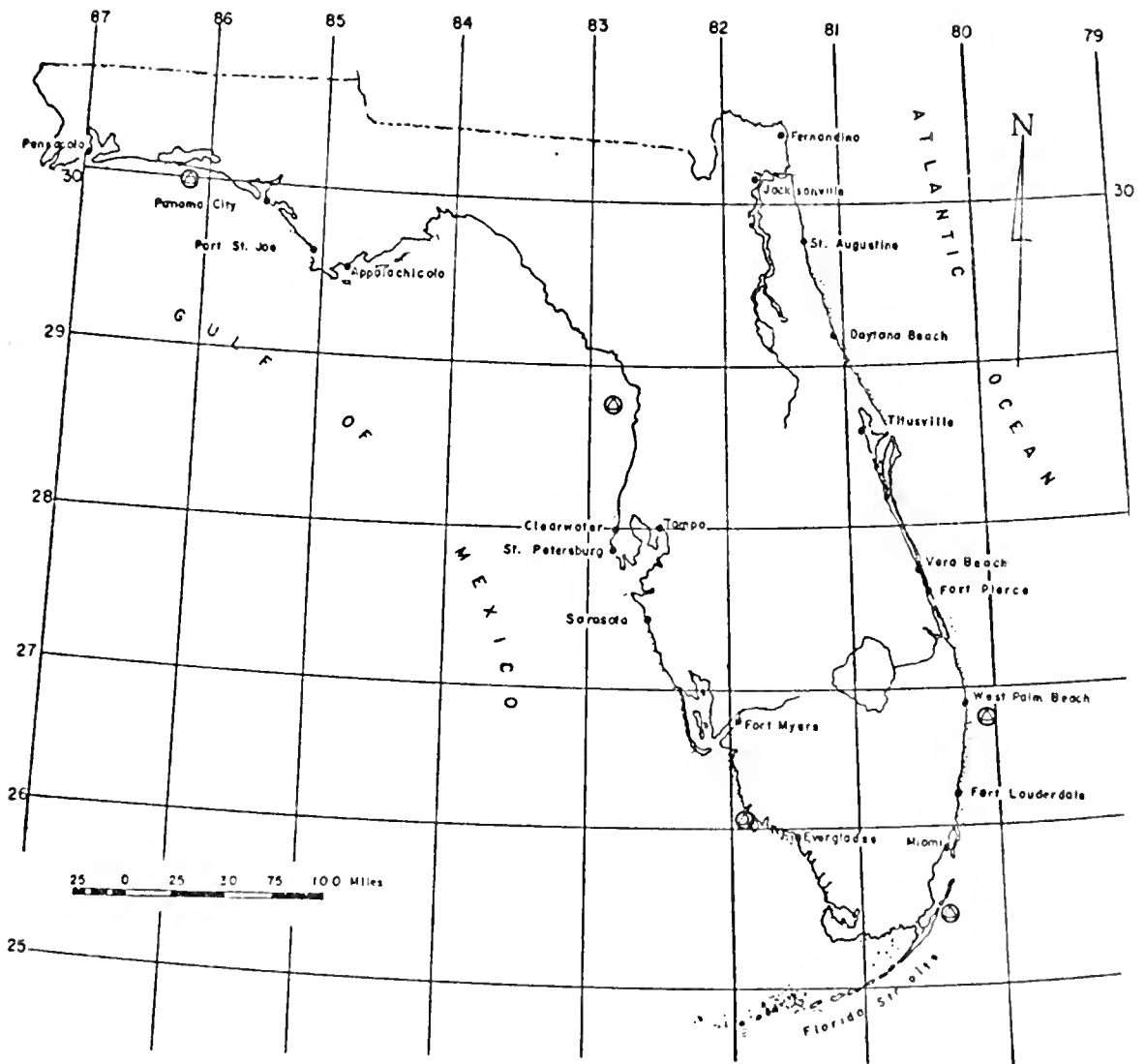
FIGURE 5-3 NUMBER OF TIMES DESTRUCTION WAS CAUSED BY TROPICAL STORMS, 1901-1955 (FROM REFERENCE [37])

Note:

Instrumentation Sites Designated by ⊚

FIGURE 5-4   PROPOSED FIXED, CONTINUOUSLY
MAINTAINED INSTRUMENTATION SITES
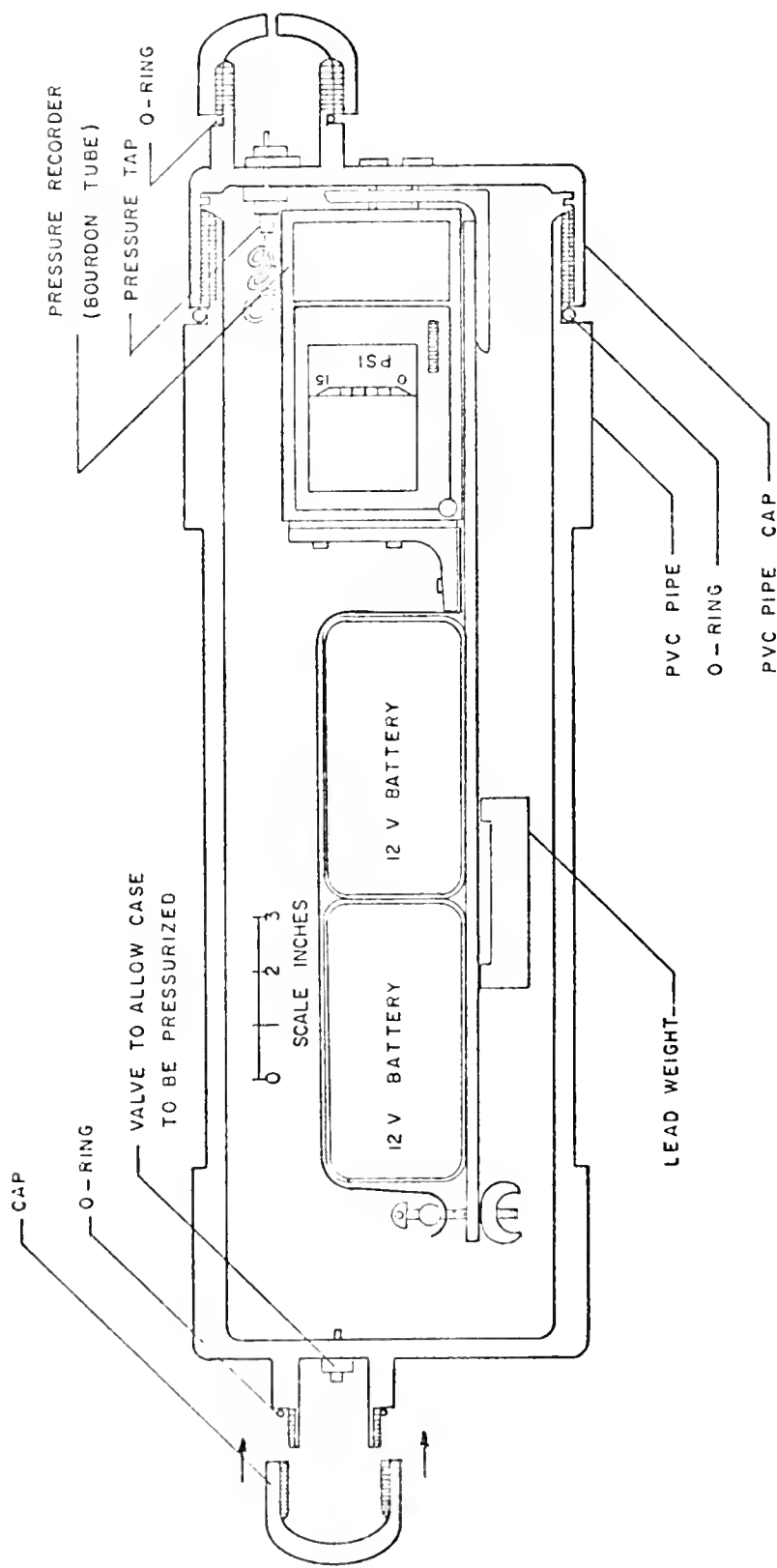
FIGURE 5-5   SCHEMATIC OF RECORDING UNDERWATER TIDE GAUGE

FIGURE 5-6 RECORDING UNDERWATER TIDE GAUGE
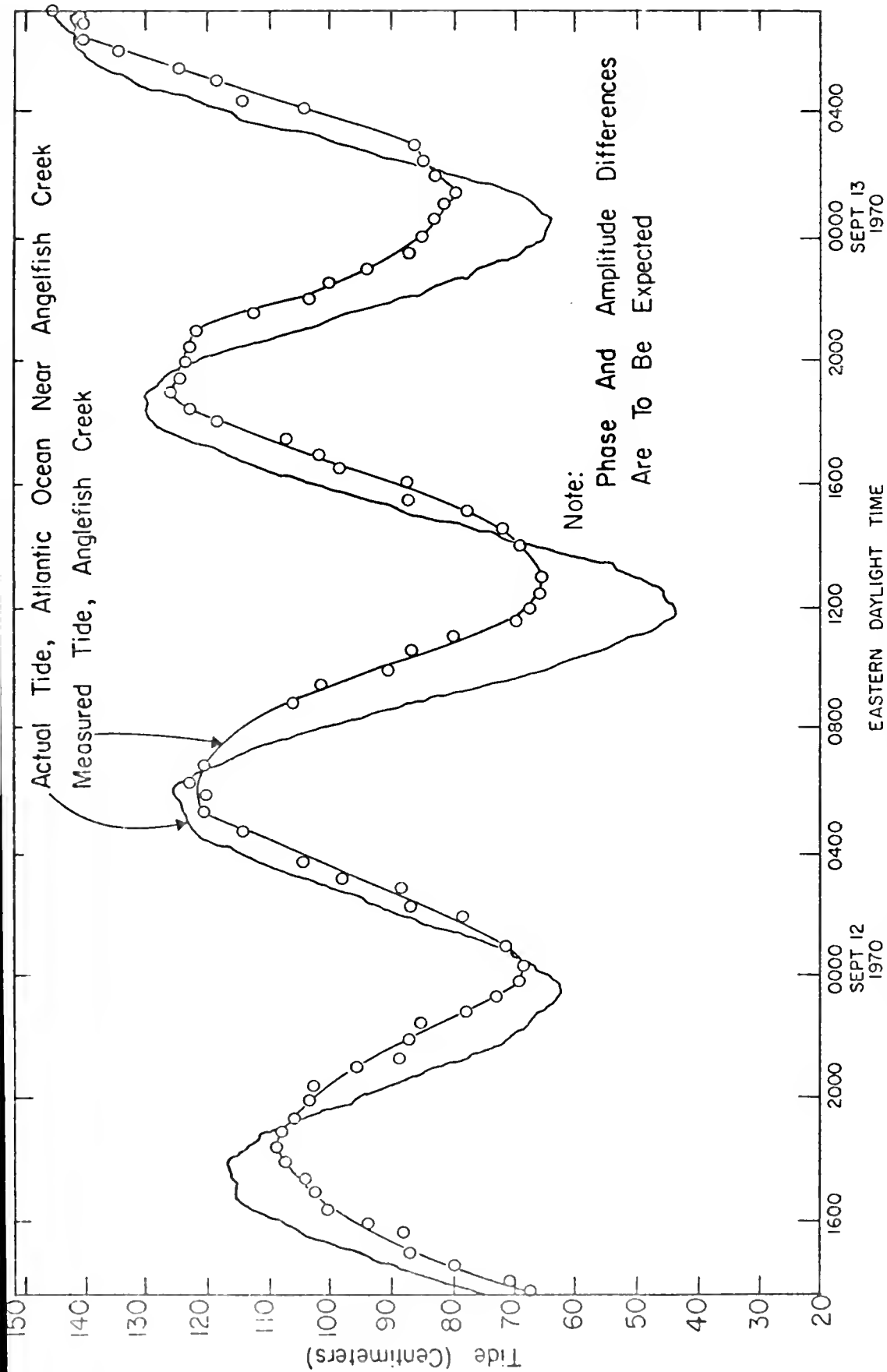
FIGURE 5-7 TIDE MEASUREMENT—UNDERWATER GAUGE

The current meter presents a formidable problem since the instrument must be rugged yet sensitive enough to obtain a mean flow from the highly turbulent environment existing in shallow water during storm conditions. The current meter illustrated in Figures 5-8a and 5-8b was developed in conjunction with General Oceanics, Inc.*   It is inexpensive but proved to have a threshold velocity of 0.56 feet/second, high enough to render calibration impossible in a turbulent environment. If the threshold velocity can be reduced this device would prove to be ideally suited for the measurement of hurricane driven currents.

Future work on hurricane surges and currents is especially needed in three areas: improved representations of bottom friction, considerably more field data, and development of physical modeling techniques. It is evident that the accurate prediction of storm driven currents lies in a better understanding of the dissipation mechanism (i.e. friction) during a hurricane. This development will rely to a great extent on availability of data upon which a better model can be based. Data will become available from prototype situations and also from physical models of which there are none at present. There are many problems in developing a physical model. The problem of scaling is difficult since the length/depth ratio for a typical prototype case would be of the order of 1,000-10,000. Thus any laboratory model would probably require highly distorted length scales. The modeling of friction resulting from turbulent flows

---

*Miami, Florida

FIGURE 5-8a   CURRENT METER DEPLOYED
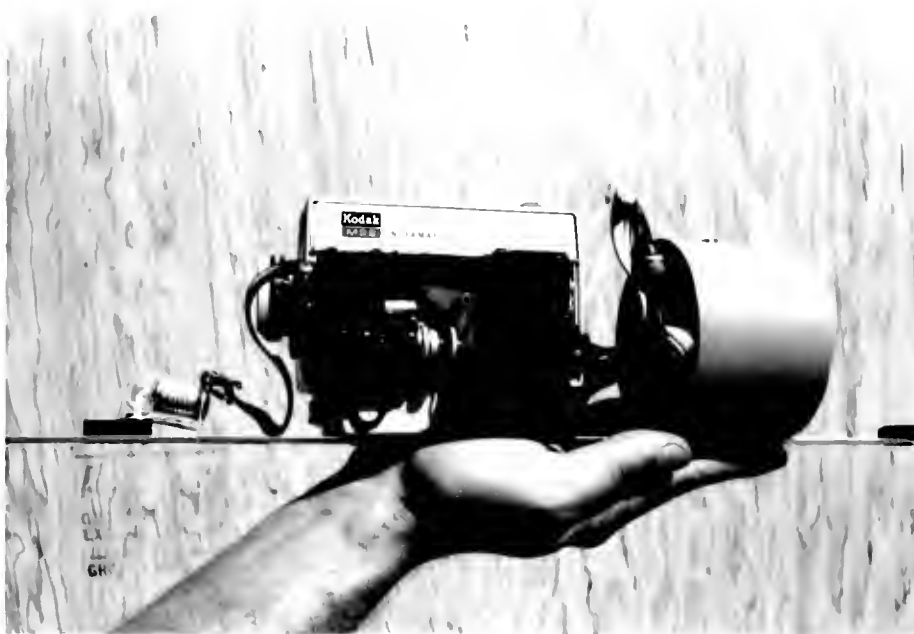
FIGURE 5-8b   PHOTOGRAPHIC RECORDING MECHANISM
OF CURRENT METER

and pressure and shear stress distributions will all require a sophis-
ticated experimental technique, yet would produce invaluable data
and data that could represent a considerable equivalent time span in
the prototype situation.

CHAPTER 6

SUMMARY AND CONCLUSIONS

The response of coastal or shelf waters to the passage of an orga-
nized storm system is studied by 1) simplified analytical techniques,
2) finite difference numerical calculations and 3) comparison of the nu-
merical calculations to field observations. The momentum equations for
fluid motion and the continuity equation are placed in turbulent form with
the instantaneous velocities being replaced by time mean velocities and
with the laminar stresses replaced by Reynolds stresses.

These equations are then integrated in the vertical, eliminating the
z-equation, with the result that all velocities represent an average over
the depth. Boundary conditions for the model boundaries are presented,
including the surface and bottom shear stresses. Initially the model is
assumed quiet and the disturbance to begin traveling far enough from the
region of interest to make the effect of the initial conditions negligible.

A simple analytical hurricane model which calculates the gradient
winds and takes the forward velocity of the hurricane into consideration
is used to predict storm winds from the central pressure index Δp, the
radius to maximum winds R, and the forward velocity V of the storm.

Simplified, steady state, one-dimensional, analytical models with
both uniform depth and uniform slope are presented with solutions in
graphical form. Also presented is an analytical treatment of a one-
dimensional uniform depth shelf subjected to a triangular shear stress

132

distribution moving at constant velocity C. Dimensionless maximum response to the latter treatment is given as a function of dimensionless storm width λ^* and velocity c^*. These solutions allow simplified calculations and verification of the numerical methods.

One-and two-dimensional models are developed including the finite difference equations as used in the computer simulation. Several techniques are presented for verifying the results of the numerical calculations and of determining the effect of the use of discrete elements.

Hurricane Camille of August 17-22,1969 was chosen as a test case for the numerical techniques. Two-dimensional plots of surge elevation at various times are included as well as the surge maximum at each point along the coast; the latter being compared to high water marks compiled by the U.S. Army Corps of Engineers. The sensitivity of the surge calculations to bottom friction coefficient f, and to starting point of the storm X_s, was investigated. A comparison of a measured tide curve to the numerical calculations is made for the data from Dauphin Island, Alabama. The currents calculated at Eglin AFB, Florida are compared to the data taken by Murray [16]. Techniques to be used for field measurements of surges and storm driven currents are discussed.

The further development of models such as the one presented will rely on a better understanding of the physical processes involved. Interaction between the wind and the sea surface is not well quantified. The use of the quadratic bottom friction, predicated on steady open channel flow, can probably be improved upon. The availability of field measurements, especially during hurricane conditions would add to a better understanding of the subject.

APPENDIX A

DERIVATION OF GOVERNING EQUATIONS FOR SURGE HYDRODYNAMICS

In this appendix the equations of momentum and continuity will be developed for the general case of long period flows in estuaries, bays, and coastal regions. The detailed velocity variations over depth are not considered to be necessary for the purpose of this study. The problem is therefore formulated, in two dimensions, in terms of the vertically integrated equations of motion and continuity as explained in Section 2-1 of the main text. Referring to the definition sketch Figure 2-1, the equations of motion are Equations (2-3) of the main text.

$$\frac{\partial u}{\partial t} + u\frac{\partial u}{\partial x} + v\frac{\partial u}{\partial y} + w\frac{\partial u}{\partial z} - 2\omega(\sin\phi)v = -\frac{1}{\rho}\frac{\partial p}{\partial x} + \frac{1}{\rho}(\frac{\partial \tau'_{xx}}{\partial x} + \frac{\partial \tau'_{xy}}{\partial y} + \frac{\partial \tau'_{xz}}{\partial z}) \quad (2\text{-}3a)$$

$$\frac{\partial v}{\partial t} + u\frac{\partial v}{\partial x} + v\frac{\partial v}{\partial y} + w\frac{\partial v}{\partial z} + 2\omega(\sin\phi)u = -\frac{1}{\rho}\frac{\partial p}{\partial y} + \frac{1}{\rho}(\frac{\partial \tau'_{xy}}{\partial x} + \frac{\partial \tau'_{yy}}{\partial y} + \frac{\partial \tau'_{yz}}{\partial z}) \quad (2\text{-}3b)$$

$$\frac{\partial w}{\partial t} + u\frac{\partial w}{\partial x} + v\frac{\partial w}{\partial y} + w\frac{\partial w}{\partial z} = -\frac{1}{\rho}\frac{\partial p}{\partial z} - g + \frac{1}{\rho}(\frac{\partial \tau'_{xz}}{\partial x} + \frac{\partial \tau'_{yz}}{\partial y} + \frac{\partial \tau'_{zz}}{\partial z}) \quad (2\text{-}3c)$$

The vertical accelerations are considered to be small as are stresses acting on any vertical plane.

The differential form of the equation of continuity for an imcompressible fluid is:

$$\frac{\partial u}{\partial x} + \frac{\partial v}{\partial y} + \frac{\partial w}{\partial z} = 0 \quad (2\text{-}3d)$$

In developing the vertically integrated equations of motion it will be

necessary to utilize Leibnitz' rule:

$$\frac{\partial}{\partial x}\int_{g(x)}^{h(x)} f(x,z,t)\ dz = \int_{g(x)}^{h(x)} \frac{\partial f}{\partial x}(x,z,t)\ dz + f(x,h(x),t)\ \frac{\partial h}{\partial x}$$

$$-f(x,g(x),t)\ \frac{\partial g}{\partial x}$$

Specifically for the first term of Equation (2-3a) we have, referring to Figure 2-1 for the notation:

$$\int_{-h(x,y)}^{\eta(x,y,t)} \frac{\partial u}{\partial t}\ dz = \frac{\partial}{\partial t}\int_{-h(x,y)}^{\eta(x,y,t)} u\ dz - u_\eta\ \frac{\partial \eta}{\partial t} + u_{-h}\ \frac{\partial(-h)}{\partial t}$$

where $u_{-h}\ \frac{\partial(-h)}{\partial t} = 0$ since h is not a function of time.

To render Equations (2-3a) and (2-3b) into better forms for integration, the following combinations of the equations of motion and continuity are formed

$$\text{Eq.(2-3a)} + u \cdot [\text{Eq. (2-3d)}] \tag{A-1}$$

$$\text{Eq.(2-3b)} + v \cdot [\text{Eq. (2-3d)}] \tag{A-2}$$

Recalling that only the stresses occurring on planes perpendicular to the z coordinate will be considered and carrying out the combinations indicated by Equations (A-1) and (A-2) the resulting equations are:

$$\frac{\partial u}{\partial t} + \frac{\partial u^2}{\partial x} + \frac{\partial(uv)}{\partial y} + \frac{\partial(uw)}{\partial z} - 2\omega(\sin\phi)v = -\frac{1}{\rho}\frac{\partial p}{\partial x} + \frac{1}{\rho}\frac{\partial \tau'_{xz}}{\partial z} \tag{A-3}$$

$$\frac{\partial v}{\partial t} + \frac{\partial(uv)}{\partial x} + \frac{\partial v^2}{\partial y} + \frac{\partial(vw)}{\partial z} + 2\omega(\sin\phi)u = -\frac{1}{\rho}\frac{\partial p}{\partial y} + \frac{\partial\tau'_{xy}}{\partial z} \tag{A-4}$$

Integrating Equation (A-3) over depth, employing Leibnitz' rule, and grouping terms leads to the following:

$$\frac{\partial}{\partial t}\int_{-h}^{\eta} u\,dz + \frac{\partial}{\partial x}\int_{-h}^{\eta} u^2\,dz + \frac{\partial}{\partial y}\int_{-h}^{\eta} uv\,dz - \int_{-h}^{\eta} 2\omega(\sin\phi)\,v\,dz$$

$$-u_{\eta}\left[\frac{\partial\eta}{\partial t} + u\frac{\partial\eta}{\partial x} + v\frac{\partial\eta}{\partial y} - w\right]_{\eta}$$

$$+u_{-h}\left[u\frac{\partial(-h)}{\partial x} + v\frac{\partial(-h)}{\partial y} - w\right]_{-h} = -\frac{1}{\rho}\int_{-h}^{\eta}\frac{\partial p}{\partial x}\,dx + \frac{1}{\rho}(\tau_{n_x} - \tau_{-h_x}) \tag{A-5}$$

To further reduce Equation (A-5) the kinematic free surface and the bottom boundary conditions, Equations (A-6) and (A-7) are employed.

$$\frac{\partial\eta}{\partial t} + u\frac{\partial\eta}{\partial x} + v\frac{\partial\eta}{\partial y} = w \quad ; \quad \text{at } z = \eta \tag{A-6}$$

$$u\frac{\partial(-h)}{\partial x} + v\frac{\partial(-h)}{\partial y} = w \quad ; \quad \text{at } z = -h \tag{A-7}$$

The assumptions stated earlier that the vertical acceleration is negligible and that only stress on horizontal planes is of importance, imply that the motion is hydrostatic; integrating Equation (2-3c) over depth yields

$$p(x,y,z) = p_{\eta}(x,y) + \gamma(\eta(x,y) - z) \tag{A-8}$$

where $\gamma = \rho g$ is the specific weight of water and $p_{\eta}(x,y)$ is the distribution of (barometric) pressure on the free surface.

We now have the necessary equations to further reduce Equation (A-5). Combining Equations (A-6), (A-7) and (A-8) with Equation (A-5) yields

$$\frac{\partial}{\partial t} \int_{-h}^{\eta} u \; dz + \frac{\partial}{\partial x} \int_{-h}^{\eta} u^2 \; dz + \frac{\partial}{\partial y} \int_{-h}^{\eta} uv \; dz = -\frac{1}{\rho} (h+\eta) \frac{\partial p_\eta}{\partial x} \qquad (A-9)$$

$$-g(h+\eta) \frac{\partial \eta}{\partial x} + \frac{1}{\rho} (\tau_{\eta_x} - \tau_{-h_x})$$

The form for the equation of motion in the y-direction is:

$$\frac{\partial}{\partial t} \int_{-h}^{\eta} v \; dz + \frac{\partial}{\partial x} \int_{-h}^{\eta} uv \; dz + \frac{\partial}{\partial y} \int_{-h}^{\eta} v^2 \; dz = -\frac{1}{\rho} (h+\eta) \frac{\partial p_\eta}{\partial y} \qquad (A-10)$$

$$-g(h+\eta) \frac{\partial \eta}{\partial y} + \frac{1}{\rho} (\tau_{\eta_y} - \tau_{-h_y})$$

Integration of the continuity equation over depth and employing Leibnitz' rule, yields

$$\frac{\partial}{\partial x} \int_{-h}^{\eta} u \; dz + \frac{\partial}{\partial y} \int_{-h}^{\eta} v \; dz - [\, u \, \frac{\partial \eta}{\partial x} + v \, \frac{\partial \eta}{\partial y} - w \,]_\eta$$

$$(A-11)$$

$$+ [\, u \, \frac{\partial(-h)}{\partial x} + v \, \frac{\partial(-h)}{\partial y} - w \,]_{-h} \; = 0$$

Combining Equations (A-6), (A-7), and (A-11) leads to the vertically integrated equation of continuity, Equation (A-12).

$$\frac{\partial \eta}{\partial t} + \frac{\partial}{\partial x} \int_{-h}^{\eta} u \ dz + \frac{\partial}{\partial y} \int_{-h}^{\eta} v \ dz = 0 \tag{A-12}$$

The governing equations will be more convenient for later use if the following definitions are made and the form of the equations modified accordingly:

$$q_x \equiv \int_{-h}^{\eta} u \ dz$$

$$q_y \equiv \int_{-h}^{\eta} v \ dz$$

$$D(x,y,t) \equiv h(x,y) + \eta(x,y,t)$$

The vertically integrated equations of motion and continuity are summarized as:

$$\frac{\partial q_x}{\partial t} + \frac{\partial}{\partial x} \int_{-h}^{\eta} u^2 \ dz + \frac{\partial}{\partial y} \int_{-h}^{\eta} uv \ dz - 2\omega(\sin\phi)q_y = - \frac{D}{\rho} \frac{\partial p_\eta}{\partial x} - gD \frac{\partial \eta}{\partial x}$$

$$+ \frac{1}{\rho} (\tau_{\eta_x} - \tau_{-h_x})$$

$$\frac{\partial q_y}{\partial t} + \frac{\partial}{\partial x} \int_{-h}^{n} uv \ dz + \frac{\partial}{\partial y} \int_{-h}^{n} v^2 \ dz + 2\omega(\sin\phi)q_x = -\frac{D}{\rho}\frac{\partial p_n}{\partial y} - gD\frac{\partial n}{\partial y}$$

$$+ \frac{1}{\rho}(\tau_{n_y} - \tau_{-h_y})$$

$$\frac{\partial q_x}{\partial x} + \frac{\partial q_y}{\partial y} + \frac{\partial n}{\partial t} = 0$$

To express these equations completely in finite-difference form, further approximations must be made as discussed in Appendix B.

APPENDIX B

TRANSFORMATION OF GOVERNING DIFFERENTIAL EQUATIONS
INTO FINITE DIFFERENCE FORM

1. Transformation Without Convective Terms

Transforming the vertically integrated equation of motion into a finite difference form is straightforward if the nonlinear friction and convective terms are neglected. If they are not to be neglected then some form of approximations must be made in addition to the approximations introduced by discretization. Writing the vertically integrated equations of motion and continuity and including the convective terms yields Equations (B-1a), (B-1b), and (B-1c).

$$\frac{\partial q_x}{\partial t} + \frac{\partial}{\partial x} \int_{-h}^{\eta} u^2 \; dz + \frac{\partial}{\partial y} \int_{-h}^{\eta} uv \; dz - 2 \; \omega(\sin\phi)q_y + gD \; \frac{\partial \eta}{\partial x} =$$

$$-\frac{D}{\rho} \; \frac{\partial p_\eta}{\partial x} + \frac{1}{\rho} \; \tau_{\eta_x} - \frac{f|q|q_x}{8D^2} \tag{B-1a}$$

$$\frac{\partial q_y}{\partial t} + \frac{\partial}{\partial x} \int_{-h}^{\eta} uv \; dz + \frac{\partial}{\partial y} \int_{-h}^{\eta} v^2 \; dz + 2 \; \omega(\sin\phi)q_x + gD \; \frac{\partial \eta}{\partial y} =$$

$$-\frac{D}{\rho} \frac{\partial p_\eta}{\partial y} + \frac{1}{\rho} \; \tau_{\eta_y} - \frac{f|q|q_y}{8D^2} \tag{B-1b}$$

$$\frac{\partial \eta}{\partial t} + \frac{\partial q_x}{\partial x} + \frac{\partial q_y}{\partial y} = 0 \qquad \text{(B-1c)}$$

where, as before, $q_x = \displaystyle\int_{-h}^{\eta} u\ dz$, $q_y = \displaystyle\int_{-h}^{\eta} v\ dz$, and where the

Darcy-Weisbach friction coefficient, f, is used, to represent the

bottom friction.

The numerical computations presented herein were carried out

without the convective terms represented by the integrals in Equations

(B-1a) and (B-1b). These equations then assume the form of Equations

(3-6) in the text.

$$\frac{\partial q_x}{\partial t} - 2\omega(\sin\phi)q_y + gD\frac{\partial \eta}{\partial x} = \frac{-D}{\rho}\frac{\partial P_\eta}{\partial x} + \frac{1}{\rho}\ \tau_{x_\eta} - \frac{f|q|q_x}{8D^2} \qquad \text{(3-6a)}$$

$$\frac{\partial q_y}{\partial t} + 2\omega(\sin\phi)q_x + gD\frac{\partial \eta}{\partial y} = -\frac{D}{\rho}\frac{\partial P_\eta}{\partial y} + \frac{1}{\rho}\ \tau_{y_\eta} - \frac{f|q|q_y}{8D^2} \qquad \text{(3-6b)}$$

$$\frac{\partial \eta}{\partial t} + \frac{\partial q_x}{\partial x} + \frac{\partial q_y}{\partial y} = 0 \qquad \text{(3-6c)}$$

To transform Equation (3-6a) into finite difference form integrate

from t to t + Δt. Using the indicial notation described in Chapter

3 of the text, the result of that integration is approximately

$$q_x(i,j,n+1) - q_x(i,j,n) = 2 \, \omega(\sin\phi) \, [\int_n^{n+1} \overline{q}_y(i,j,\xi) \, d\xi]$$

$$+ \frac{g\Delta t}{2\Delta x} [\, D(i,j,n+1/2) + D(i-1,j,n+1/2)] \, [\eta(i-1,j,n+1/2) - \eta(i,j,n+1/2)]$$

$$+ \frac{\Delta t}{2\rho\Delta x} [\, D(i,j,n+1/2) + D(i-1,j,n+1/2)] \, [p_\eta(i-1,j,n+1/2) - p_\eta(i,j,n+1/2)]$$

$$+ \frac{\Delta t}{2\rho} [\tau_{x_\eta} (i,j,n+1/2) + \tau_{x_\eta} (i-1,j,n+1/2)]$$

$$- \frac{f/2}{[D(i,j,n+1/2) + D(i-1,j,n+1/2)]^2} \int_n^{n+1} |q(i,j,\xi)| \, q_x(i,j,\xi) \, d\xi \quad \text{(B-2)}$$

where ξ is a dummy variable and $\overline{q}_y(i,j,\xi)$ is defined in Figure 3-4. The value of D at the location of $q_x(i,j,n)$ is assumed to be the average of $D(i,j,n)$ and $D(i-1,j,n)$ and furthermore the value at time $(n+1/2)$ is assumed to be adequately represented by the average value from time (n) to time $(n+1)$. To evaluate the integral terms in Equation B-2 the assumption is first made that the parameters q_x, q_y are slowly varying with respect to the time scale Δt.

$$\Delta t \int_t^{t + \Delta t} \overline{q}_y(i,j,\xi) \, d\xi$$

is then approximated by $\overline{q}_y(i,j,n)\Delta t$, remembering that $\overline{q}_y(i,j,n+1/2)\Delta t$ would be a better approximation but that the value at $(n+1/2)$ is not available. An iterative technique could be used to obtain $\overline{q}_y(i,j,n+1/2)$ but the magnitude of the error is small since $\overline{q}_y$ is seen to change slow-

ly with respect to Δt (see Figure 4-10), and cost in increased computer time is large so that a change to an implicit scheme is not warranted at the present time.

A more critical problem is that of placing the

$$\int_n^{n+1} |q(i,j,\xi)|\ q_x(i,j,\xi)\ d\xi$$

term into finite-difference form. To maintain an explicit form the following approximation is made:

$$\int_n^{n+1} |q(i,j,\xi)|\ q_x(i,j,\xi)\ d\xi = |q(i,j,n)|\ q_x(i,j,n+1)\ \Delta t$$

To show that this is correct to second order, it is sufficient to demonstrate that to second order in Δt

$$\int_{t_0}^{t_0+\Delta t} q^2 dt = q(t_0)\ q(t_0+\Delta t)$$

Expanding about $q(t_0)$

$$\int_{t_0}^{t_0+\Delta t} [q + \frac{\partial q}{\partial t}(t-t_0) + \frac{\partial^2 q}{\partial t^2}(t-t_0)^2]^2\ dt$$

$$\approx \int_{t_0}^{t_0+\Delta t} [q^2 + 2q\frac{\partial q}{\partial t}(t-t_0) + \frac{\partial^2 q}{\partial t^2}(t-t_0)^2 + (\frac{\partial q}{\partial t})^2(t-t_0)^2/4]dt$$

Making the change of variable $t' = t - t_o$

$$\int_0^{\Delta t} [q^2 + 2q \frac{\partial q}{\partial t} t' + q \frac{\partial^2 q}{\partial t^2} t'^2 + \frac{1}{4}(\frac{\partial q}{\partial t})^2 t'^2] \, dt'$$

$$\simeq q^2 \Delta t + 2q \frac{\partial q}{\partial t} \frac{\Delta t^2}{2} + q \frac{\partial^2 q}{\partial t^2} \frac{\Delta t^3}{3} + (\frac{\partial q}{\partial t})^2 \frac{\Delta t^3}{12}$$

$$= q [q + 2\frac{\partial q}{\partial t} \Delta t + O(\Delta t^2)]\Delta t$$

Now changing back to $t = t' + t_o$ and expressing the result in indicial notation yields to second order in Δt,

$$= q(i,j,n) [q(i,j,n+1)]\Delta t$$

The desired result with the introduction of the x-component and absolute value is

$$|q(i,j,n)| \, q_x(i,j,n+1)\Delta t$$

Introducing this into Equation (B-2a) and solving for $q_x(i,j,n+1)$ yields Equation (B-3a)

$$q_x(i,j,n+1) = \frac{1}{F_x} [q_x(i,j,n) + 2\omega(\sin\phi)\overline{q}_y(i,j,n)\Delta t$$

$$+ \frac{\Delta t}{2\Delta x} \{D(i,j,n+1/2)+D(i-1,j,n+1/2)\}\{\frac{1}{\rho}[p_n(i-1,j,n+1/2)-p_n(i,j,n+1/2)]$$

$$+ g [n(i-1,j,n+1/2) - n(i,j,n+1/2)]\}$$

$$+ \frac{\Delta t}{2\rho} \{\tau_{n_x}(i,j,n+1/2) + \tau_{n_x}(i-1,j,n+1/2)\}] \tag{B-3a}$$

with

$$F_x = 1 + \frac{f \Delta t}{2} \{[q_x(i,j,n)]^2 + [q_y(i,j,n)]^2\} \ . \qquad \text{(B-3b)}$$

$$[D(i-1,j,n+1/2) + D(i,j,n+1/2)]^{-2}$$

These are Equations (3-7a) and (3-7b) of the main text respectively. It can be seen that forward differences in time have been used throughout. Application of this procedure to the y-equation and the continuity equation is identical in concept to the above and the equations in finite difference form are given by Equations (3-8a), (3-8b), and (3-9) of the main text.

2. Effect of Convective Terms

The convective terms for the x-equation are: $\dfrac{\partial}{\partial x} \displaystyle\int_{-h}^{\eta} u^2 \, dz$ and

$\dfrac{\partial}{\partial y} \displaystyle\int_{-h}^{\eta} uv \, dz.$ Since the form of the velocity profile is an unknown,

evaluation of the convective terms is difficult. An approximation

could be made by assuming that the flow is highly turbulent (a

physically reasonable condition), and similar in form to that of open

channel flow, that is steady state. This would then provide a velocity

distribution that is logarithmic in form and reasonably uniform above

a distance 0.2 x depth. Making the more restrictive assumption that the

velocity distribution in the vertical is uniform enables one to evaluate

the integral terms,

$$\frac{\partial}{\partial x} \int_{-\eta}^{\eta} u^2 \, dz = \frac{\partial}{\partial x} [\, Du^2 \,] = \frac{\partial}{\partial x} [\frac{q_x^2}{D}]$$

$$\frac{\partial}{\partial y} \int_{-\eta}^{\eta} uv \, dz = \frac{\partial}{\partial y} [\, Duv \,] = \frac{\partial}{\partial y} [\, \frac{q_x \bar{q}_y}{D} \,]$$

where $q_x = Du$ and $q_y = Dv$ as a result of the uniform velocity distribu-
tion.

If one continues at this point as in part 1 of this appendix and
assumes

$$q_x(n+1/2) \; \bar{q}_y(n+1/2) = q_x(n+1) \; \bar{q}_y(n)$$

an implicit scheme would still be necessary because of the required spatial derivatives in x and y. Keeping in mind the magnitude of the error in part 1 of this appendix it is reasonable to approximate q_x^2, $q_x\bar{q}_y$, and $\bar{q}_y^2$ by their values at one time step earlier, this is especially true near the time of peak surge and currents where

$\dfrac{\partial q_x}{\partial t} \to 0$ and $\dfrac{\partial q_y}{\partial t} \to 0$. The x-equation of motion then becomes Equation (B-4)

$$q_x(i,j,n+1) = \frac{1}{F_x} \left[q_x(i,j,n) + 2\omega(\sin \phi)\bar{q}_y(i,j,n) \; \Delta t \right.$$

$$+ \frac{\Delta t}{2\Delta x} \{D(i-1,j,n+1/2) + D(i,j,n+1/2)\} \; \{ \frac{1}{\rho} [p_n(i-1,j,n+1/2)-p_n(i,j,n+1/2)]$$

$$+ g [n(i-1,j,n+1/2) - n(i,j,n+1/2)]\}$$

$$+ \frac{\Delta t}{2\rho} \{\tau_{n_x}(i-1,j,n+1/2) + \tau_{n_x}(i,j,n+1/2)\}$$

$$- \frac{\Delta t}{4\Delta x} [D(i-1,j,n+1/2) + D(i,j,n+1/2)]^{-1} [q_x^2(i+1,j,n) - q_x^2(i-1,j,n)]$$

$$- \frac{\Delta t}{4\Delta y} [D(i-1,j,n+1/2) + D(i,j,n+1/2)]^{-1} [q_x(i,j+1,n) \; \bar{q}_y(i,j+1,n)$$

$$\left. -q_x(i,j-1,n) \; \bar{q}_y(i,j-1,n)]\right] \tag{B-4}$$

where, as before

$$F_x = 1+ \frac{f \; \Delta t}{2} \{ [q_x(i,j,n)]^2 + [\bar{q}_y(i,j,n)]^2 \}^{1/2} \; .$$

$$[D(i-1,j,n+1/2) + D(i,j,n+1/2)]^{-2}$$

The convective terms for the y-equation of motion are

$$\frac{\partial}{\partial x} \int_{-\eta}^{\eta} uv \ dz \ \text{and} \ \frac{\partial}{\partial y} \int_{-\eta}^{\eta} v^2 dz,$$

applying the approximations used for the x-equation, the y-equation can be written as Equation (B-5).

$$q_y(i,j,n+1) = \frac{1}{F_y} [q_y(i,j,n) - 2\omega \ \sin\phi \ \overline{q}_x(i,j,n) \Delta t$$

$$+ \frac{\Delta t}{2\Delta x} \{D(i,j,n+1/2) + D(i,j-1,n+1/2)\}$$

$$\{ \frac{1}{\rho} [p_\eta \ (i,j-1,n+1/2) - p_\eta(i,j,n+1/2)]$$

$$+ g \ [\eta(i,j-1,n+1/2) - \eta(i,j,n+1/2)] \}$$

$$+ \frac{\Delta t}{2\rho} \{\tau_{\eta_y} (i,j,n+1/2) + \tau_{\eta_y} (i,j-1,n+1/2) \}$$

$$- \frac{\Delta t}{4\Delta x} [D(i,j,n+1/2) + D(i,j-1,n+1/2)] [q_y(i+1,j,n) \ \overline{q}_x(i+1,j,n)$$

$$-q_y(i-1,j,n) \ \overline{q}_x(i-1,j,n)]$$

$$- \frac{\Delta t}{4\Delta y} [D(i,j,n+1/2) + D(i,j-1,n+1/2)] [q_y^2(i,j+1,n) - q_y^2(i,j-1,n)]]$$

$$(B-5)$$

where

$$F_y = 1 + \frac{f\Delta t}{2} \{[\overline{q}_x(i,j,n)]^2 + q_y(i,j,n)]^2\}^{-1/2} \ .$$

$$[D(i,j,n+1/2) + D(i,j-1,n+1/2)]^{-2}$$

A better smoothing of D as in Section 3-b of the text may be desirable but the simplicity of the averages used in Equations (B-4) and (B-5) dictate that they be used since the goal here is to obtain a numerical

estimate of the changes due to the inclusion of the convective terms.

Introduction of these forms for the convective terms into the numerical model changed the calculated maximum surge by about 1.2% and changes the surge height at any grid element adjacent to the coast by less than 5%. Because of the complexity and their relatively small effect, the convective terms were not further considered in this study.

REFERENCES

1. Lamb, H., Hydrodynamics, 6th Ed., Dover Publications, New York, 1945.

2. Reid, R. O., "Approximate Response of Water Level on a Sloping Shelf to a Wind Fetch Which Moves Toward Shore," U. S. Army Corps of Engineers, Beach Erosion Board, Technical Memorandum 83, 1956.

3. Hansen, W., "Theorie zur Errechnung des Wasserstandes und der Stromungen in Randmeeren Nebst Anwendungen," Tellus, No. 3, 1956.

4. Hansen, W., "Hydrodynamical Methods Applied to Oceanographic Problems," Proceedings of the Symposium, Mathematical-Hydrodynamical Methods of Physical Oceanography, Institute Fur Meereskunde Der Universitat Hamburg, 1962.

5. Platzman, G. W., "A Numerical Computation of the Surge of 26 June 1954 on Lake Michigan," Geophysica, Vol. 6, 1958.

6. Miyazaki, M., "A Numerical Computation of the Storm Surge of Hurricane Carla 1961 in the Gulf of Mexico," University of Chicago, Department of Geophysical Sciences, Technical Report No. 10, 1963.

7. Reid, R. O., "Modification of the Quadratic Bottom-Stress Law for Turbulent Channel Flow in the Presence of Surface Wind Stress," U. S. Army Corps of Engineers, Beach Erosion Board, Technical Memorandum 93, 1957.

8. Marinos, G., and J. W. Woodward, "Estimation of Hurricane Surge Hydrographs," Journal of the Waterways and Harbors Division, ASCE, Vol. 94, No. WW2, 1968.

9. Freeman, J. C., Jr., L. Baer, and G. H. Jung, "The Bathystrophic Storm Tide," Journal of Marine Research, Vol. 16, No. 1, 1957.

10. Reid, R. O., and B. R. Bodine, "Numerical Model for Storm Surges in Galveston Bay," Journal of the Waterways and Harbors Division, ASCE, Vol. 94, No. WW1, 1968.

11. Harris, D. L. and C. P. Jelesnianski, "Some Problems Involved in the Numerical Solutions of Tidal Hydraulics Equations," Monthly Weather Review, Vol. 92, No. 9, 1964.

12. Jelesnianski, C. P., "A Numerical Computation of Storm Tides Induced by a Tropical Storm Impinging on a Continental Shelf," Monthly Weather Review, Vol. 93, No. 6, 1965.

13. Jelesnianski, C. P., "Numerical Computations of Storm Surges Without Bottom Stress," Monthly Weather Review, Vol. 94, No. 6, 1966.

14. Jelesnianski, C. P., "Numerical Computations of Storm Surges with Bottom Stress," Monthly Weather Review, Vol. 95, No. 11, 1967.

15. Jelesnianski, C. P., "Bottom Stress Time-History in Linearized Equations of Motion of Storm Surges," Monthly Weather Review, Vol. 98, No. 6, 1970.

16. Murray, S. P., "Bottom Currents Near the Coast During Hurricane Camille," Journal of Geophysical Research, Vol. 75, No. 24, 1970.

17. Murray, S. P., "Turbulence in Hurricane-Generated Coastal Currents," Proceedings of the Twelfth Coastal Engineering Conference, American Society of Civil Engineers, Chapter 124, New York, 1970.

18. Schlichting, H., Boundary-Layer Theory, McGraw-Hill Book Co., New York, 1968.

19. Van Dorn, W., "Wind Stress on an Artificial Pond," Journal of Marine Research, Vol. 12, No. 3, 1953.

20. Wu, J., "Wind Stress and Surface Roughness at Air-Sea Interface," Journal of Geophysical Research, Vol. 74, No. 2, 1969.

21. Dean, R. G. and B. R. Pearce, "Storm Tide Response on Idealized Continental Shelves: Effects of Steady Wind Fields of Limited Lateral Extent," Department of Coastal and Oceanographic Engineering, University of Florida, Technical Report No. 9, January, 1972.

22. Tickner, E. G., "Transient Wind Tides in Shallow Water," U. S. Army Corps of Engineers, Beach Erosion Board, Technical Memorandum 123, 1961.

23. Wilson, B. L., "Hurricane Wave Statistics for the Gulf of Mexico," U. S. Army Corps of Engineers, Beach Erosion Board, Technical Memorandum 98, 1957.

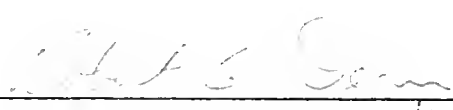24. Gordon, A. H., Elements of Dynamic Meteorology, D. Van Nostrand Company, Inc., London, 1962.

25. Holmboe, J., G. E. Forsythe, and W. Gustin, Dynamic Meteorology, John Wiley & Sons, New York, 1945.

26. U. S. Department of Commerce, National Weather Service, Memorandum HUR 7-113, 1969.

27. U. S. Department of Commerce, National Weather Service, Memorandum HUR 7-113A, 1970.

28. Verma, A. P. and R. G. Dean, "Numerical Modeling of Hydromechanics of Bay Systems," Proceedings, Civil Engineering in the Oceans II, Miami, 1969.

29. Hildebrand, F. B., Advanced Calculus For Applications, Prentice-Hall, Inc., Englewood Cliffs, 1962.

30. Dean, R. G. and B. R. Pearce, "Numerical Modeling Aspects of Storm Tide and Current Response to Hurricane Systems," Department of Coastal and Oceanographic Engineering, University of Florida Technical Report No. 10, January, 1972.

31. U. S. Army Corps of Engineers, Mobile District, Hurricane Camille 14-22 August 1969, May, 1970.

32. U. S. Army Corps of Engineers, New Orleans District, Report on Hurricane Camille, 14-22 August 1969, May, 1970.

33. U. S. Department of Commerce, NOAA, Tide Tables, High and Low Water Predictions, 1969, U. S. Government Printing Office, Washington, D. C., 1968.

34. Dean, R. G. and B. R. Pearce, unpublished data.

35. Sonu, C. J., "Beach Changes by Extraordinary Waves Caused by Hurricane Camille," Coastal Studies Institute, Louisiana State University, Technical Report 77, February, 1970.

36. U. S. Department of Commerce, National Weather Service, "Preliminary Report - Hurricane Camille - August 14-22, 1969," 1969.

37. Harris, D. L., "Meteorological Aspects of Storm Surge Generation," Journal of Hydraulics Division, ASCE, Vol. 84, No. HY7, 1958.

BIOGRAPHICAL SKETCH

Bryan Rowell Pearce was born October 9, 1944, at Washington, D.C. In June 1962, he graduated from Melbourne High School, Melbourne, Florida. In June 1966, he received the degree Bachelor of Science with a major in Physics from the Massachusetts Institute of Technology. From July through December of 1966 he served as a scientific crew member on an oceanographic expedition to the Red and Mediterranean Seas conducted by the Woods Hole Oceanographic Institution. He spent the spring semester 1966-67 in graduate study in Geophysics at Harvard University. He worked as a graduate assistant in the Department of Naval Architecture and Marine Engineering at the Massachusetts Institute of Technology from September 1967 until June 1969 when he received the degree of Master of Science in Ocean Engineering. From September 1969 until the present time he has worked as a research assistant in the Department of Coastal and Oceanographic Engineering at the University of Florida. From September 1969 until the present time he has also pursued his work toward the degree Doctor of Philosophy in Civil Engineering.

Bryan Rowell Pearce is married to the former Aphrodite Maria Pananos. He is a member of American Geophysical Union, American Society of Civil Engineers, and the Marine Technology Society.

I certify that I have read this study and that in my opinion it conforms to acceptable standards of scholarly presentation and is fully adequate, in scope and quality, as a dissertation for the degree of Doctor of Philosophy.

Robert G. Dean, Chairman
Professor of Civil and Coastal
Engineering

I certify that I have read this study and that in my opinion it conforms to acceptable standards of scholarly presentation and is fully adequate, in scope and quality, as a dissertation for the degree of Doctor of Philosophy.

Bent A. Christensen, Cochairman
Professor of Civil and Coastal
Engineering

I certify that I have read this study and that in my opinion it conforms to acceptable standards of scholarly presentation and is fully adequate, in scope and quality, as a dissertation for the degree of Doctor of Philosophy.

F. Michael Wahl
Professor of Geology

This dissertation was submitted to the Dean of the College of Engineering and to the Graduate Council, and was accepted as partial fulfillment of the requirements for the degree of Doctor of Philosophy.

August, 1972

Dean, College of Engineering

Dean, Graduate School